

**THE ROLE OF THE GAS-WATER INTERFACE ON  
THE TRANSPORT OF  
COLLOIDS AND BACTERIA IN POROUS MEDIA**

by

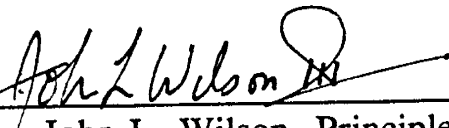
**Jiamin Wan**

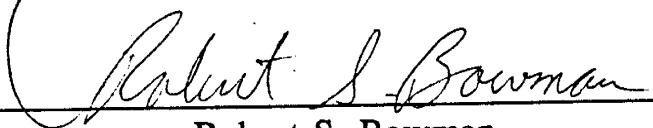
Submitted in partial fulfillment of the requirements for  
the degree of the Doctor of Philosophy in Hydrology

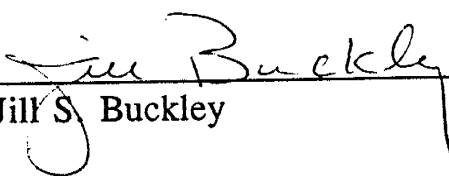
Department of Geoscience  
New Mexico Institute of Mining and Technology  
Socorro, New Mexico

April 1993

This dissertation is accepted on behalf of the faculty of the  
Institute by the following committee:

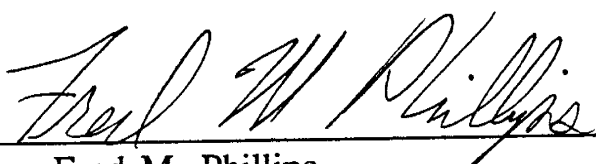
Approved by:   
John L. Wilson, Principle Adviser

  
Robert S. Bowman

  
Jill S. Buckley

  
Thomas L. Kieft

Norman R. Morrow  
Norman R. Morrow

  
Fred M. Phillips

---

## ACKNOWLEDGEMENTS

---

I gratefully acknowledge John Wilson, my advisor; his advice, help, trust, and encouragement has made this achievement possible. I am grateful, also, to my dissertation committee members: Robert Bowman, Jill Buckley, Thomas Kieft, Norman Morrow, and Fred Phillips for their warm support, helpful discussions, attention to my progress reports, and for their reading of this thesis. I would like to thank Liyuan Liang as well for reading my proposal and this thesis. I am appreciative for the funding provided by the Subsurface Science Program of the Department of Energy, DOE Grant Number DE-FG04-89ER60829 through Dr. J.L. Wilson and NMT.

I would like to especially acknowledge my friends, Robert Mace, Robert TerBerg, Grace Haggerty, LuAnn Pavletich, and many others. They have greatly helped me with my English, supported me with love and patience, and shown me good times.

I am also grateful to Edith Montoya and Loretta Murillo from the hydrology office, who have made so many things easier and smoother for me.

I would like to dedicate this thesis to my parents in memory of their love, the hopes they had for me, and the education they gave me. I seem to feel, at this moment, their joyful smiles, and hear their voices. As usual, Mum says, "You look tired, have a break." Dad says, "Don't stop, you've just started..."

---

**ABSTRACT**

---

In this dissertation a new mechanism governing the transport of colloids and microorganisms through unsaturated porous media is suggested, and a new method for directly visualizing colloids and bacterial behavior within a porous medium under controlled chemical and flow conditions is developed.

Different types of polystyrene latex microspheres, clay particles, and resting-cells of bacterial strains with various surface hydrophobicities were used as model particles. The degree of hydrophobicity was determined by contact angle measurements. Glass micromodels allowed the direct observation of particle behavior on a pore scale, and sand columns with three types of different gas saturations (water-saturated, gas as residual bubbles, and gas as a continuous phase) provided quantitative measurements of the observed phenomena on a porous medium scale. The reproducibility of each breakthrough curve was established in five repeated experiments. Both the cause and effect were revealed by combining the visualization and quantification of these two methods.

The retention rate of particles is proportional to the gas saturation in porous media, due to the preferential sorption of particles onto the gas-water interface rather than onto the rock-water interface. The degree of sorption is chiefly controlled by particle surface hydrophobicity under the simulated groundwater conditions, due to

## II

hydrophobic forces between the particles and the interfaces. The sorption onto the gas-water interface is essentially irreversible due to capillary forces. Because of the preferential and irreversible sorption, a static gas-water interface behaving as a sorbent phase sorbs and retains colloids, thus reducing particle transport. The static gas-water interface along with the previously sorbed colloids can be mobilized by increasing shear stress, thereby increasing the transport and redistributing the particles in the porous medium.

With potential applications to wastewater disposal, in-situ bioremediation, and microbially enhanced oil recovery, etc., the gas-water interface is a significant factor strongly influencing the movement and spatial distribution of colloids and microorganisms in the subsurface environment.

---

**TABLE OF CONTENTS**

---

	Page
Abstract .....	I
Table of Contents.....	III
List of Figures .....	VII
List of Tables .....	XI
Chapter 1 Introduction .....	1
Statement of the Problem .....	1
Theoretical Background .....	5
Adhesion of Partices on Gas Bubbles and Froth Flotation .....	5
Interfacial Forces and Stability of Colloids .....	8
References .....	16
Chapter 2 Visualization of the Role of the Gas-water Interface on the	
Fate and Transport of Colloids in Porous Media .....	21
Abstract .....	21
Introduction .....	22
Materials and Methods .....	23
Glass Micromodels .....	23
Colloidal Particles .....	27
Characterization of Particle Surface Hydrophobicity .....	29

### III

	Page
Experimental Procedure .....	30
Results and Discussion .....	32
Gas-water Interface and Hydrophilic Particles .....	32
Sorption and Particle Surface Hydrophobicity .....	38
Sorption and Particle Surface Charge Sign .....	39
Sorption and Ionic Strength .....	42
Desorption .....	45
Summary and Conclusions .....	52
Acknowledgements .....	53
References .....	54
Appendix 2A: Procedure for Making Glass Micromodels .....	57
Chapter 3 Colloid Transport in Unsaturated Porous Media .....	61
Abstract .....	61
Introduction .....	62
Materials and Methods .....	65
General Methodology .....	65
Colloids and Surface Characterization .....	68
Preparation of Medium Surface .....	72
Preparation of the Columns .....	72
Procedure for Column Experiments .....	74
Results and Discussion .....	76

IV

	Page
Micromodel Experiments .....	76
Column Experiments with Hydrophilic Colloids .....	79
Column Experiments with Hydrophobic Colloids .....	82
Conclusions .....	86
Acknowledgements .....	87
References .....	88
Appendix 3A: Breakthrough Data of Latex Particles .....	91
Appendix 3B: Breakthrough Curves of Latex Particles .....	101
Appendix 3C: Parameters of Columns in Latex	
Particle Experiments .....	108
Chapter 4 The Gas-water Interface as an Influence on Transport	
of Microorganisms through Unsaturated Porous Media .....	111
Abstract .....	111
Introduction .....	112
Materials and Methods .....	115
Glass Micromodels .....	115
Solutions and Cell Suspensions .....	116
Bacterial Strains .....	119
Apparatus and Procedure for Micromodel Experiments .....	121
Materials and Procedure for the Column Experiments .....	122



	Page
Results and Discussion .....	126
Cell Surface Hydrophobicity .....	126
Micromodel Experiments .....	127
Column Experiments .....	134
Acknowledgements .....	140
References .....	141
Appendix 4A: Breakthrough Data of Bacterial Strains .....	145
Appendix 4B: Breakthrough Curves of Bacterial Strains .....	152
Appendix 4C: Parameters of Columns in Experiments with Bacterial Strains .....	159
Chapter 5 Summary and Recommendations .....	162
Appendix 5A: Dynamic Gas-Water Interfaces .....	165

---

 LIST OF FIGURES
 

---

Figure	Page
1.1. Schematic energy vs. distance profiles of DLVO interactions .....	12
2.1. Three pore networks used in this study: (a) quadrilateral network; (b) hexagonal network; (c) heterogeneous network .....	25
2.2. A glass micromodel plate containing four micromodels with heterogeneous networks.....	26
2.3. Hydrophilic negatively charged latex particles ( $0.95 \mu\text{m}$ ) preferentially sorbed onto air bubbles vs. pore walls .....	34
2.4. Sketch of trapped air bubble in pore body of glass micromodel, explaining the dark ring of air bubble .....	35
2.5. Na-montmorillonite particles ( $\sim 0.5 \mu\text{m}$ ) accumulated on downstream side of air bubble trapped in pore body of hexagonal network .....	36
2.6. Hydrophilic bacteria 3N3A ( $1.3 \times 0.8 \mu\text{m}$ ) preferentially sorbed on air bubble trapped in pore body of hexagonal network .....	37
2.7. Hydrophobic negatively charged latex particles sorbed on both air-water and glass-water interfaces .....	40
2.8. Relatively hydrophobic bacteria S-139 ( $1.0 \times 0.8 \mu\text{m}$ ) accumulated on air bubble in pore body of hexagonal network .....	41
2.9. Positively charged hydrophobic latex particles ( $0.6 \mu\text{m}$ ) have very strong affinity for both gas-water and glass-water interfaces .....	43
2.10. The effect of solution ionic strength on sorption: (a) in low ionic strength (1.0 mM) solution. (b) ionic strength is increased by a factor of 100 .....	44
2.11. Desorption as solution ionic strength decreases .....	46
2.12. The capillary free energy change $E_{\text{cap}}$ fixes the particles on the interface after the rupture of liquid film .....	49

## VII

Figure	Page
2.13.	The calculated capillary free energy as a function of contact angles for a one micron spherical particle near a large air bubble ..... 50
3.1.	Cross sections of columns with three different saturations..... 67
3.2.	Contact angle measurement with particle layer-captive drop method used on hydrophobic latex particles ..... 71
3.3.	Hydrophilic latex particles (0.95 $\mu\text{m}$ ) preferentially sorb onto the downstream portion of an air bubble. Few particles sorb onto the pore walls..... 77
3.4.	Hydrophobic negatively charged latex particles sorb onto both air-water and glass-water interfaces. .... 78
3.5.	Breakthrough curves of hydrophilic latex particles through three types of columns ..... 80
3.6.	Breakthrough curves of hydrophobic latex particles through three types of columns ..... 85
3.7	Breakthrough curves of hydrophilic latex particles through water-saturated columns..... 102
3.8	Breakthrough curves of hydrophilic latex particles through columns with 15% gas..... 103
3.9	Breakthrough curves of hydrophilic latex particles through unsaturated columns with 46% gas..... 104
3.10	Breakthrough curves of hydrophobic latex particles through water-saturated columns..... 105
3.11	Breakthrough curves of hydrophobic latex particles through columns with 15% gas..... 106
3.12	Breakthrough curves of hydrophobic latex particles through unsaturated columns with 46% gas..... 107
4.1.	Photo of a glass multi-micromodel plate containing four micromodels with a heterogeneous network pattern ..... 117

## VIII

Figure	Page
4.2. Microphotographs of three types of networks showing different saturations .....	118
4.3. Cross-sectional sketch of three column types with different saturations .....	124
4.4. Hydrophilic bacteria 3N3A (1.3x0.8 $\mu\text{m}$ ) preferentially sorbed on air bubble trapped in a pore body of hexagonal network.....	128
4.5. Relatively hydrophobic bacteria S-139 (1.0x0.8 $\mu\text{m}$ ) accumulated on an air bubble and sorbed onto the pore walls in a pore body of a hexagonal network .....	129
4.6. Dark field photographs; bacteria are white; heterogeneous network. (a) A large number of bacteria S-139 (1.0x0.8 $\mu\text{m}$ ) sorbed on a trapped air bubble. (b) The air bubble with sorbed bacteria was removed by increasing water flow rate .....	131
4.7. Bacterial strain ZAL001 (1.1x0.8 $\mu\text{m}$ ) with a strong affinity to the organic carbon liquid-water interface. Dark field.....	133
4.8. Breakthrough curves of bacterial strain 3N3A from columns with three different saturations (3 to 5 replications each) .....	136
4.9. Breakthrough curves of bacterial strain S-139 from columns with three different saturations .....	137
4.10. Breakthrough curves of bacterial strain 3N3A from water-saturated columns.....	153
4.11. Breakthrough curves of bacterial strain 3N3A from columns with 15% gas.....	154
4.12. Breakthrough curves of bacterial strain 3N3A from columns with 46% gas.....	155
4.13. Breakthrough curves of bacterial strain S-139 from water-saturated columns.....	156
4.14. Breakthrough curves of bacterial strain S-139 from columns with 15% gas.....	157

IX

Figure	Page
4.15. Breakthrough curves of bacterial strain S-139 from columns with 46% gas.....	158
5.1. Effect of moving gas-water interfaces.....	166

## LIST OF TABLES

---

Table	Page
2.1. Particles used in the micromodel experiments.....	28
3.1. Latex particles and their surface properties.....	70
3.2. Parameters of column experiments.....	75
3.3. Breakthrough data of hydrophilic latex particles through water-saturated columns.....	92
3.4. Breakthrough data of hydrophilic latex particles through columns with 15% gas.....	93
3.5. Breakthrough data of hydrophilic latex particles through columns with 46% gas.....	94
3.6. Breakthrough data of hydrophobic latex particles through water-saturated columns.....	95
3.7. Breakthrough data of hydrophobic latex particles through columns with 15% gas.....	97
3.8. Breakthrough data of hydrophobic latex particles through columns with 15% gas.....	99
3.9. Parameters of columns in experiments with hydrophilic latex particles.....	109
3.10. Parameters of columns in experiments with hydrophobic latex particles.....	110
4.1. Bacterial strains used in the experiments.....	120
4.2. Parameters for the column experiments.....	125
4.3. Breakthrough data of hydrophilic strain 3N3A through water-saturated columns.....	146

XI

Table	Page
4.4. Breakthrough data of hydrophilic strain 3N3A through columns with 15 % gas .....	147
4.5. Breakthrough data of hydrophilic strain 3N3A through columns with 46 % gas.....	148
4.6. Breakthrough data of hydrophobic strain S-139 through water-saturated columns.....	149
4.7. Breakthrough data of hydrophobic strain S-139 through columns with 15 % gas.....	150
4.8. Breakthrough data of hydrophobic strain S-139 through columns with 46 % gas.....	151
4.9. Parameters of columns in experiments with hydrophilic bacteria .....	160
4.10. Parameters of columns in experiments with hydrophobic bacteria .....	161

---

## CHAPTER 1

---

### INTRODUCTION

#### STATEMENT OF THE PROBLEM

The transport of mobile colloids through porous media is an important process in environmental and biological systems. In the subsurface environment colloid transport significantly facilitates the migration of particulate contaminants and colloid-bound pollutants in groundwater and soils (Gshwend and Wu, 1985; McDowell-Boyer et al. 1986; Buddemeier and Hunt, 1988; McCarthy and Zachara, 1989). In the water and wastewater treatment industries, granular-bed filtration separates fine particles, pathogens and colloid-associated pollutants from suspensions (Ives and Gregory, 1966; Yao et al., 1971; O'Melia, 1989). Historically, research on colloid transport has focused on water-saturated porous media, and has been concerned with the movement, sorption to and desorption from the solid medium surface. Quantitative models for predicting particle transport in the water filtration literature (e.g., Yao et al., 1971; Spielman et al., 1973; Tien and Payatakes, 1979; Tien, 1989) account for the deposition mechanisms of particle-medium collisions and attachment. For Brownian particles, diffusion and advection control the collision rate. Attachment is determined by the interfacial forces between the mobile particles and fixed solid surfaces (collectors). These forces include electrical double layer, van der Waals, structure (hydration or hydrophobic), and



hydrodynamic forces (Israelachvili, 1985; Derjaguin et al., 1987; Hirasaki, 1991; Israelachvili, 1991). A large discrepancy between controlled laboratory experiments and theory is a common feature of colloid transport studies. For instance, under conditions unfavorable to particle deposition, the predictions for particle transport greatly exceed any laboratory and field observations (FitzPatrick, 1972; Bomen and Epstein, 1979; Elimelech and O'Melia, 1990 a,b). Various explanations for these discrepancies have been proposed over the past two decades (e.g. Spielman, 1977; Gregory and Wishart, 1980; Adamczyk et al., 1983; O'Melia, 1989; Litton and Olson, 1993). The research presented in this dissertation suggests a new explanation: a residual gas phase present in porous media can effectively reduce the transport distance.

Research on the fate and transport of microorganisms in the subsurface environment has been stimulated by interest in in-situ bioremediation of contaminated soils and aquifers (Lee et al., 1988; Thomas and Ward, 1989), transport of microbe-associated radionuclides (Champ, 1986), and enhancement of crude-oil recovery (Chase et al., 1990). A traditional and important concern is also the disposal of sewage by infiltration through soil to remove pathogenic microorganisms. Transport of microorganisms is governed by sorption onto immobile substrates, and also by inactivation (Yates et al. 1987; Bales et al., 1991). Many factors contributing to sorption have been studied: the nature of the porous medium including soil type, grain size, heterogeneity, and clay and organic matter content (Bales et al., 1989; Baven and Germann, 1982; Fontes et al., 1991; Powelson et al., 1991); water chemistry including pH and ionic strength (Martln et al, 1973; Bales et al., 1991 ); cell types including size

and surface hydrophobicity (van Loosdrecht, et al., 1987; Doyle and Rosenberg, 1990; Grotenhuis et al., 1992); infiltration rate (Vaughn et al., 1981); and clogging efficiency (Vandevivere and Baveye, 1992). Most of the transport studies have focused on saturated porous media, but a few have studied unsaturated conditions such as those found in the vadose zone. Lance and Gerba (1984) observed that unsaturated flow resulted in a higher degree of virus retention through loamy sand. Powelson et al. (1990) reported that viruses were more strongly removed from the soil water under unsaturated than saturated conditions, and they suggested that the unrecovered viruses were inactivated.

Gas is one of the major fluid phases in the subsurface. In the vadose zone, a continuous gas phase shares pore space with the aqueous phase. In the saturated zone, gas bubbles may be generated by various processes: entrapment of air as the water table fluctuates, organic and biogenic activities, or the emergence of gas from the solution as the aqueous phase pressure drops. In addition to occupying the pore space, the appearance of the gas phase generates the gas-water interface. The area of the gas-water interface depends on the ratio of gas saturation to water saturation, as well as the structure of the porous medium. In a common three-phase system of rock, water and gas, with a water-wet rock surface, we have two principle interfaces: rock-water and gas-water. Although the rock-water interface has been studied for decades, the gas-water interface has not been considered in the research of subsurface transport phenomena or has been assumed to be inactive. The initial motivation of this research was curiosity as to whether or how the presence of this interface affects the transport of particulate contaminants.

The objectives of this research have been: (a) To assess the adhesion of particles on the gas-water interface as a function of particle type, particle surface hydrophobicity, surface charge sign, and the ionic strength of solutions. (b) To identify theoretically the interfacial forces responsible for the observed behavior. (c) To develop a general technique for visualizing the interfacial interactions in a pore scale, and quantifying the interaction on an extended scale such as in a sand column. (d) To explore the potential applications of this interfacial phenomenon for soil and aquifer cleanup.

Glass micromodels generated by a modified method were used to visualize the interfacial interactions of particles and interfaces in a pore and pore network scale under strictly controlled chemical and flow conditions. The observed phenomena were quantified by filtration experiments using packed sand columns. Columns with three different saturations, water-saturated, gas trapped as the residual bubbles, and gas contained as a continuous phase, represented different subsurface conditions. Although polystyrene latex particles were used as the model colloids; clay particles and bacterial strains were also studied. The particle surface hydrophobicities were characterized by contact angle measurements. The results are described in the following three chapters. Chapter 2 presents the glass micromodel methods and visualized phenomena; Chapter 3 emphasizes the column experimental methods and results; Chapter 4 presents the methods and results related to bacterial strains; and Chapter 5 concludes with the significance of the research. The remaining portion of this chapter presents a theoretical background for the experiments.

## THEORETICAL BACKGROUND

### Adhesion of Particles on Gas Bubbles and Froth Flotation

Gas bubbles have been intensively studied in the flotation field (Derjaguin and Dukhin, 1981; Jameson, 1985; Lekki and Laskowsky, 1976; Hornsy and Leja, 1982) due to their economic importance. Froth flotation is a physical-chemical process commonly used for beneficiating a wide variety of ores, coal, oil shale, tar sand, industrial waste and biological substances. The success of the flotation process depends on rendering selected minerals in a pulp to become hydrophobic and hence floatable, while keeping or making all the other minerals hydrophilic. In the simplest case, this is achieved by adding a surface-active agent called a collector which has a selectivity for the mineral to be floated. Depressants are added to prevent flotation of unwanted minerals and activators are used to promote the adsorption of the collector on a given mineral. Air bubbles blown into the pulp and stabilized by the addition of a frother, most commonly a non-ionic surfactant, collect the hydrophobic particles and carry them to the froth layer at the top of the slurry, where they concentrate and overflow into a launder. The hydrophilic minerals or tailings are rejected from the bottom of the flotation cell. From a dynamic viewpoint, the events leading to flotation are usually considered to occur in three main stages (Derjaguin and Dukhin, 1961; Laskowski, 1975). (1) Bubble-particle collision with the formation of a thin wetting film, which is known as the disjoining film. (2) Thinning of the disjoining film which separates the colliding bubble and particle, and

film rupture at the critical thickness under the influence of interfacial surface forces. (3) Formation of a stable bubble-particle aggregates in the flotation cell. The first of these stages is controlled by the hydrodynamic conditions in the cell and the related solution chemistry that determines the production of bubbles of suitable size while the other two stages, which deal with the attachment efficiency, depend mainly on the physical-chemical conditions, particularly the degree of hydrophobicity of the mineral particles. The second stage, the thinning and rupture of the wetting film, is regarded as the most important stage in flotation (Derjaguin and Shukakidse, 1961; Finch and Smith, 1979) because it is a slow process and, therefore, is the rate-determining step. During the approach of a bubble to a mineral particle the intervening film undergoes thinning and, usually, it becomes unstable and subsequently ruptures under the influence of interfacial surface forces.

Sutherland (1948) provided a framework for quantifying the probability of bubble-particle flotation. He expressed the overall probability of particle flotation  $P$  as:

$$P = P_a P_c ( 1 - P_d ) \quad (1)$$

where  $P_c$ ,  $P_a$ , and  $P_d$  are the probabilities of collision, adhesion and detachment, respectively. Recently, Al Taweel et al. (1986) have pointed out that the probability of particle flotation  $P$ , is a compromise between  $P_c$  and  $P_a(1-P_d)$ . For strongly hydrophobic material such as coal,  $P_a(1-P_d)$  approaches one and the flotation rate is determined primarily by  $P_c$ , which increases with particle size. On the other hand, for relatively large particles of less hydrophobic nature the recovery is expected to be mainly

determined by  $P_a(1-P_d)$ , and is therefore strongly affected by the surface properties. Quantification of these parameters is difficult. Many researchers have provided different models (Al Taweel et al., 1986; Yoon and Luttrell, 1986). In the flotation literature it has been recognized that processing fine particles is extremely difficult due to the special properties of fines. For the same minerals, fine particles have lower flotation rates because of their low inertia. As the particle size decreases to colloidal dimensions, the differences in the surface properties of different kinds of fine mineral particles become less pronounced, thereby causing low separation efficiency. It is obvious that fine particles have a high specific surface area and low mass, a fact which yields low inertia and low momentum. This fact regarding the nature of fines makes it very difficult to avoid entrainment of unwanted fine particles (Warren, 1985; Fuerstenau, 1980; Anfruns and Kitchner, 1977; Jamesin, 1985; Derjaguin and Dukhin, 1981). This phenomenon implies that for particles with colloidal dimension, the general flotation theory may not provide a complete explanation.

The major differences between flotation and colloid movement through subsurface porous media which containing gas bubbles are: (1) Particle sizes are different, the mineral particles of concern in flotation ( $\geq 100 \mu\text{m}$ ) are much larger than the colloids ( $\leq 10 \mu\text{m}$ ) we consider in subsurface environments. (2) The interests are different; in the flotation industry the purpose is to separate the desired mineral from the gangue or non-mineral-containing material, while we are interested in all kinds of particles occurring in natural porous media. (3) The chemical conditions are different. The surfaces of mineral particles in flotation are usually covered with surface-active agents and the

surface of the bubbles is covered with a frother. The attachment of particles and bubbles is actually the attachment of molecules in these two phases. The similarity of these two processes is that the governing forces for adhesion, which determines the attachment efficiency, are theoretically the same.

### **Stability of Colloids and Interfacial Forces**

When colloidal particles or a particle and a surface approach each other in an aqueous phase, various types of interactions arise. The major types of interactions are described as follows:

**Van der Waals Force Between Surfaces.** The Van der Waals force ( $V_D$ ) is a long-range force contributed by three distinct types of forces: the induction force, the orientation force, and the dispersion force.  $V_D$  may be repulsive or attractive depending on the medium (Gregory, 1969; Israelachvili and Tabor, 1973; Nir, 1976). There are two approaches for calculating  $V_D$  between macroscopic bodies (Israelachvili and Tabor, 1973; Nir, 1976): one based on a molecular model attributed to Hamaker (Hamaker, 1937) and the other based on a model of condensed media, attributed to Lifshitz (Lifshitz, 1955). The former approach, also known as the microscopic approach, is widely used. In this approach Hamaker (1937) used the well known London expression for the dispersion attraction between two isolated molecules and integrated it for all the molecules in two separate particles in order to obtain the dispersion energy of interaction

between two macroscopic bodies. For two spheres of unequal radii, the dispersion potential (van der Waals interaction) is given by:

$$V_D = -\frac{A_{123}R_1R_2}{6h(R_1+R_2)} \quad (2)$$

Where  $A_{123}$  is the complex Hamaker constant for the interaction of two bodies of composition 1 and 3 in a medium of composition 2.  $R_1$  and  $R_2$  are the radii of two bodies, respectively, and  $h$  is the separation of surfaces along the line of their centers.  $A_{123}$  is evaluated by the equation:

$$A_{123} = (A_{11}^{1/2} - A_{22}^{1/2}) (A_{33}^{1/2} - A_{22}^{1/2}) \quad (3)$$

In this research the particle surface (solid phase) 1 and the gas phase 3 interact in the aqueous medium 2,  $A_{11}$  is the Hamaker constant for the particle,  $A_{33}$  the Hamaker constant for the air bubble, and  $A_{22}$  the Hamaker constant for the medium water. Note that, if the value of  $A_{22}$  is intermediate between the values of  $A_{11}$  and  $A_{33}$ , as is typically the case in flotation, then the Hamaker constant is negative. In this case the  $V_D$  force is repulsive. The concept of the negative Hamaker constant was first suggested in the classical paper of Hamaker (1937), and later discussed by Visser (1972, 1981). Experimental evidence for the existence of negative-Hamaker constants was summarized by Van Oss et al. (1983).

**Electrostatic Force between Surfaces.** The electrostatic energy ( $V_E$ ) arises from



the interaction between two double layers. When two surfaces approach each other, the overlap of diffuse double layers causes a change in the free energy of the system. For interacting double layers with equal signs, an increase in the free energy occurs causing repulsion and  $V_E$  to be positive. With opposite signs, a decrease in the free energy causes attraction;  $V_E$  is negative. Derjaguin and Landau (1941), and Verwey and Overbeek (1948) derived quantitative expressions for the double layer interaction energy. For an unequally charged spherical particle and a flat plate interacting at constant surface potential,  $V_E$  is given by (Hoggs, 1966):

$$V_E = P \left[ Q \ln \frac{(1 + e^{-\kappa h})}{(1 - e^{-\kappa h})} + \ln(1 - e^{-2\kappa h}) \right] \quad (4)$$

$h$  is the separation distance between the interaction bodies, and  $\kappa$  is the Debye reciprocal length given by the expression:

$$\kappa = \left( \frac{2Z^2F^2C}{\epsilon_0 \epsilon_r RT} \right)^{1/2} \quad (5)$$

$F$  is the Faraday constant,  $R$  is the gas constant,  $T$  is the absolute temperature,  $\epsilon_0$  and  $\epsilon_r$  are dielectric constant and dielectric permittivity, respectively.  $Z$  the valence of the counterions and  $C$  the concentration of the electrolyte.  $P$  and  $Q$  are constants given by:

$$P = \frac{\epsilon_r (\psi_1^2 + \psi_2^2)}{4} \quad (6)$$

$$Q = \frac{2(\psi_1\psi_2)}{(\psi_1^2 + \psi_2^2)} \quad (7)$$

$\epsilon$  is the dielectric constant of the medium and  $r$  is the radius of the particle,  $\psi_1$  and  $\psi_2$  are the surface potentials of the two bodies, which are approximated by their respective zeta potentials.

**Colloid Stability and DLVO Theory.** On the basis of van der Waals and electrostatic double layer forces, DLVO theory, has been developed to explain quantitatively the stability of colloids. According to the classical DLVO theory, the total interaction potential  $V_T$  between two particles embedded in a third liquid medium consists of two components, i.e.,

$$V_T = V_D + V_E \quad (8)$$

$V_D$  and  $V_E$  are the van der Waals dispersion and electrostatic interaction energies. This total interaction is indeed a simplified model since it does not include other important factors such as surface roughness, charge heterogeneity (Adamczyk et al., 1983) and short range structural forces (Israelachvili, 1985). Figure 1.1 shows the general energy profile obtained from Equation (8). The DLVO theory are summarized as follows:

(1) The energy barrier hinders the approach of particles and prevents their contact with the collector when electrical repulsion exceeds van der Waals attraction over a certain range of separation distances.

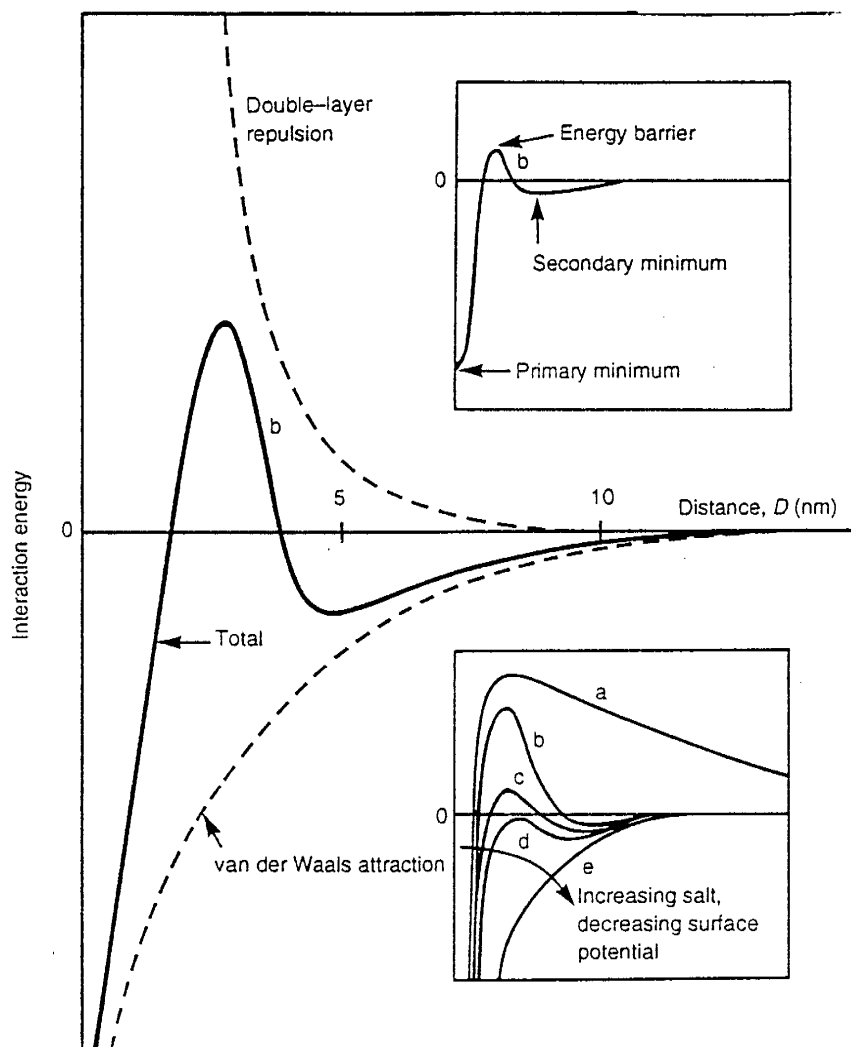


Fig. 1.1. Schematic energy vs. distance profiles of DLVO interactions. (a) Surfaces repel strongly; particles remain "stable". (b) Surfaces come into stable equilibrium at secondary minimum if it is deep enough; colloids remain "kinetically" stable. (c) Surface come into secondary minimum; colloids coagulate slowly. (d) The "critical coagulation concentration". Surfaces may remain in secondary minimum or adhere; colloids coagulate rapidly. (e) Surfaces and colloids coalesce rapidly. (After Israelachvili, 1992).

(2) Particle deposition rates on to the collector can be increased by lowering the energy barrier. This can be achieved by increasing the salt concentration of the solution, which reduces electrostatic double layer repulsion. The effect is more pronounced when the valence of the counterions is higher.

(3) When electrostatic double layer repulsion is sufficiently reduced such that the energy barrier is eliminated, particles will deposit on the collector due to the strong attractive  $V_D$  force.

**Structural Force.** The stability of very hydrophobic colloidal suspensions cannot be adequately described by the classical DLVO theory. Many investigators have provided both theoretical and experimental evidence for the existence of forces other than the dispersion and electrostatic forces considered in the DLVO theory. Structural force is the most general term, since it refers to the free energy change due to the unspecified solvent structuring, exhibited by the intervening liquid between approaching surfaces. The terms solvation, hydration, and hydrophobic forces are also used for this purpose. Our understanding of the nature of the structural force is still in its infancy due to the lack of a mature theory for describing the basic phenomenon. The origin of the structural force is believed to be the overlapping of the boundary layers of surfaces when they are approaching one another. However, many related problems remain unsolved: e.g., what is the special structure within the boundary layer? How do the boundary layers interact with each other? Some investigators (Laskowski and Kitchener, 1969; Rabinovich and Derjaguin, 1988; Claesson, 1987; Israelachvili and Pashley, 1982) have

suggested that the structural force arises mainly from the configurational rearrangement of water molecules in the vicinity of the surfaces, while others believe it is due to phase changes within the interlayer confined by the two approaching surfaces (Claesson, 1987; Pashley, 1981; Christenson, et al., 1987) or to the anomalous polarization of water molecules in the boundary (Laskowski and Kitchener, 1969; Marcelja and Radic, 1976; Claesson, et al., 1987).

Israelachvili and Pashley (1982) gave the isotherms of the structural force  $V_s$ , i.e., the dependence of the structural force on the thickness,  $h$ , of a liquid interlayer between a spherical particle and a flat surface as:

$$V_s(h) = -CrD_0 e^{(-h/D_0)} \quad (9)$$

where  $r$  is the radius of the sphere near the flat surface,  $h$  is the thickness of the liquid interlayer between the interacting bodies,  $D_0$  the decay length, and  $C$  a constant that has negative values for liquids that wet the substrate (hydrophilic), and positive values for hydrophobic substrats. When  $C$  is negative,  $V_s$  is more commonly known as hydration energy. On the other hand, when  $C$  is positive,  $V_s$  becomes attractive and is named hydrophobic interaction energy.

**Capillary Force.** If by any means a particle with a contact angle  $> 0^\circ$ , can pass through the energy barrier that arises from the superposition of van der Waals force, double layer force, and structural forces, the particle will contact the interface and a three-phase contact line will be formed. As long as the contact angle is greater than zero, such a line must exist. The resulting equilibrium forces can be calculated by applying force balance analyses and

Young's equation. The capillary forces, arises as soon as the three-phase (particle, gas, and liquid) contact line is established, will fix the particles at an equilibrium position at the gas-liquid interface. The exact calculation of such force involves solving a non-linear ordinary differential equation for the meniscus profiles and is only possible for the simplest geometries. A comprehensive treatment of capillary force was given by Rapacchietta and Neumann (1977). In their work, both force and free energy were analyzed to determine the particle's equilibrium position at the interface. These calculations are quite complex. However, the problem can be significantly simplified in the case of particles of colloidal size, where the effect of the gravitational force can be ignored when compared to the surface tension and the meniscus can be approximated as a flat one. This asymptotic behavior, presented in chapter 2 (Figure 2.13), was checked by examining the James matched asymptotic expansion (James, 1963; Williams, 1991) for the meniscus profile about a small circular meniscus and using it to calculate the particle position with the model of Rapacchietta and Neumann. No significant deviation from the results was found.

## REFERENCES

- Al Taweel, A.M., B. Delory, M. Stefanski, N. Andersen and H.A. Hamza. Influence of the surface characteristics of coal on its floatability. *Colloids and surfaces* 18:9-18. 1986.
- Adamczyk, Z., T. Dabros, J. Czarnecki and T.G.M. Van der Ven. Particle transport to solid surfaces. *Adv. Colloid Interface Sci.* 19:183-252. 1983.
- Anfruns, J.F., and J.A. Kitchener. Rate of capture of small particles in flotation. *Trans. IMM* 86:C9-C15. 1977.
- Bales, R.C., C.P. Gerba, G.H. Grondin, and S.L. Jensen. Bacteriophage transport in sandy soil and fractured tuff. *Appl. Environ. Microbiol.* 55:2061-2067. 1989.
- Bales, R.C., S.R. Hinkle, T.W. Kroeger, and K. Stocking. Bacteriophage adsorption during transport through porous media: chemical perturbations and reversibility. *Environ. Sci. Technol.* 25:2088-2095. 1991.
- Baven, K., and P.F. Germann. Macropores and water flow in soils. *Water Resour. Res.* 18:1311-1325. 1982.
- Bowen, B.D., and N. Epstein. Fine particle deposition in smooth parallel-plate channels. *J. Colloid Interface Sci.* 72:81-97. 1979.
- Buddemeier, R.W., and J.R. Hunt. Transport of colloidal contaminants in groundwater: radionuclide migration at the Nevada Test Site. *Appl. Geochem.* 3:535-548. 1988.
- Chase, K.L., R.S. Bryant, K.M. Bertus, and A.K. Stepp. Investigations of mechanisms of microbial enhanced oil recovery by microbes and their metabolic products. Dept. of Energy Report No. NIPER-483. Bartlesville, OK. 1990.
- Christenson, H.K., P.M. Claesson and R.M. Pashley. The hydrophobic interaction between macroscopic surfaces. *Proc. Indian Acad. Sci. (Chem. Sci.)*. 98:379-386. 1987.
- Claesson, P.M. Experimental evidence for repulsive and attractive forces not accounted for by conventional DLVO Theory. *Progr Colloid & Polymer Sci.* 74:48-54. 1987.
- Claesson, P.M., P.C. Herder, C.E. Bolm and B.W. Ninham. Interactions between a positively charged hydrophobic surface and a negatively charged bare mica surface. *J. Colloid Interface Sci.* 118:68-77. 1987.
- Derjaguin, B.V., and S.S. Dukhin. Theory of flotation of small and medium size particles. *Trans. IMM.* 70:221-258. 1961.

- Derjaguin, B.V., and S.S. Dukhin. Kinetic theory of the flotation of fine particles. in: Mineral Processing: Developments in Mineral processing (Proc. XIII, Int. Miner. Processin Congr. Warsaw, Poland). J.E. Laskowski (Ed): Amsterdam; Polish Scientific Publishers, Warsaw. 2:21-79. 1981.
- Derjaguin, B.V., N.V. Churave and V.M. Muller. Surface forces. Consultants Bureau. New York City. 1987.
- Elimelech M., and C.R. O'Melia. Effect of particle size on collision efficiency in the deposition of Brownian particles with electrostatic energy barriers. *Langmuir*. 6:1153-1163. 1990a.
- Elimelech M., and C.R. O'Melia. Kinetics of deposition of colloidal particles in porous media. *Envir. Sci. Technol.* 24:1528-1536. 1990b.
- Fontes, D.E., A.L. Mills, G.M. Hornberger, and J.A. Herman. Physical and chemical factors influencing transport of microorganisms through porous media. *Appl. Environ. Microbiol.* 57:2473-2481. 1991.
- Fuerstenau, D.W., Fine particle flotation. in: Fine Particle Processing, P. Somasundaran (Ed). AIME Inc. New York. 2:669-723. 1980.
- FitzPatrick, J.A., and L.A. Spielman. Filtration of aqueous latex suspensions through beds of glass spheres. *J. Colloid Interface Sci.* 43:350-360. 1973.
- Gregory, J., The calculation of Hamaker Constant, *Advances in colloid and interface science.* 2:396-417. 1969.
- Grotenhuis, J.T.C., C.M. Plugge, A.J.M. Stams, and A.J.B. Zehnder. Hydrophobicities and electrophoretic mobilities of anaerobic bacterial isolates from methanogenic granular sludge. *Appl. Environ. Microbiol.* 58:1054-1056. 1992.
- Gschwend, P.M., and S.C. Wu. On the constancy of sediment-water partition coefficients of hydrophobic organic pollutants. *Environ. Sci. Technol.* 19:90-96. 1985.
- Hamaker, H.C., The London-van der Waals attraction between spherical particles. *Physica.* 4:1058-1072. 1937.
- Hirasaki, G.J., Wettability: fundamentals and surfaces. *SPE Formation Evaluation.* 1:217-226. 1991.
- Hornsy, D., and J. Leja. Selective flotation and its surface chemical characteristics. *Surface Colloid Sci.* 12:217-225. 1982.



- Israelachvili, J.N., and R.M. Pashley. The hydrophobic interaction is long range, decaying exponentially with distance. *Nature*. 300:341-352. 1982.
- Israelachvili, J.N. Measurements of hydration forces between macroscopic surfaces. *Chemica Scripta*. 25:7-14. 1985.
- Israelachvili, J.N., *Intermolecular & Surface Force*. Academic Press Inc. 1992.
- James, D.F., The meniscus on the outside of a small circular cylinder. *J. Fluid Mechanics*. 63:657-664. 1963.
- Jameson, G.J., Physical aspects of fine particle flotation. p215. in *Principles of Mineral Flotation*. J.T. Woodcock (Ed). The Australia Institute of Mining and Metallurgy. Victoria, Australa. 1985.
- Lance, J.C., and C.P. Gerba. Virus movement in soil during saturated and unsaturated flow. *Appl. Environ. Microbiol.* 47:335-337. 1984.
- Laskowski, J., and J.A. Kitchener. The hydrophilic-hydrophobic transition on silica. *J. Colloid & Interface Sci.* 29:670-678. 1969.
- Lee, M.D., J.M. Thomas, R.C. Borden, P.B. Bedient, J.T. Wilson, and C.H. Ward. Biorestitution of aquifers contaminated with organic compounds. *Crit Rev. Environ. Control.* 18:29-89. 1988.
- Lekki, J., and J. Laskowsky. Dynamic interaction in particle-bubble attachment in floatation. p65. in *Colloid and Interface Science Vol. IV*. M. Kerker (Ed). Academic Press. New York. 1976.
- Litton, G.M., and T.M. Olson. Colloid deposition rates on silica bed media and artifacts related to collector surface preparation methods. *Environ. Sci. Technol.* 27:185-193. 1993.
- Marcelja, S., and N. Radic. Repulsion of interfaces due to boundary water. *Chem. Phys. Lett.* 42:129-136. 1976.
- Martln, R.E., E.J. Bouwer, and L.M. Hanna. Application of clean-bed filtration theory to bacterial deposition in porous media. *Environ. Sci. Technol.* 26:1053-1058. 1992.
- McCarthy, J.F., and J.M. Zachara. Subsurface transport of contaminants. *Environ. Sci. Technol.* 23:496-502. 1989.
- McDowell-Boyer, L.M., J.R. Hunt and N. Sitar. Particle transport through porous media. *Water Resour. Res.* 22:1901-1921. 1986.

- O'Melia, C.R., Kinetics of colloid chemical processes in aquatic systems. p32. Presented at workshop on: Aquatic Chemical Kinetics: Reaction Rates of Processes in Natural Waters, at Warth, Thurgau, Switzerland. March, 1989.
- Pashley, R.M., and J.N. Israelachvili. A comparison of surface forces and interfacial properties of mica in purified surfactant solutions, *Colloids and Surfaces*. 2:169-187. 1981.
- Powelson, D.K., J.R. Simpson, and P. Gerba. Virus transport and survival in saturated and unsaturated flow through soil columns. *J. Environ. Qual.* 19:396-401. 1990.
- Powelson, D.K., J.R. Simpson, and P. Gerba. Effects of organic matter on virus transport in unsaturated flow. *Appl. Environ. Microbiol.* 57:2192-2196. 1991.
- Rabinovich, Ya. I., and B. V. Derjaguin. Interaction of hydrophobilized filaments in aqueous electrolyte solutions. *Colloids and Surfaces*. 30:243-251. 1988.
- Rapacchietta, A.V., and A.W. Neuman. Force and free energy analysis at fluid interfaces: 2. spheres. *J. Colloid and Interface Sci.* 59 :555-564. 1977.
- Spielman, L.A., and S.K. Friedlander. Role of electric double layer in particle deposition by convective diffusion. *J. Colloid and Interface Sci.* 46:22-31. 1974.
- Spielman, L.A., Particle capture from low-speed laminar flow. *Annu. Rev. Fluid Mech.* 9:297-319. 1977.
- Thomas, J.M., and C.H. Ward. In situ biorestitution of organic contaminants in the subsurface. *Environ. Scil. Technol.* 23:760-766. 1989.
- Tien, C., and A.C. Payatakes, *Advances in deep bed filtration, AICHE J.*, 25, 737-759, 1979.
- Tien, C., *Granular filtration of aerosols and hydrosols*. Butterworths. Stoneham, Mass. 1989.
- Vandevivere, P., and P. Baveye. Relationship between transport of bacteria and their clogging efficiency in sand columns. *Appl. Environ. Microbiol.* 58:2523-2530. 1992.
- Van Loosdrecht, M.C.M., J. Lyklema, W. Norde, G. Schraa, and A.J.B. Zehnder. Electrophoretic mobility and hydrophobicity as a measure to predict the initial steps of bacterial adhesion. *Appl. Environ. Microbiol.* 53:1898-1901. 1987.
- Van Oss, C.J., J. Visser, D.R. Absolom, S.N. Omenyi and A. W. Neumann. The concept of negative Hamaker constant. *Advances in Colloid and Interface Science.* 18: 133-148. 1983.

- Vaughn, J.M., E.F. Landry, C.L. Beckwith, and M.C. Thomas. Virus removal during groundwater recharge: effects of infiltration rate on adsorption of poliovirus to soil. *Appl. Environ. Microbiol.* 41:139-147. 1981.
- Visser, J., On Hamaker constants: A comparison between Hamaker constants and Lifshitz-van der Waals constants, *Advances in Colloid and Interface Science.* 3:331-363. 1972.
- Visser, J., The concept of negative hamaker coefficients. *Adv. Colloid and Interf. Sci.* 15:157-169. 1981.
- Warren, L.J., Ultrafine particles in flotation. p185. in *Principles of Mineral Flotation.* M.H. Jones and J.T. Woodcock (Ed). The Australasian Institute of Mining and Metallurgy. Victoria, Australi. 1985.
- Williams, D.F., Aggregation of colloidal particles at the air-water interface, Ph.D. dissertation, University of Washington, 1991.
- Yao, K.M., M.T. Habibian and C.R. O'Melia. Water and wastewater filtration: concepts and applications. *Environ. Sci. Technol.* 5:1105-1112. 1971.
- Yates, M.V., C.P. Gerba, and L.M. Kelly. Virus persistence in groundwater. *Appl. Environ. Microbiol.* 49:778-781.1985.
- Yates, M.V., S.R. Yates, J. Wagner, and C.P. Gerba. Modeling virus survival and transport in the subsurface. *J. Contam. Hydrol.* 1:329-345. 1987.

---

## CHAPTER 2

---

# VISUALIZATION OF THE ROLE OF THE GAS-WATER INTERFACE ON THE FATE AND TRANSPORT OF COLLOIDS IN POROUS MEDIA

(Submitted to Water Resources Research, January 26, 1993)

### ABSTRACT

This paper exposes the significant role played by the gas-water interface in the fate and transport of colloids in porous media, and also introduces a micromodel method to allow direct visualization of colloid behavior in pore networks. The gas-water interface was created by trapping air in the pore space. Various types of latex and clay particles, as well as bacteria, were studied. The results suggest that the gas-water interface sorbs not only hydrophobic but also hydrophilic particles. The degree of sorption is controlled by particle surface hydrophobicity, solution ionic strength, and particle charge sign. Sorption increases with increasing particle hydrophobicity and solution ionic strength, while positively charged particles have a very strong affinity to the gas-water interface. The sorption on the gas-water interface is essentially irreversible, in that the capillary free energy provides a large attractive force to hold particles on the gas-water interface after its rupture. These findings reveal a mechanism of vadose zone transport: a static gas-water interface behaves as a sorbent phase retarding the transport of particulate

contaminants. The method developed in this research is very useful for the investigation of particulate contaminant behavior and interface-related transport, especially in the context of bioremediation.

## INTRODUCTION

Organic and inorganic pollutants adsorb onto mobile colloids in the subsurface environment, thereby enhancing pollutant mobility (McDowell-Boyer et al. 1986; Buddemeier and Hunt, 1988; McCarthy and Zachara, 1989; Gschwend, 1992). In addition, some colloids are themselves toxic or virulent (i.e., bacteria and viruses). Colloid transport is concerned with the movement, sorption to, and desorption from rock surfaces in porous aquifer media. Historically, research on transport has focused on water-saturated porous media, but there are often other fluid phases present. Gas is one of the major fluid phases in the subsurface. In the vadose zone, a continuous gas phase shares pore space with the aqueous phase. In the saturated zone, gas bubbles may be generated by various processes: entrapment of air as the water table fluctuates, organic and biogenic activities, or the emergence of gas from solution as the aqueous phase pressure drops, etc. In a common three-phase system of rock, water, and gas, with a water-wet rock surface, we have two principal interfaces: rock-water and gas-water. Although the rock-water interface has been extensively studied, the gas-water interface has been neglected. In this paper we present a study of the role of this interface using a visualization tool, the etched glass micromodel.

Interactions of fine-grained minerals and gas bubbles have been extensively studied in the field of froth flotation (Laskowski, 1974; Derjaguin et al., 1984; Fuerstenau, 1980; Leja, 1982; Hornaby and Leja, 1983; Jameson, 1985). In froth flotation, valuable metals are separated from gangue minerals by selective sorption to gas bubbles running up through a mineral-surfactant-water slurry. The important differences between the present research and the flotation process are: (1) The mineral particles in a flotation process are macroscopic particles compared to the microscopic colloids in a groundwater system. (2) In flotation the mineral particle surfaces are treated with the specific surfactants that impart a hydrophobic character to the desired particles. The surfaces of the bubbles are stabilized by adding reagents. Natural porous media systems are essentially free of surfactant. (3) Flotation applications occur in a reactor vessel, whereas our study concerns porous media. The similarity between the two processes is in the surface forces that control the adhesion when particles and bubbles approach each other. These forces are also universal for any interacting surfaces in a liquid phase. They are electrostatic, van der Waals, and structural forces (Israelachvili, 1985; Derjaguin et al., 1987; Hirasaki, 1991).

## EXPERIMENTAL METHOD AND MATERIALS

### Glass Micromodels

Glass micromodels are created by etching a pore network pattern onto two glass plates which are then fused together in a furnace (Chatzis, 1982; Wilson et al., 1990; Buckley, 1991). Micromodel transparency allows microscopic investigation of fluid flow

in a pore network composed of pore bodies connected by pore throats. Although the network is only two-dimensional, the pores have a complex three-dimensional structure. Pore wedges, composed of corners of the pore bodies and throats where the glass plates meet, are a feature of the third dimension. The glass used for making micromodels has a chemical composition of 72% SiO<sub>2</sub>, 14% Na<sub>2</sub>O, 3.8% CaO, and other trace metal oxides. In the presence of water, glass is covered with surface hydroxyl groups; the glass-water interface is negatively charged at neutral pH. The surface energy of glass is very similar to that of bulk aquifer rock. Thus, the glass surface plays the role of a rock surface. Figure 1 shows three pore network patterns used in this study. The photos were taken from actual micromodel networks. Figure 1a shows a portion of a homogeneous quadrilateral network with 1225 pore bodies. An air bubble is trapped in each of the pore bodies in this photo. Pore bodies and pore throats are sized at about 200  $\mu\text{m}$  and 50  $\mu\text{m}$  in diameter, respectively. Figure 1b shows part of a homogeneous hexagonal network with 1116 pore bodies in each model. Pore bodies and throats are sized 300  $\mu\text{m}$  and 20-100  $\mu\text{m}$ , respectively, in diameter. Figure 1c has a heterogeneous network with preferential flow paths. Pore sizes vary from 4 to 400  $\mu\text{m}$  in diameter. The pore volume in all micromodels is about 0.1 to 0.2 ml, measured by water-weight. The pore network covers an area of only 3.0 cm<sup>2</sup>. In order to facilitate efficient micromodel production, experimental repeatability and comparison, we fabricated four similar micromodels on one plate at a time (see Figure 2). Micromodels are not amenable to reuse in colloid research because of the difficulties of removing all of the attached particles while preserving a homogeneous surface chemistry.

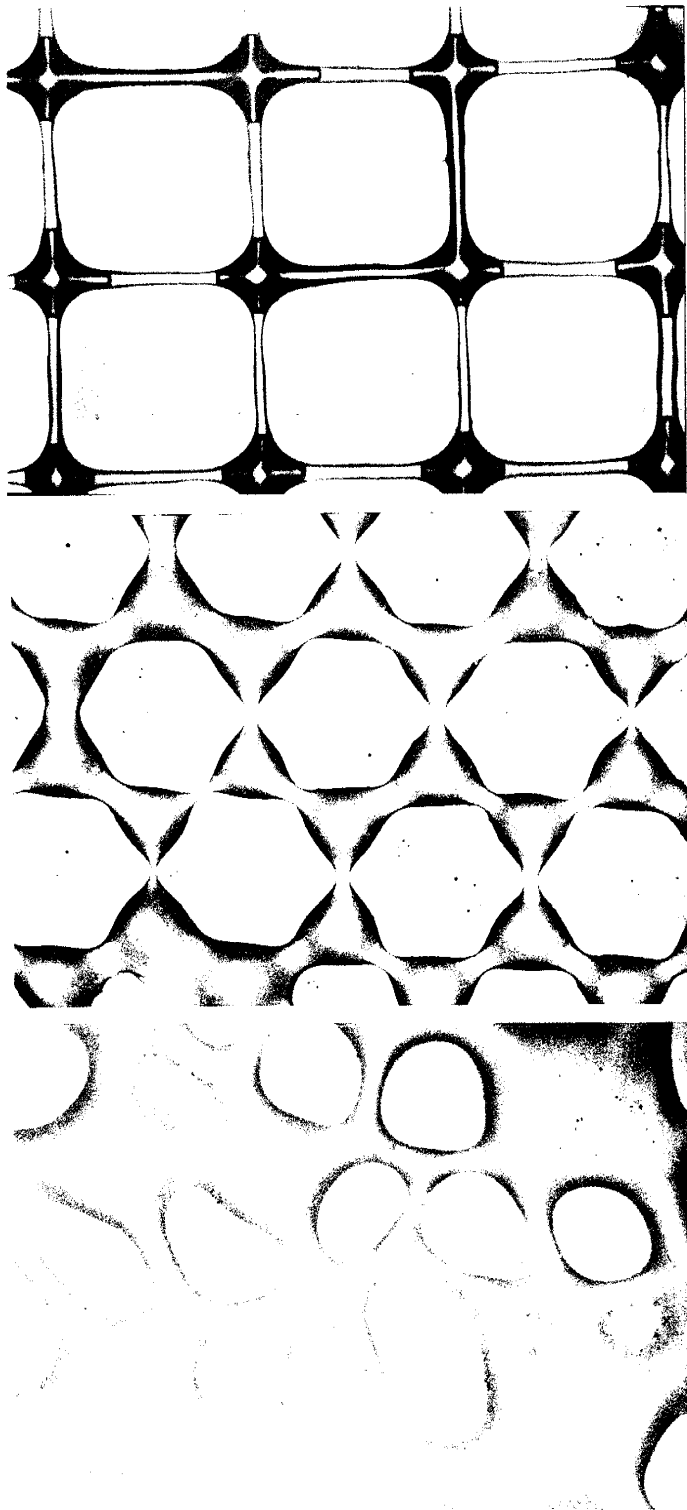


Figure 2.1. Three pore networks used in this study: (a) quadrilateral network; (b) hexagonal network; (c) heterogeneous network.



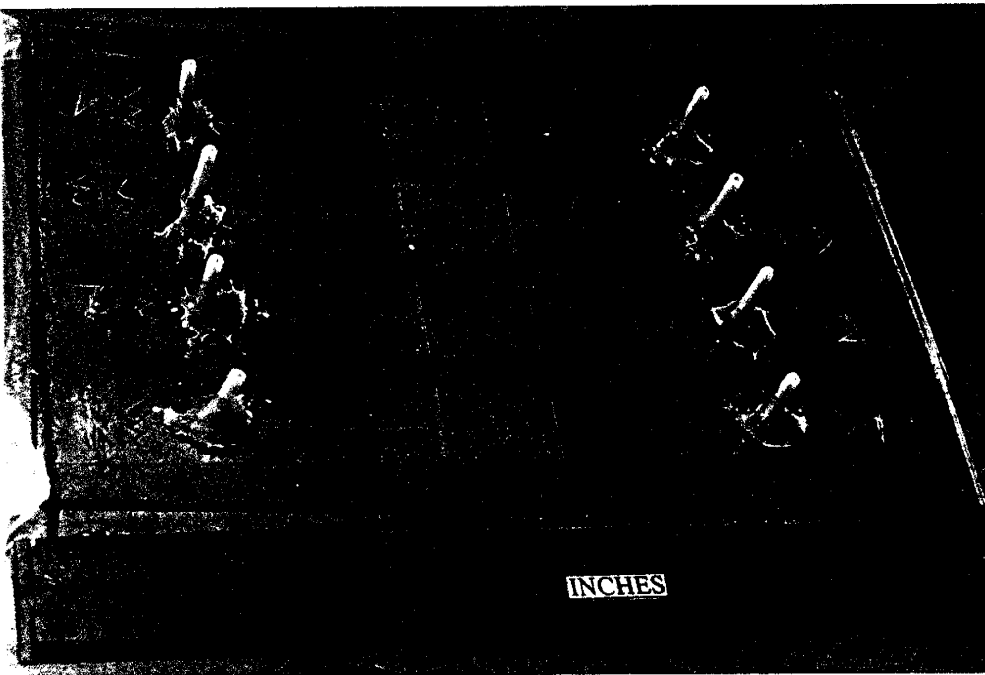


Figure 2.2. A glass micromodel plate containing four micromodels with heterogeneous networks.

## Colloidal Particles

Fluorescent latex microspheres (Interfacial Dynamics Co.) were used as model particles in this research because they were easy to observe, had well-defined physico-chemical characteristics, and were manufactured without surfactant. The yellow-green fluorospheres we chose can be more efficiently illuminated than other color types. According to the manufacturer's report, the fluorescent dyes have no significant effect on the surface properties of the latex particles. Clay and bacteria were also tested because of their importance in groundwater. The six types of particles, and their size and surface characteristics are listed in Table 1: (1) Hydrophilic negatively charged latex: these high-surface charge density, hydrophilic latexes are manufactured from hydrophobic sulfate-charge stabilized latexes. The process consists of grafting carboxylic acid polymers to the particle surface to produce a porous, highly charged surface layer. The final functional surface groups are predominantly carboxylate with an insignificant amount of sulfate. (2) Hydrophobic negatively charged latex: these microspheres are also stabilized by sulfate charges, but the surface functional groups are sulfate and hydroxylate. Their hydrophobicity is attributed to low charge density. (3) Positively charged hydrophobic latex: the only surface functional group present on these particles is amidine. Because the surface charge density is relatively low, the particles have a hydrophobic surface. (4) Na-montmorillonite (Source Clay, Columbia, MS): particles were sorted with a centrifuge, and particle size was measured with a scanning electron microscope. To diminish the influence of organics, the clay particles were washed with a series of solvents in the order of chloroform-methanol-water. (5) Hydrophilic bacteria: *Pseudomonas cepacia*

Table 2.1 Particles Used in Micromodel Experiments

Descriptive Term	Particle Types	Size ( $\mu\text{m}$ )	Electrophoretic Mobility ( $\mu\text{m}/\text{sec}/\text{volt}/\text{cm}$ )	Contact Angle $\theta_a$
Hydrophilic negatively charged latex	Carboxylate Latex	0.95	$-7.10 \pm 0.24$	$< 10^\circ$
Hydrophobic negatively charged latex	Sulfate Latex	1.05	$-3.84 \pm 0.21$	$121.9 \pm 6.7^\circ$
Positively charged hydrophobic latex	Amidine Latex	0.60	$+5.00 \pm 0.26$	$109.5 \pm 5.3^\circ$
Clay	Na-montmorillonite	$\sim 0.5$	$-2.90 \pm 0.12$	$36.7 \pm 2.7^\circ$
Hydrophilic bacteria	Bacteria 3N3A	1.2x0.8	$-0.96 \pm 0.28$	$24.7 \pm 3.1^\circ$
Hydrophobic bacteria	Bacteria S-139	1.0x0.8	$-4.48 \pm 0.36$	$77.1 \pm 2.5^\circ$

3N3A was isolated by Brockman et al. (1989) from sediment samples from a depth of 203 m near Aiken, South Carolina. (6) Relatively hydrophobic bacteria S-139: This strain was isolated by Aaron Mills et al. from a shallow groundwater aquifer, but they have not been identified yet. Bacteria sizes were measured with an optical microscope. Both strains were grown in 10% PTYG broth at 27 °C on a shaker (200 rpm). When the culture reached a late logarithmic stage of growth (36 to 48 hours), cells were harvested by centrifugation (7,000 rpm for 10 minutes) and washed three times in a sterile solution of 1.0 mM NaNO<sub>3</sub>, at pH 6.6. Cells were then suspended in the same solution. The concentrated suspension was stored by refrigeration.

### **Characterization of Particle Surface Hydrophobicity**

Particle electrophoretic mobility is an indirect measurement of particle surface hydrophobicity. The measurements of electrophoretic mobility were conducted in a solution of 1.0 mM NaNO<sub>3</sub> and pH 6.6 at 25 °C (see Table 1). Analyses were carried out in a Coulter DELSA 440 (Doppler Electrophoretic Light Scattering Analyzer). The instrument monitors the light scattered from the moving particles at four angles. The reported mean was computed from these four analyses.

Water contact angle is a more direct measurement of surface hydrophobicity. We modified a technique to measure surface relative contact angles of all particles presented in this paper using a smear-layer in a classic captive-drop method (Gaudin et al., 1963). A "flat" layer of particles for measuring contact angles was prepared by smearing a highly concentrated particle suspension onto a clean glass slide which was allowed to dry

by evaporation for 2 to 3 hours at 24 °C. The thickness of the particle layer was about 50-100  $\mu\text{m}$ . Contact angles were measured directly with a microscope (Carl Zeiss Stereoscope) fitted with a goniometer eyepiece (Tiyoda, No. 4443, Tokyo) at the junction of the drop of the solution, the layer of particles, and the atmosphere at 24 °C. The solution was 1.0 mM  $\text{NaNO}_3$  with pH 6.6. The initial water advancing and receding angles were recorded. The readings of the initial advancing angles were taken about 2 seconds after the water drop contacted the surface. The receding angles were taken just before the water drop snapped from the pipet. The limitations of this method are that the layer is formed by the packed particles and the contact angle decreases with time because the "porous medium" of packed particles imbibes water. The measured value depends on many factors, including particle size, layer thickness and layer moisture content, etc. The initial advancing angle is more significant as a relative measurement of particle surface hydrophobicity. Data reported in Table 1 are the mean of  $\geq 15$  measurements.

In general, the greater the electrophoretic mobility, the higher the surface charge density, and, therefore, the more hydrophilic and the smaller the water contact angle. This relationship is shown by the data for latexes and clay particles. Data for bacteria show an opposite correlation, that is, water contact angle increases with the increasing electrophoretic mobility. Van Loosdrecht (1987) reported the same correlation for bacteria.

### **Experimental Procedure**

A high resolution optical microscope (Zeiss Axiophot) with fluorescent lighting,

dark field image and long working distance objectives was used. During experiments a prepared micromodel was mounted horizontally on the stage of the microscope. Flow rate was precisely controlled by a syringe pump (Harvard Apparatus, Model 4400-001). Microphotographs and a video recording were taken simultaneously. The visualization experiment procedure was as follows: (1) A selected number of pore volumes of particle-free solution were pumped through a clean micromodel to saturate the micromodel and obtain the desired chemical conditions for the porous medium. (2) The gas-water interface was created, as residual air bubbles in the glass pore networks, by draining the model with air and then reimbibing particle-free solution. The concept of a residual non-wetting phase was described by Morrow (1970). (3) The micromodel was placed on the stage of the microscope. A dilute particle suspension was injected at a constant rate (1.5 ml/hr) for 30 pore volumes. Particle behavior was observed and recorded. (4) The particle suspension was replaced with a particle-free solution at the same flow rate until all free particles were displaced, leaving only particles attached on interfaces. Most photos showing sorbed particles were taken after this step.

In order to simulate groundwater conditions, the solution chemistry was designed conservatively with exceptions noted later. The ionic strength of solution and suspension was 1.0 mM  $\text{NaNO}_3$ . A pH of 6.6 was maintained in all the solutions and suspensions. Air was used as the gas phase. All chemicals used were analytical reagent grade. Solutions and suspensions were prepared using distilled and deionized water.

## EXPERIMENTAL RESULTS AND DISCUSSION

### Gas-water Interface and Hydrophilic Particles

Although classical criteria separating hydrophilic and hydrophobic surfaces involves a water contact angle that is less or greater than some reference angle (usually  $0^\circ$  or  $90^\circ$  depending on the preference), this study refers, instead, to relative hydrophilicity and hydrophobicity. We classify particles with high charge density and low water contact angle as hydrophilic particles, and those with low charge density and greater contact angle as hydrophobic particles. For instance, we believe that most of the naturally generated abundant inorganic colloids, such as fines of clay, silica, and the other metal oxides are hydrophilic.

Within the framework of the DLVO theory, the sum of the van der Waals and electrical double layer interaction forces form the total energy of interaction (Derjaguin and Landau, 1941; Verwey and Overbeek, 1948). We calculated two pairs of interaction potentials based on our experiment conditions: those involving the hydrophilic particle with the glass surface and the hydrophilic particle with the gas bubble. For the hydrophilic particle-glass pair, the absolute value of repulsive electrical energy is greater than the attractive van der Waals energy; thus the net interaction potential is repulsive. For the hydrophilic particle-gas bubble pair the electrostatic force is repulsive because both the particle surface and the bubble surface (Lee and McCammon, 1984; Yoon and Yordan, 1986) are negatively charged, and van der Waals force is repulsive due to the positive complex Hamaker constant (Hamaker, 1937; Van Oss et al., 1983; Li and

Somasundaran, 1991). Hence, the net interaction energy is repulsive. Therefore, according to DLVO theory, the hydrophilic particles used in this research should not sorb onto either the glass-water or the gas-water interfaces.

Fluorescent carboxyl latex (diameter =  $0.95 \mu\text{m}$ ,  $\theta_a < 10^\circ$ ), Na-montmorillonite (diameter =  $0.5 \mu\text{m}$ ,  $\theta_a = 37^\circ$ ) and bacteria 3N3A ( $1.2 \times 0.8 \mu\text{m}$ ,  $\theta_a = 25^\circ$ ) were used to test the behavior of hydrophilic particles at interfaces. The visualized phenomena were recorded photographically and on video tape. In Figure 3a a single air bubble is trapped in a pore body of a quadrilateral network, and in Figure 3b a few bubbles are trapped in a heterogeneous network. Both pictures show that hydrophilic latex particles preferentially sorb onto the air-water interface but very few particles attach to the pore walls. Figure 4 is a sketch of an air bubble trapped in a pore body of a glass micromodel. Figure 4a is a top view equivalent to Figure 3. Figure 4b is a cross-sectional view along the pore center line. In the top view the dark ring around the exterior of the bubble represents the curvature of the air bubble as it bridges the pore body from top to bottom of the micromodel. The curvature approaches the top and bottom of the micromodel at the three-phase (air-water-glass) contact line represented here as the interior circumference of the dark ring. Light does not transmit through the multiple air-water-glass layers; therefore, a dark ring is formed. Inside of this three-phase contact ring the water phase is a thin film. Usually the latex particles are too big to enter this film, but we see some particles in Figure 3b have found their way into the film. This may be caused by surface roughness. We also see a few particles have been strained by some of the fine pores, perhaps plugging the throats. The behavior of



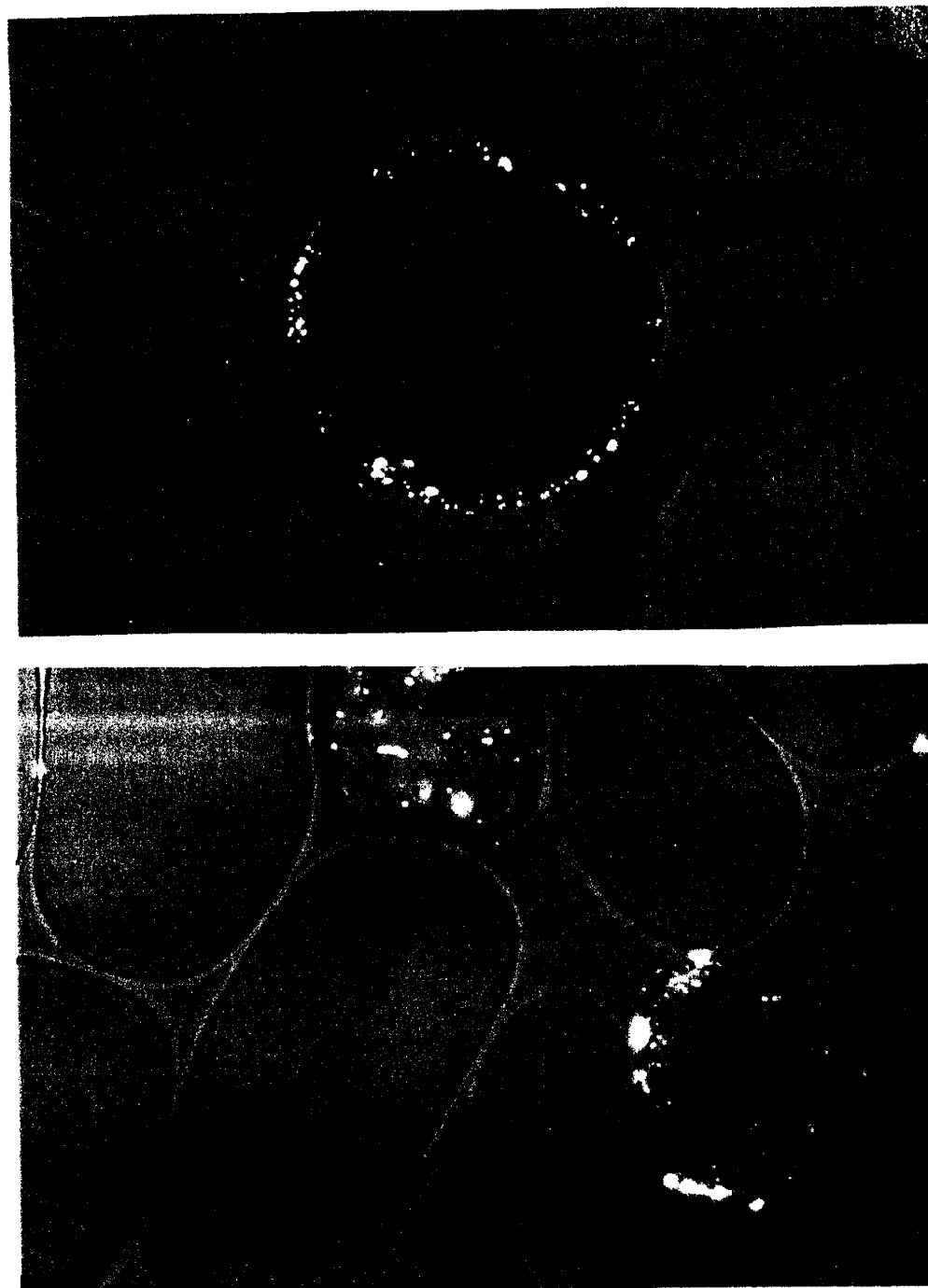
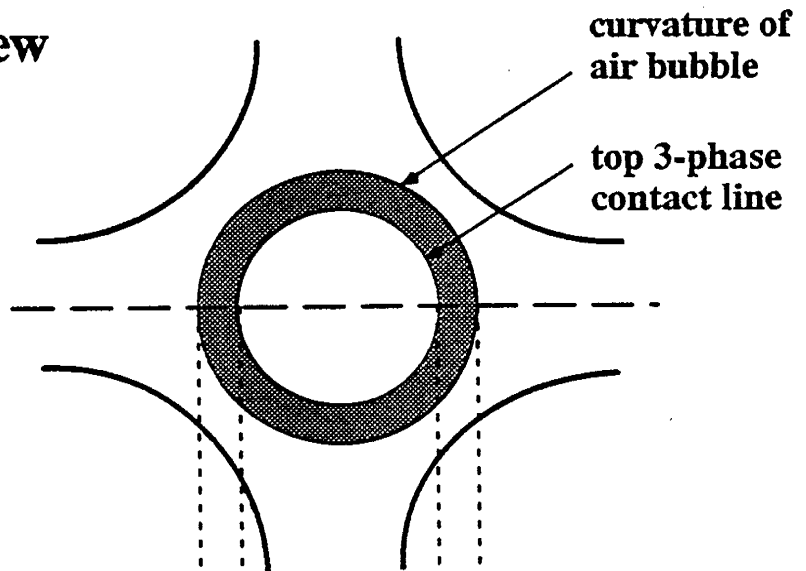


Figure 2.3. Hydrophilic negatively charged latex particles ( $0.95 \mu\text{m}$ ) preferentially sorbed onto air bubbles vs. pore walls: (a) air bubble trapped in pore body of quadrilateral network; (b) air bubbles trapped in heterogeneous network. Some fine pore throats physically plugged by particles.

a) top view



b) side view

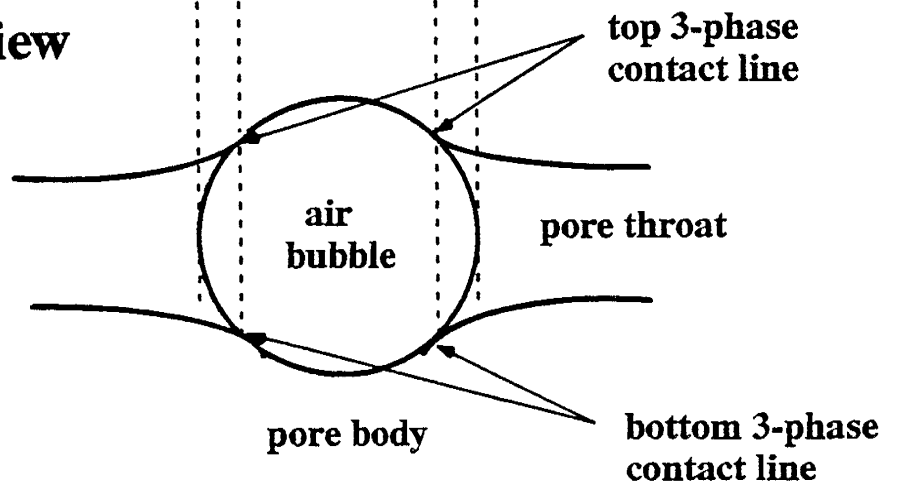


Figure 2.4. Sketch of trapped air bubble in pore body of glass micromodel, explaining the dark ring of air bubble.



Figure 2.5. Na-montmorillonite particles ( $\sim 0.5 \mu\text{m}$ ) accumulated on downstream side of air bubble trapped in pore body of hexagonal network. Air bubble is about  $300 \mu\text{m}$  in diameter.

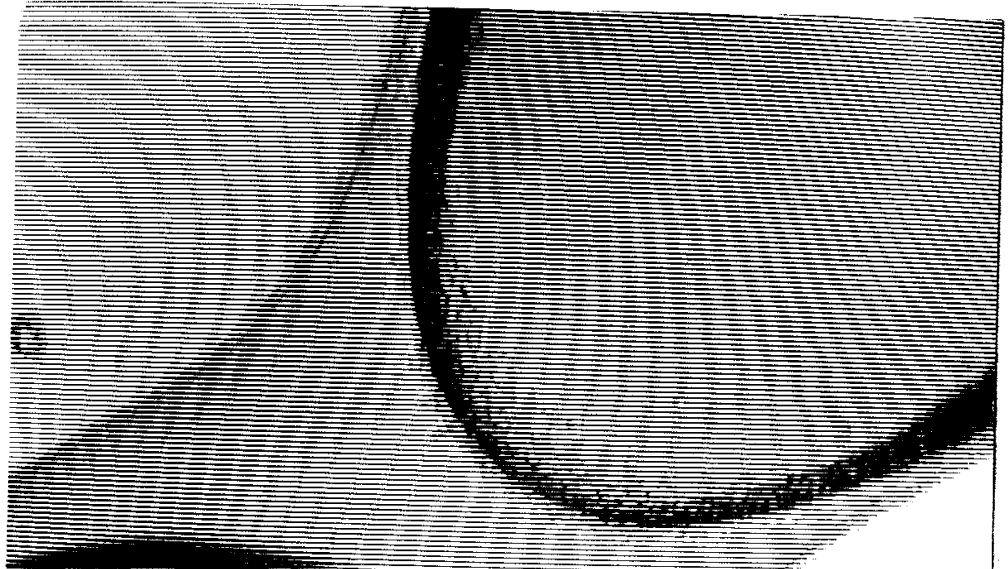


Figure 2.6. Hydrophilic bacteria 3N3A ( $1.3 \times 0.8 \mu\text{m}$ ) preferentially sorbed on air bubble trapped in pore body of hexagonal network.

hydrophilic particles on the air bubbles is inconsistent with the prediction based on DLVO theory. This unexpected phenomena was also found in the clay and bacteria experiments. Figure 5 shows Na-montmorillonite particles accumulated onto the downstream portion of an air bubble in a pore body. The lower curve is the three-phase contact line of top glass plate, air, and water. The white spots are clay particles that accumulated near this line, which is in focus. The upper curve is the curvature of the bubble, which is between two glass plates and unfocused. Figure 6 shows hydrophilic bacteria accumulated on a gas bubble trapped in a pore body.

Comparing the partitioning of particles on the two interfaces, the net pair interaction energy is repulsive between glass surface and hydrophilic particle, and attractive between the air bubble and hydrophilic particle. It is clear that the gas-water interface has an attractive potential which is not associated with the glass-water interface. The observation is consistent with the prediction for the pair of glass and hydrophilic particle, but inconsistent for that of air bubble and hydrophilic particle. Therefore, we hypothesize that the structural force between gas bubble and hydrophilic particle is attractive, and large enough to overcome repulsive van der Waals and electrostatic forces, if there is no additional fourth force dominating.

### **Sorption and Particle Surface Hydrophobicity**

Colloids in the subsurface environment have a wide range of surface wettability. Various types of natural and manmade organic colloids are hydrophobic. Also, the adsorption of organic matter onto hydrophilic particles can alter their surface wettability.

Figure 7 shows the distribution of hydrophobic latex particles (diameter =  $1.05 \mu\text{m}$ ,  $\theta_a = 122^\circ$ ) in a single pore with a trapped air bubble. In comparing sorptive behavior as a function of hydrophobicity (all the other experimental conditions are the same), we see many more hydrophobic particles sorbed onto both the air bubble and the pore walls (Figure 7) than we saw earlier with hydrophilic particles (Figure 3). Hydrophobic particles show a greater affinity to both air-water and glass-water interfaces because, firstly, a hydrophobic surface has a lower charge density than a hydrophilic one does, therefore, the electrostatic repulsive force is lower. Secondly, the structural force for hydrophobic particles is more attractive than for hydrophilic ones. This phenomenon is also shown by the bacteria experiments. In Figure 8, the relatively hydrophobic bacteria S-139 ( $1.0 \times 0.8 \mu\text{m}$ ,  $\theta_a = 77^\circ$ ) greatly prefer the gas-water interface. In addition, many more bacteria sorbed onto the glass surface relative to the hydrophilic bacteria in Figure 6. Comparing the sorption of latex particles and bacteria on the gas-water interface, we notice that many bacteria appear to have crossed the three-phase contact line and to have entered into the apparent two-phase contact area of glass and air (where there is a thin water film).

### **Sorption and Particle Surface Charge Sign**

The interaction of positively charged particles with the gas-water interface should reveal the charge status of the gas-water interface. A suspension of positively charged latex particles (diameter =  $0.60 \mu\text{m}$ ,  $\theta_a = 109^\circ$ ) was pumped through the micromodels using the same experimental procedure. Figure 9 shows an entire air bubble



Figure 2.7. Hydrophobic negatively charged latex particles sorbed on both air-water and glass-water interfaces; air bubble is trapped in pore body of quadrilateral network. Observe the effect of particle surface hydrophobicity by comparing to Figure 2.3.

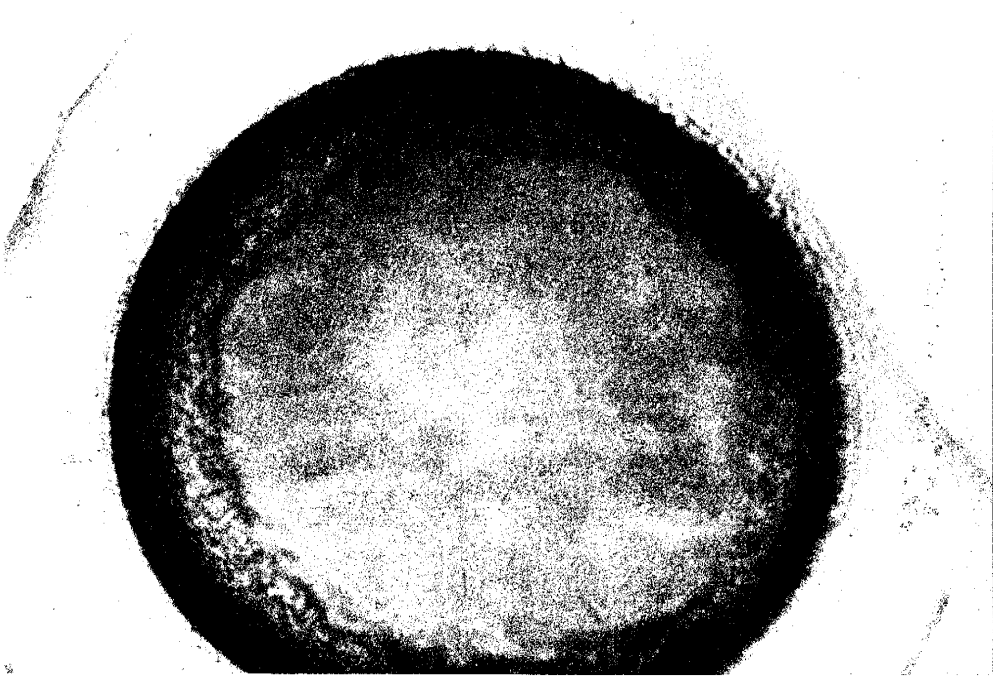


Figure 2.8. Relatively hydrophobic bacteria S-139 ( $1.0 \times 0.8 \mu\text{m}$ ) accumulated on air bubble in pore body of hexagonal network.



and the adjacent glass surface covered by sorbed particles, where both interfaces have a higher affinity to positively charged hydrophobic particles rather than to the negatively charged hydrophobic particles shown earlier in Figure 7. Those particles were more hydrophobic ( $\theta_a = 122^\circ$ ), and larger ( $1.05 \mu\text{m}$ ). In Figure 9, the focus is on the top three-phase contact line and the curvature is slightly off focus, but we can see that the whole boundary area is solid with the sorbed particles. The increased sorption of particles on the glass surface is easy to understand, because the glass surface and the particle surface are oppositely charged, thus the electrostatic force is attractive. The increased sorption on the gas-water interface indicates that the gas-water interface must be negatively charged.

### Sorption and Solution Ionic Strength

Sorption in solutions of different ionic strength was tested with hydrophilic negatively charged latex (diameter =  $0.95 \mu\text{m}$ ,  $\theta_a < 10^\circ$ ). The results shown in Figure 10 indicate that, with increasing solution ionic strength, there is increasing sorption on both trapped bubbles and pore walls. In a 1.0 mM solution (Figure 10a), particles sorb only on the gas bubbles. In Figure 10b ionic strength is increased by a factor of 100, and sorption increases on both bubbles and pore walls due to double layer compression; thus, the double layer theory also applies to the gas-water interface.

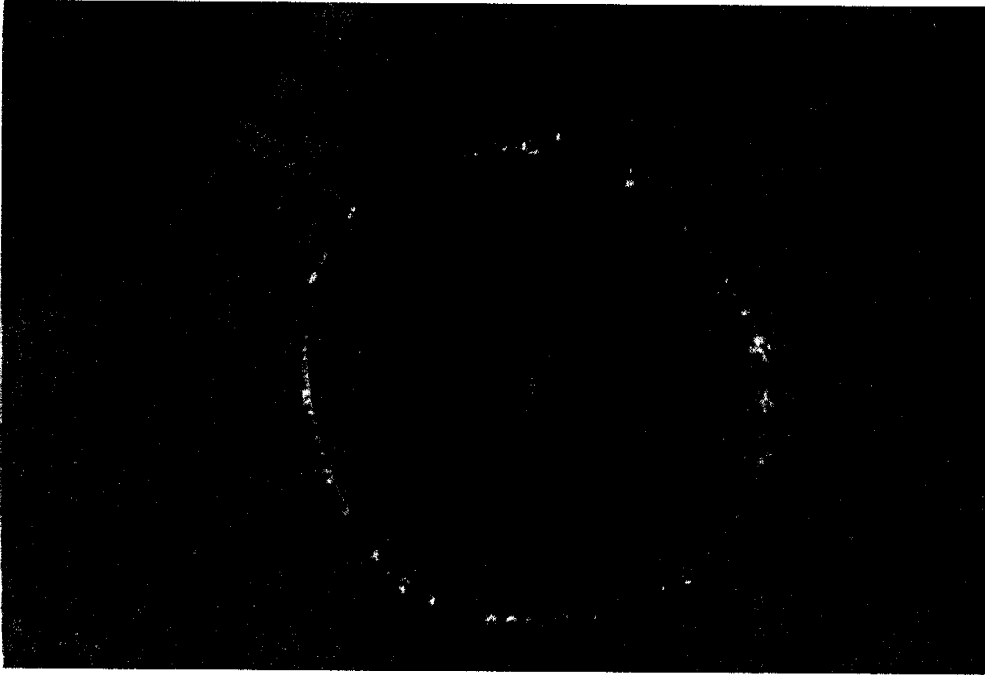


Figure 2.9. Positively charged hydrophobic latex particles ( $0.6 \mu\text{m}$ ) with very strong affinity to both gas-water and glass-water interfaces. Hexagonal network was used.

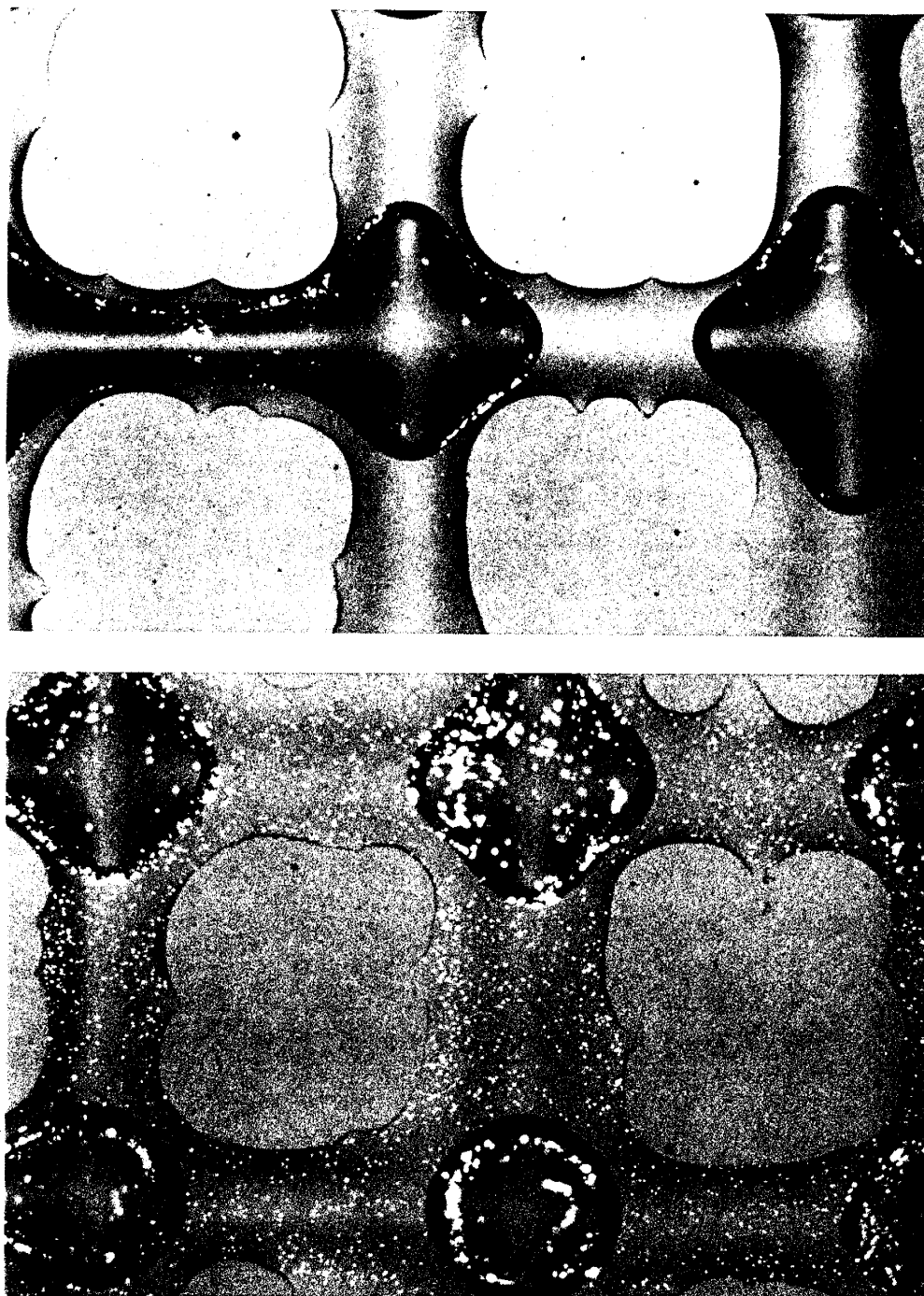


Figure 2.10. The effect of solution ionic strength on sorption: (a) in low ionic strength (1.0 mM) solution, hydrophilic latex particles only sorb on gas-water interface; (b) ionic strength is increased by a factor of 100; many more particles sorb on both bubbles and pore walls. The experiment was carried out in quadrilateral network.

## Desorption

Examination of particle desorption helps to reveal the energy status of interfaces and the sorption mechanism. In these experiments we tested desorption from interfaces by decreasing ionic strength and by increasing flow rate, using hydrophilic negatively charged latex particles (diameter =  $0.95 \mu\text{m}$ ,  $\theta_a < 10^\circ$ ). In the first step, 30 pore volumes of particle suspension with high ionic strength (100.0 mM) was flushed through a prepared micromodel at 1.5 ml/hr; then a particle-free solution with the same ionic strength (100.0 mM) displaced the particle suspension at the same flow rate. In Figure 11a we see that a high population of particles was sorbed onto both glass and the residual air bubble due to the double layer compression. After this, 30 pore volumes of distilled and deionized water were injected at the same flow rate in order to facilitate desorption behavior in a solution of decreasing ionic strength. The result is shown in Figure 11b. Most of the particles attached on the glass were desorbed. No particles were desorbed from the air-water interface. Instead, some of the particles desorbed from the glass surface were captured on the bubble. In other experiments where we increased flow rate rather than changed ionic strength, the result was similar, except that shear stress moved the sorbed particles to the down-stream side of the bubbles. These experiments indicate that the attractive force is larger at the gas-water interface than at the rock-water interface for the same particles under the same chemical conditions, and that sorption on the gas-water interface is essentially irreversible.

In the context of a general interaction potential isotherm (Hirasaki, 1991), irreversibility indicates that the sorption may occur in the primary minimum and

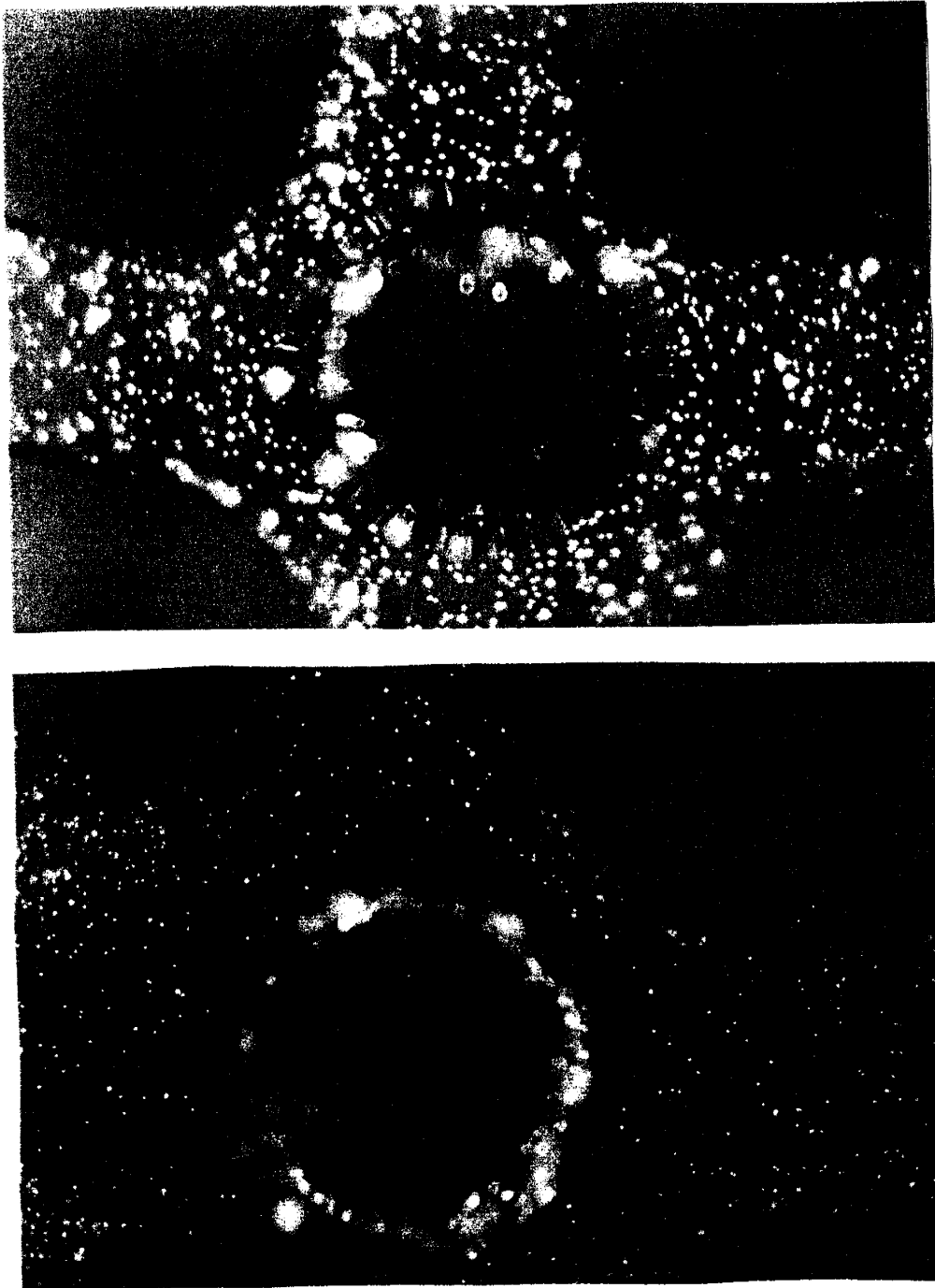


Figure 2.11. Desorption as solution ionic strength decreases: (a) in high ionic strength solution (100.0 mM) at 1.5ml/hr, hydrophilic latex particles sorbed onto the interfaces; (b) after the passage of 30 pore volumes of distilled and deionized water at same flow rate. Air-bubble ( $\sim 200 \mu\text{m}$  dia.) is trapped in pore body of quadrilateral network.

the particles must have overcome the energy barrier. A question arises: what is the high adhesion energy between particles and air bubbles? We suggest capillary energy, based on the work done by James (1974), Rapacchietta and Neumann (1977), Morrow (1988), and Williams (1991). If by any means the non-wetting particles (contact angle  $> 0$ ) can overcome the energy barrier caused by the superposition of van der Waals force, double layer force, and structural force, their surfaces will contact the interface and a three-phase contact line (gas, water, particle) will be formed on the particle surface. The capillary force, developed as soon as the three-phase contact line is established, will fix the particle at an equilibrium position at the interface. The exact calculation of such force involves solving a non-linear ordinary differential equation for the meniscus profiles and is only possible for the simplest geometries. A comprehensive treatment of capillary force was given by Rapacchietta and Neumann (1977). In their work, both force and free energy were analyzed to determine the particle's equilibrium position at the interface. These calculations are quite complicated. However, the problem can be significantly simplified in the case of particles of colloidal size, where the effect of gravitational force can be ignored when compared to the surface tension, and the meniscus can be approximated as a flat one. This asymptotic behavior was checked by examining the James matched asymptotic expansion (James, 1974; Williams, 1991) for the meniscus profile about a small circular meniscus and using it to calculate the particle position with the model of Rapacchietta and Neumann. This simplified analysis is schematically described in Figure 12. Consider a particle (radius =  $r$ ), which is fully immersed in a liquid with initial wetted semi-arc  $\phi = \pi$ , that passes through the gas-water interface and

becomes partially immersed ( $\phi = \pi - \theta$ ,  $\theta$  is contact angle). The free energy variation in this case is due to two contributions: the work ( $dE_1$ ) required to replace area  $A_{sg}$  of surface energy  $\sigma_{sl}$  with equivalent area of surface energy  $\sigma_{sg}$  and the work ( $dE_2$ ) done by eliminating the gas-water interface.

$$dE_1 = A_{sg} (\sigma_{sg} - \sigma_{sl}) = A_{sg} \sigma_{lg} \cos \theta = 2\pi r^2 \sigma_{lg} (1 - \cos \phi) \cos \theta \quad (1)$$

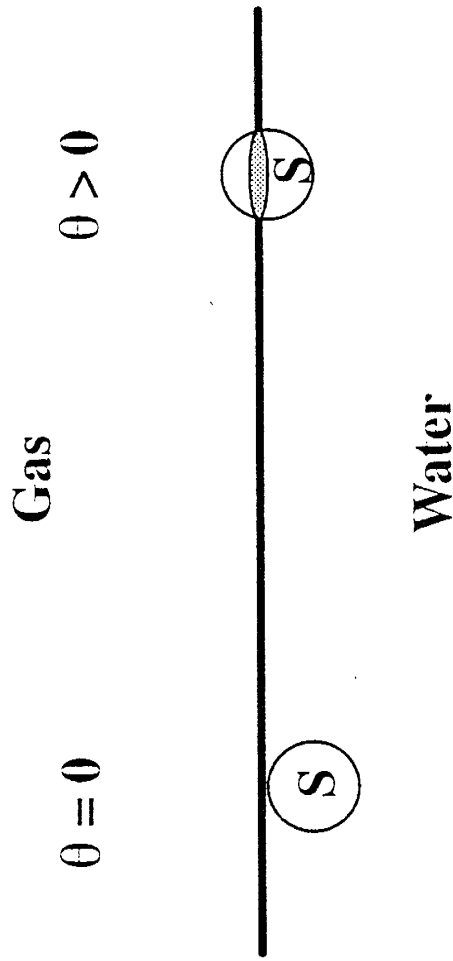
$$dE_2 = -A_{lg} \sigma_{lg} = -\pi r^2 \sin^2 \phi \sigma_{lg} \quad (2)$$

The capillary potential  $E_{cap}$ , which is defined as the total free energy variation, can be expressed as:

$$E_{cap} = dE_1 + dE_2 = \pi r^2 \sigma_{lg} [2\cos \theta (1 - \cos \theta) - \sin^2 \phi] \quad (3)$$

Figure 13 shows the calculated result of the capillary free energy change as a function of the contact angle. In this calculation, the particle was assumed to be  $1.0 \mu\text{m}$  in diameter. Capillary potential increases rapidly with the increasing of the contact angle.

Therefore, we suggest that the sorption of particles onto the gas-water interface has two energy stages. The DLVO and structural forces control the first stage, rupture; and after the three-phase contact line is established, the capillary force fixes each particle at an equilibrium position on the interface in the second stage. The capillary force strongly binds particles on the gas-water interface, so that they essentially cannot be desorbed from the gas-water interface. In fact, the whole bubble-particle unit can be



$$E_{\text{cap}}(\theta) = A_{\text{SG}}(\sigma_{\text{SG}} - \sigma_{\text{SL}}) - A_{\text{LG}}\sigma_{\text{LG}}$$

Figure 2.12. The capillary free energy change  $E_{\text{cap}}$  fixes the particles on the interface after the rupture of liquid film. Where  $\phi$  = wetted semi-arc;  $\theta$  = contact angle;  $A_{\text{sg}}$  = area of dewetted particle surface, function of contact angle;  $A_{\text{lg}}$  = area of gas-water interface displaced by particle, function of contact angle;  $\sigma_{\text{sg}}$  = particle-gas interface energy;  $\sigma_{\text{sl}}$  = particle-water interface energy;  $\sigma_{\text{lg}}$  = gas-water interface energy.



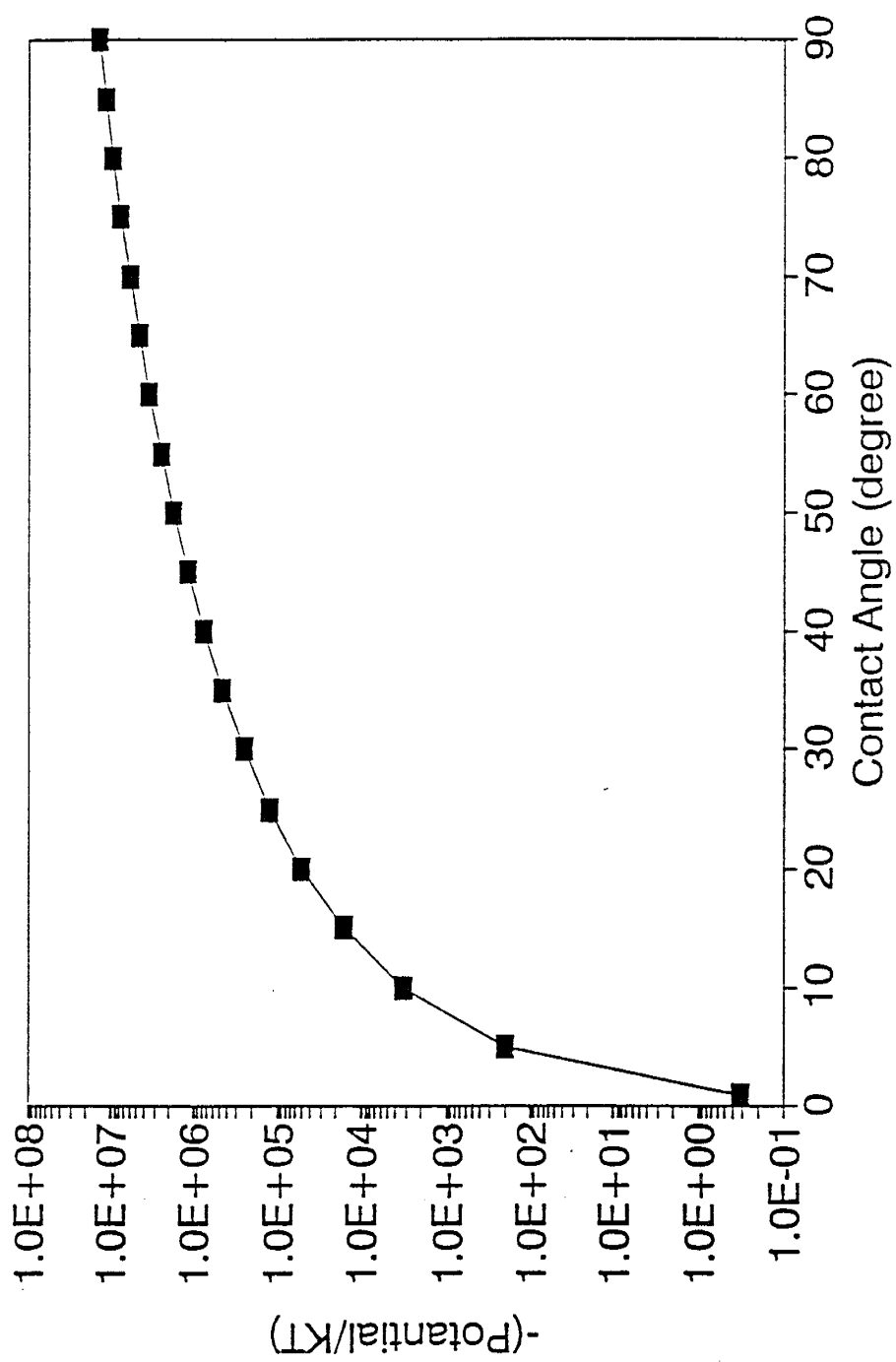


Figure 2.13. The calculated capillary free energy change as function of contact angles for a one micron spherical particle near a large air bubble. Normalized by  $KT$ , where  $K$  = Boltzmann's constant and  $T$  = absolute temperature.

moved under high shear stress without particle desorption.

A subsidiary observation, especially apparent on video tapes of the experiments, was the rapid circulation of particles along the bubble surface in all of the micromodel experiments. Most of the circulation paths were localized on a bubble surface, and the speed was proportional to the flow rate. This is probably related to the interaction between the outside shear stress and the air movement inside the bubble. Particles also tended to accumulate on the downstream portions of bubbles at higher flow rates because of the lower shear stress there. The particles sorbed on air bubbles also tended to form aggregates especially if they were hydrophobic (see Figures 3a, 7, 10, 11). This tendency is presumably due to a capillary attraction of particles on the interface. It becomes stronger when the system is disturbed, for example, by increasing flow rate, changing flow direction, and especially by moving the bubbles. The video tape recordings dramatize the dynamic aspects of these phenomena.

The preferential sorption of colloid particles onto the gas-water interface suggests a mechanism in vadose zone transport. A stationary gas-water interface in porous media can retard the transport of particulate contaminants. Moving interfaces, such as during infiltration, drainage or near a fluctuating water table may enhance colloid mobility. Colloids may also be preferably attached to the interfaces between non-aqueous phase liquids (NAPL's) and water. Thus, as NAPL's move through the saturated zone they may redistribute colloids. Alternatively, this attachment suggests a mechanism to deliver colloid-sized packages (bacteria, capsules, etc.) to a NAPL-contaminated zone. One

would simply control the chemistry to insure their mobility in the water saturated portions of the aquifer. When they reach the NAPL residual zone, they would be easily sorbed. We also believe that the visualization of colloid behavior can be used to mimic the behavior of dissolved contaminants. In this case the capillary force is irrelevant, but we have seen other forces leading to the attraction of particles to the gas-water interface. This suggests that, depending on the chemistry, in the vadose zone some or perhaps even most of the aqueous concentration of hydrophobic contaminants will be concentrated near the gas-water interface.

## SUMMARY AND CONCLUSIONS

We developed a method to visualize the behavior of colloid particles at interfaces within pore networks. Visualization was achieved by using glass micromodels with a UV epifluorescent light and dark field microscope. This method allowed direct observation of the interactions of colloids and interfaces both globally throughout the network and locally within individual pores. Besides fluorescent latex particles, common natural colloids, such as clay and bacteria were directly observable. The wettability of the pore walls, the fluid phase distribution within the pore network, the flow rate, and the chemical conditions of the system could all be closely controlled. Thus, the method reveals both cause and effect. This method can be used in future studies of particulate transport, interface-related transport, and the facilitation of bioremediation schemes.

We isolated several phenomena in our interface-related colloid transport study.

The gas-water interface preferentially sorbs colloidal particles relative to the rock-water interface under simulated groundwater conditions. The degree of this sorption increases with increasing particle surface hydrophobicity, and increasing solution ionic strength. Positively charged particles have greater affinity to the gas-water interface. The sorption at the gas-water interface is irreversible due to the capillary free energy change. Once sorbed onto the interface, few particles can be desorbed by chemistry or shear stress. The preferential sorption of colloid particles onto fluid-fluid interfaces suggests a role for this mechanism in vadose zone transport, NAPL behavior, and bioremediation.

**Acknowledgments.** The authors would like to acknowledge Norman Morrow, Robert Bowman, Jill Buckley, and Tom Kieft for their helpful discussions. We thank Robert TerBerg for help with editing this manuscript. We also would like to acknowledge the Subsurface Science Program, Office of Health and Environmental Research, U.S. Department of Energy for supporting this work.

## REFERENCES

- Buddemeier, R.W., and J.R. Hunt, Transport of colloidal contaminants in groundwater: radionuclide migration at the Nevada test site, *Appl. Geochem.*, 3, 535-548, 1988.
- Brockman, F.J., B.A. Denovan, R.J. Hicks and J.K. Fredrickson, Isolation and characterization of quinoline-degrading bacteria from subsurface sediments, *Applied and Environmental Microbiology*, 55, 1029-1032, 1989.
- Buckley, J.S., Multiphase displacements in micromodels, in *Interfacial Phenomena in Petroleum Recovery*, ed. by N.R. Morrow, Marcel Dekker, Inc., New York and Basel, 157-189, 1991.
- Chatzis, I., Photofabrication technique of two-dimensional glass micromodels. PRRC report no. 82-12, New Mexico Institute of Mining and Technology, Socorro, NM, 1982.
- Derjaguin, B.V., and L. Landau, Theory of the stability of strongly charged lyophobic sols and of the adhesion of strongly charged particles in solutions of electrolytes, *Acta Physicochemica, U.R.S.S.*, 14, 633-662, 1941.
- Derjaguin, B.V., N.V. Churave and V. M. Muller, *Surface forces*, Consultants Bureau, New York City, 1987.
- Derjaguin, B.V., S.S. Dukhin, and N. N. Rulyov, Kinetic theory of the flotation of fine particles, *Surface Colloid Sci.*, 13, 71-113, 1984.
- Fuerstenau, D.W., Fine particle flotation, in *Fine Particle Processing*, ed. by P. Somasundaran, AIME, Inc., New York, 2, 669-691, 1980.
- Gaudin, A.M., A.F. Witt, and T.G. Decker, Contact angle hysteresis: principles and application of measurement methods. *Trans. AIME*, 226, 107-112, 1963.
- Gschwend, P.M., Colloids in groundwater: their mobilization, subsurface transport, and sorption affinity for toxic chemicals, DOE/ER/60846-3, Office of Health and Environmental Research Subsurface Science Program, 1992.
- Hamaker, H.C., The London-van der Waals attraction between spherical particles, *Physica*, 4, 1058-1072, 1937.
- Hirasaki, G.J., Wettability: fundamentals and surfaces, *SPE Formation Evaluation*, 1, 217-226, 1991.

- Hornaby, D., and J. Leja, Selective flotation and its surface chemical characteristics, *Surface Colloid Sci.*, 12, 217-314, 1983.
- Israelachvili, J.N., *Intermolecular and Surface Forces*, Academic Press, New York City, 1985. James, D.F., The meniscus on the outside of a small circular cylinder, *J. Fluid Mechanics*, 63, 657-64, 1974.
- Jamis, D.F., The meniscus on the outside of a small circular cylinder. *J. Fluid Mechanics*. 63:657-664. 1963.
- Jameson, G.J., Physical aspects of fine particle flotation, in *Principles of Mineral Flotation*, ed. by M.H. Jones and J.T. Woodcock, The Australia Institute of Mining and Metallurgy, Victoria, Australia, 215-236, 1985.
- Laskowski, J., Particle-bubble attachment in flotation, *Miner. Sci. Eng.*, 6(4), 223-235, 1974.
- Lee, C.Y., and J.A. McCammon, The structure of liquid water at an extended hydrophobic surface, *J. Chem. Phys.*, 80, 4448-4456, 1984.
- Leja, J., *Surface Chemistry of Froth Flotation*, Plenum, New York, 1982.
- Li, C., and P. Somasundaran, Reversal of bubble charge in multivalent inorganic salt solutions: effect of magnesium, *J. Colloid and Interface Sci.* 146, 215-218, 1991.
- McCarthy, J.F., and J.M. Zachara, Subsurface transport of contaminants, *Environ. Sci. Technol.* 23, 496-502, 1989.
- McDowell-Boyer, L.M., J.R. Hunter and N. Sitar, Particle transport through porous media, *Water Resour. Res.*, 22, 1901-1921, 1986.
- Morrow, N.R., Physics and thermodynamics of capillary action in porous media, *Industrial Engineering Chem.*, 62(6), 20-30, 1970.
- Morrow, N.R., I. Chatzis, and J.J. Taber, Entrapment and mobilization of residual oil in bead packs. *SPE Reservoir Engineering*, 3(3), 927-934, 1988.
- Rapacchietta, A.V., and A.W. Neumann, Force and free energy analysis at fluid interfaces: II. spheres, *J. Colloid and Interface Sci.* 59, 555-567, 1977.
- Van Loosdrecht, M.C.M., J. Lyklema, W. Norde, G. Schraa, and A.J.B. Zehnder, Electrophoretic mobility and hydrophobicity as a measure to predict the initial steps of bacterial adhesion, *Applied and Environmental Microbiology*, 53, 1898-1901, 1987.

Van Oss, C.J., J. Visser, D.R. Absolom, S.N. Omenyi and A. W. Neumann, The concept of negative Hamaker constant, *Advances in Colloid and Interface Science*, 18, 133-148, 1983.

Verwey, E.J.W., and J.Th.G. Overbeek, *Theory of Stability of Lyophobic Colloids*, Elsevier, Amsterdam, 1948. Williams, D.F. Aggregation of colloidal particles at the air-water interface, Ph. D. dissertation, University of Washington, 1991.

Williams, D.F., Aggregation of colloidal particles at the air-water interface, Ph.D. dissertation, University of Washington, 1991.

Wilson, J.L., S.H. Conrad, W.R. Mason, W. Peplinski, and E. Hagan, Laboratory investigation of residual liquid organics from spills, leaks, and the disposal of hazardous waters in groundwater, R. S. Kerr Environmental Research Laboratory; EPA/600/690/004, 1990.

Yoon, R.H., and J.L. Yordan, Zeta potential measurements on microbubbles generated using various surfactants, *J. Colloid and Interface Sci.*, 113(2), 430-438, 1986.

## APPENDIX 2A

## THE PROCEDURE FOR MAKING GLASS MICROMODELS

The following is a summary of the procedure for generating glass multi-micromodels.

**1. Preparing a micromodel pattern:** A micromodel is composed of a pore network, reservoirs at both ends of the network, and an inlet and outlet at each reservoir, respectively. A drawing of a micromodel pattern is created on a computer, and then reproduced photographically on plastic transparencies in a desired size and number of models.

**2. Preparing glass mirrors:** Glass mirrors can be specially purchased from manufacturers. These mirrors are glass plates coated with silver and copper but without the additional protective enamel backing covering the copper layer. We recommend 5x8 inch mirrors that are 0.08 inch thick. The quality of the image decreases with the thickness of glass, but a very thin glass is not easy to handle. The non-backed mirrors must be protected from scratching and corrosion. If the mirror has an enamel backing it must be removed. The backing stripper is composed of 95% dichloromethane and 5% formic acid. The stripper is placed in a glass pan which is slightly larger than a mirror. A mirror is immersed in the stripper with its backing face up for about 10 seconds. When the backing peels off, remove the mirror and rinse thoroughly with tap water. The mirror is immediately washed, in steps, with toluene, acetone, and soapy water. Then it is rinsed thoroughly and dried with compressed air. Once the backing is removed, the copper layer is checked on the light table to see that it is unblemished. Only the good



pieces are retained for the next step.

**3. Covering the mirror with photo-resist:** This step is performed in a dark room. Kodak thin film resist (KTFR) is used to transfer the micromodel pattern onto the mirror surface. Prepare a mixture of 1:2 of KTFR to xylene (dimethylbenzene). Hold the mirror horizontally and with the copper side face up. Pour enough of the mixture to coat the copper evenly; leave the excess resist on for 30 seconds, then pour off the resist and place the plate vertically to drain the excess resist. Leave the plates to air-dry overnight in a dark place.

**4. Exposure:** Uniform light intensity is required. In a dark room, four 15 W long wave ultraviolet light lamps are put in a row. A fresnel lens is set under the light source and 8.5 inches above the table. The emulsion-side of the pattern transparency is put on the coated side of a mirror; the pattern is covered with a piece of clean glass to ensure a good contact, then the whole set is placed under the fresnel lens and on the table. The exposure time varies from 1.5 to 3 minutes depending on the fineness of the patterns, intensity of the light source, the thickness of film resist, and the age of the resist. Longer exposure reduces the fine detail, and a thicker resist requires longer exposure. Therefore, the exact exposure time needs to be experimentally determined for each pattern in the fixed conditions. If the resist is underexposed, it will be washed off during the next step, and if it is overexposed, the pattern will lose details.

**5. Development:** When the exposure is complete and the room light is still dim, hold the mirror horizontally and spray xylene on the surface. The plate is tipped back and forth for 2 minutes to dissolve the undeveloped resist. The plate is rinsed with warm tap

water and then dried with compressed air. Place the plate in concentrated nitric acid for about 10 seconds, or until the unprotected copper and silver layers are dissolved to reveal the underlying glass surface. The plate is rinsed quickly with cold tap water. Check the plate under a microscope, and keep only the unblemished ones for the next step.

**6. Etching:** All areas of glass that needed to be unetched, such as the model edges and back, are coated with resist and air-dried. During etching the plate is placed pattern-side down in a tray of concentrated hydrofluoric acid for about 4 to 18 minutes, depending on the difference in patterns. Longer etching time is used for models requiring deeper pores. The depth of the etching should be equal to and less than the average throat width. When the plate is removed from the hydrofluoric acid, it is rinsed in cold water, and the network is scrubbed with a hard brush to remove silica deposits formed during etching. The resist is removed with a razor, then the copper and silver with concentrated nitric acid.

**7. Fusing:** Inlet and outlet ports are drilled with a diamond drill bit on one side of a pair of plates. After drilling the plates are washed with soapy water and brushed thoroughly, then put in a ultrasonicator for 20 minutes to remove the fine silica. The two halves are aligned under a microscope, and a tiny drop of cyanoacrylate glue is added in between the plates from the edges to hold them together. The model is placed in a muffle furnace and fused at 715 °C for about 15 minutes. Higher temperature and longer fusing time result in smoother, smaller pores; however, when the temperature is too high and fusing time is too long, pores will close and the network becomes disconnected. A completed micromodel is removed after the furnace is cooled to below 100 °C.

**8. Fittings:** Hard teflon tubes 0.5 inch in length and 0.128 inch O.D. are fitted and glued in the inlet/outlet holes. Input and output fluids are conducted by tygon tubing fitted to the teflon tubes as shown in Figure 2.2.

---

**CHAPTER 3**

---

**COLLOID TRANSPORT IN UNSATURATED POROUS MEDIA**

(Submitted to Water Resources Research, March 2, 1993)

**ABSTRACT**

Using two-dimensional glass micromodels, Wan and Wilson (1993) visualized the preferential sorption of colloidal particles onto the gas-water interface relative to the glass-water interface on a pore scale. This paper quantifies those observed phenomena in packed sand columns on a porous medium scale. The porous media used in the column experiments represent different situations in the subsurface environment: (1) a completely water saturated condition, (2) gas trapped by capillary forces as a non-wetting residual phase, and (3) gas present as a continuous phase or, in other words, a vadose zone situation. These different situations produce different interfacial conditions as well as different pore geometries. An important benefit is that the column method employed here results in reproducible data. In addition, the relative particle surface hydrophobicity is more accurately characterized by the contact angle measurements used in this research. Experimental results show that the transport rate of colloids is inversely proportional to the gas content of the porous medium. The preferential and irreversible sorption of colloids onto the surface of trapped gas bubbles is the cause of the increased retention. The degree of sorption increases with the increase of colloid surface hydrophobicity.

These results demonstrate that the gas-water interface plays a significant role in colloid transport in a two-fluid porous medium.

## INTRODUCTION

The transport of mobile colloids through porous media is an important process in both natural and engineering systems. In subsurface hydrogeological environments colloid transport significantly facilitates the migration of colloidal and colloid-bound pollutants in groundwater and soils (McDowell-Boyer et al., 1986; Gschwend and Wu, 1985; Buddemeier and Hunt, 1988; McCarthy and Zachara, 1989; Bales et al., 1991; Puls and Powell, 1992). In the water and wastewater treatment industries, granular-bed filtration separates fine particles, pathogens and colloid-associated pollutants from suspensions (e.g. Ives and Gregory, 1966; Yao et al., 1971; O'Melia, 1989). Historically, research on colloid transport has focused on water-saturated porous media. Quantitative models for predicting particle transport are presented in the water filtration literature (Yao et al., 1971; Spielman and FitzPatrick and Spielman, 1973; Tien and Payatakes, 1979; Tien, 1989). These papers account for the deposition mechanisms of particle-medium collisions and the conditions for particle attachment. For Brownian particles, diffusion and advection control the collision rate. Attachment is determined by the interfacial forces between the mobile particles and fixed solid surfaces (collectors). These forces include electrical double layer, van der Waals, structural (hydration), and hydrodynamic forces. The deposition rate in an ideal medium can be calculated theoretically from the solution

of the advection diffusion equation (Spielman and Fitzpatrick, 1974; Friedlander, 1977; Adamczyk et al., 1983). The deposition rate can also be determined experimentally by measuring the particle capture rate through a clean granular bed (e.g. Gregory and Wishart, 1980; Tobiasson and O'Melia, 1988). A large discrepancy between controlled laboratory experiments and theory is a common feature of colloid transport studies. For instance, in unfavorable conditions the predictions of transport distance greatly exceed any laboratory or field observations (FitzPatrick, 1972; Bowen and Epstein, 1979; Elimelech and O'Melia, 1990a,b). Various reasons for these discrepancies have been proposed over the past two decades (e.g. Spielman, 1977; Gregory and Wishart, 1980; Adamczyk et al., 1983; O'Melia, 1989; Litton and Olson, 1993). Among these are heterogeneous surface roughness, differences in surface charge and surface potential, and differences in the methods of collector surface preparation

. However, none of these previous investigators has been aware that any residual gas phase present in porous media can reduce the transport distance effectively (Wan and Wilson, 1992a,b), or if they are aware, they have taken precautions to insure the absence of trapped gas in the laboratory packed porous media and field test sites. The preferential sorption of colloids by the gas-water interface may explain some of the discrepancies in standard single phase flow experiments.

Contaminant transport through unsaturated porous media is an important aspect of subsurface transport phenomena. Colloids generated from weathering, biological activities and human influence may be much more concentrated in soil water compared to their levels in groundwater. How these colloids move through the vadose zone and

capillary fringe to reach the water table is not well understood. In particular, the role of the gas-water interface, one of the two most important interfaces in the vadose zone, has been neglected. Powelson et al. (1990) pointed out that, under unsaturated flow conditions, viruses were strongly removed from the soil water due to their enhanced inactivation. This conclusion could mean that the viruses were mobile but no longer viable, or that they had been immobilized. Powelson et al. (1990) found inactivation, but not its cause. In two-dimensional glass micromodels, Wan and Wilson (1992c, 1993) studied the interactions between various colloids (latex spheres, bacteria and clay particles) and the solid-water and gas-water interfaces on a microscopic pore scale. They observed the preferential sorption of particles onto the gas-water interface, which they explain by, among other things, a capillary force acting on particles at fluid-fluid interfaces.

The objective of this paper is to validate and quantify those visualized phenomena on a hydrologically significant scale. Column experiments are described in which colloid suspensions are injected at one end and breakthroughs observed at the other end. Water and gas saturations are varied from experiment to experiment in order to observe the effect of the gas-water interface on breakthrough. Fully water-saturated experiments serve as the control. Other experiments are performed with capillary trapped residual gas bubbles (~ 15% gas saturation), and with a continuous gas phase (~ 46% gas saturation). In the residual gas experiments the gas-water interface is isolated on each bubble. Here we test the hypothesis that some particles will be retained, due to irreversible sorption on the isolated bubbles (Wan and Wilson, 1993). The continuous

gas phase experiments contain a continuous and largely interconnected gas-water interface. Solving the Navier-Stokes equations, modeled as a circular tube, for two phase gas-water flow in single water-wet pore leads to the conclusion that water velocity will be maximum along the gas-water interface (Byrd et al., 1960). This suggests the hypothesis that colloids sorbed at this continuous interface will move faster than the average water velocity, and will break through early. However, packed bed porous media are geometrically far more complex than a single tube model (Bear, 1972), and it is quite possible that particles attached to the gas-water interface will become trapped. The continuous gas phase experiments also have a much larger interfacial area between gas and water, suggesting much greater sorption than for the isolated bubbles. Finally, we tested transport for two different colloid particle surfaces in order to elucidate processes at the gas-water interface.

## MATERIALS AND METHODS

### General Methodology

Particle hydrophobicity and column gas saturation were the only two variables in the column experiments. Two types of polystyrene latex particles (hydrophilic and hydrophobic,  $0.2 \mu\text{m}$ ) were used; each type was tested for three different saturations. Each experiment was repeated 5 times, for a total of 30 column experiments. Figure 1 schematically illustrates the three different saturations. In Figure 1a, the columns were fully water saturated; the quartz-water interface was the only interface present. These ten experiments acted as a control for the unsaturated flow experiments. In Figure 1b, the



columns contained a capillary trapped residual gas phase occupying 15% of the pore space; two interfaces, the gas-water and quartz-water, were present. The pore scale geometry for water flow was altered by the gas bubbles trapped in the pore bodies. In Figure 1c, the columns were also unsaturated, but the gas occupied 46% of the pore space as a continuous phase. Both gas and water were interconnected and two interfaces existed. Water pore geometry was changed significantly. Experiments were performed in 30 cm long and 2.5 cm i.d. borosilicate glass chromatography columns (ACE Glass, Inc.) packed with 212-315  $\mu\text{m}$  diameter high purity quartz sand (Unimin Co.) The columns were mounted vertically and flow was directed downward by peristaltic pumps (WIZ pumps, ISCO). The pumping rate was adjusted for each column individually to maintain a constant seepage velocity at 10.0 cm/hr, as described later. Ionic strength (1.0 mM  $\text{NaNO}_3$ ) and pH (6.6) were also maintained constant for all of the solutions and suspensions. The particle number concentration of the influent suspension was approximately  $2.5 \times 10^{10} \text{ L}^{-1}$ . Particle concentrations were measured with a spectrophotometer (Perkin Elmer 330). Prior to colloid addition, solutions were filtered with a 0.22  $\mu\text{m}$  pore size filter. Particle suspensions, made with the filtered solution, were filtered (2.5  $\mu\text{m}$ , Whatman 5) to remove any particle aggregates. Air was used as the gas phase.

It should be mentioned that some abbreviations have been used in the following text: D water = distilled water; 2D water = distilled and deionized water; 3D water = distilled, deionized and degassed water (3D water was made by boiling 2D water, and storing it in a container connected to a vacuum system); 2D solution = solution made

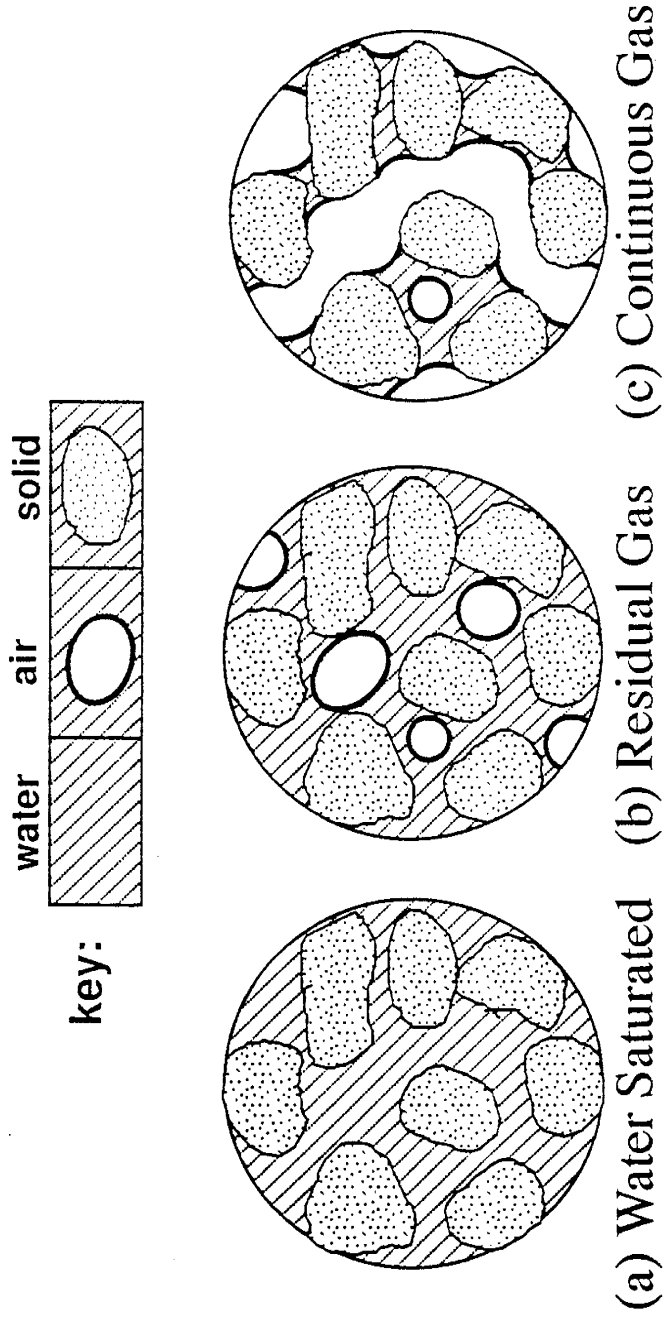


Figure 3.1. Three types of columns representing three types of groundwater conditions: (a) fully water-saturated; (b) residual gas; (c) continuous gas and water phases.

by using 2D water; 3D solution = solution made by using 3D water. 3D water and 3D solution were used in the water saturated columns to maintain an air-free condition. 2D water and 2D solution were used in unsaturated columns to keep the gas from dissolving.

Two micromodel experiments were conducted to complement the results from the column experiments. The micromodel method has been described in Wan and Wilson (1993). Fluorescent (yellow-green) hydrophilic and hydrophobic latex particles with sizes about  $1.0 \mu\text{m}$  in diameter were used in the visualization experiments because they were easy to observe.

### **Colloids and Surface Characterization**

Four types of surfactant-free polystyrene latex microspheres (Interfacial Dynamics Corp.), their surface zeta potentials, and water contact angles are listed in Table 1. Particle electrophoretic mobilities were measured with a Coulter DELSA 440 (Doppler Electrophoretic Light Scattering Analyzer) in a solution of  $1.0 \text{ mM NaNO}_3$  and pH 6.6 at  $25 \text{ }^\circ\text{C}$ . The accuracy and precision of the Coulter instrument operation were assessed for the test series through analysis of a hydrophilic electrophoresis standard particle, carboxylate modified latex. The standard of this latex particle was determined by the manufacturer. Mobility data were converted to  $\zeta$  potentials calculated from the measured mean electrophoretic mobilities by using the tabulated numerical calculations of Ottewill and Shaw (1972).

Particle hydrophobicity is an important factor controlling particle stability in an aqueous phase, but unfortunately, a quantitative measurement is not yet available. A rough estimate can be given by using  $\zeta$  potential or particle surface charge density

calculated from electrophoretic mobility. The general relationship is that the higher the mobility, the higher the  $\zeta$  potential and charge density, and the less the hydrophobicity. Many factors strongly affect the mobility value but not necessarily the surface hydrophobicity. These factors include the ionic strength, pH, and temperature of the solution, as well as particle size. This type of estimate is not accurate enough for our purpose. The direct contact angle measurement (shown in Table 1) is more accurate. The contact angles of the latex particles were measured with the smear layer-captive drop method described in Wan and Wilson (1993). Figure 2 shows a measurement of contact angles on the hydrophobic particles used in the column experiments. A glass slide with a smeared thin layer of the particles was set under the pipet in all of the four pictures. Figure 2a was taken just before the water drop attached to the surface. The shape of the water drop was not symmetric; it was caused by surface imperfection of the pipet tip. Figure 2b was taken after the water drop attached to the surface while all three phases were equilibrated with each other. The advancing contact angle was then measured. It was found that the contact angles are not constant but show relaxation because of a slow process of imbibition into the packed particle layer. Afterwards the water drop was pulled slowly off of the surface. Figure 2c records the moment just before the water drop slapped off the tip of the pipet when the receding contact angle was measured. We did not report the receding contact angle because of the large hysteresis of the system. Figure 2d is a picture taken after the measurement was finished. The accuracy of this smear layer-captive drop method is limited by many factors, including the roughness of the particle layer and pipet tip, particle size, and the moisture content of the layer.

TABLE 3.1. Latex Particles and their Surface Properties

Used In	Particle Type	Size ( $\mu\text{m}$ )	Contact Angle $\theta_a$	$\zeta$ Potential (mv)
Column Experiments	Carboxylate Hydrophilic Latex	0.19	$35.6 \pm 5.7^\circ$	-52.8
Column Experiments	Sulfate Hydrophobic Latex	0.22	$127.4 \pm 5.4^\circ$	-35.8
Micromodel Experiments	Fluorescent Carboxylate Hydrophilic Latex	0.95	$< 10^\circ$	-89.2
Micromodel Experiments	Fluorescent Sulfate Hydrophobic Latex	1.05	$121.9 \pm 6.7^\circ$	-48.2

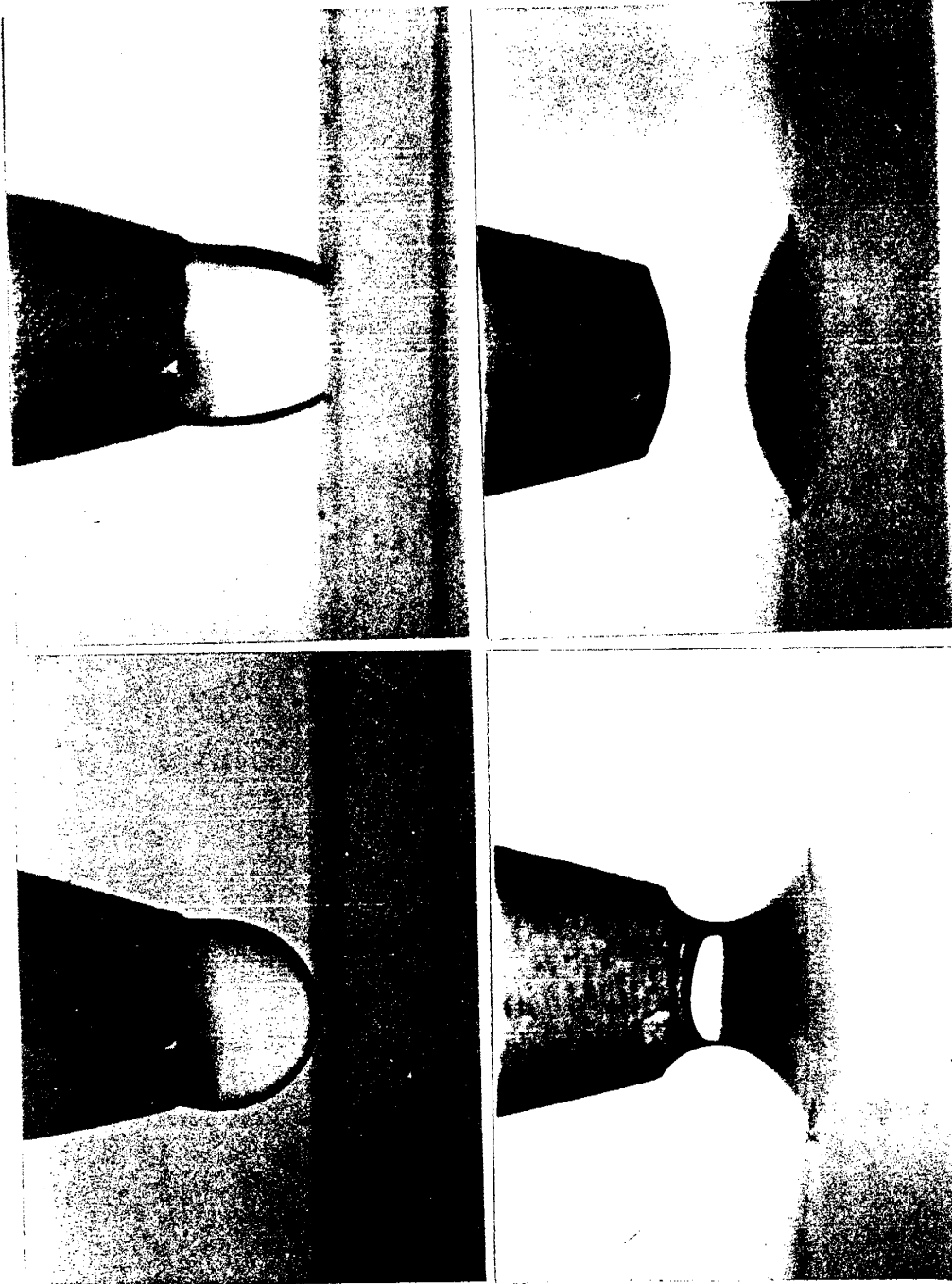


Figure 3.2. Contact angle measurement with particle layer-captive drop method used on hydrophobic latex particles: (a) before the water drop attaches to the particle layer; (b) as the advancing contact angle is measured; (c) as the receding contact angle is measured; (d) when measurement is finished.

### Preparation of Medium Surface

We present the detailed procedure here because a clean medium surface is one of the most important factors controlling the reproducibility of particle deposition rate (from our own experience as well as that of Litton and Olson, 1993). High purity quartz sand was used in the column experiments as the porous medium. The quartz sand was size-fractionated with stainless steel sieves to a 212-315  $\mu\text{m}$  range. In order to reduce surface contaminants and remove attached amorphous and fine material, we used the following cleaning procedure: soak ~ 500 grams of sorted dry sand in 50%  $\text{HNO}_3$  solution for 24 hr in a 1000 ml glass beaker. Boil the sand in a fresh 50%  $\text{HNO}_3$  for 20 min. Batch wash the sand with D water 20-30 times until the pH reaches that of the D water. Soak the sand in a 1.0% sodium polyphosphate solution and sonicate it for 20 min. Batch wash the sand with D water until the pH reaches that of D water. Sonicate the sand in 2D water for 20 min, then batch wash with 2D water 5 times. Dry the sand in a clean oven at 110°C for 24 hr. Then the sand is ready to be used for packing.

### Preparation of the Columns

A column apparatus consists of a glass chromatographic column, 30 cm long and 2.5 cm i.d. with two tetrafluoroethylene (TFE) endcaps and associated plumbing. The endcaps were screwed into threaded ends on the glass column and sealed against the column with o-rings. A network of small channels, approximately 1 mm deep and 1.5 mm wide, was machined onto the surface of each endcap. The grooves allow for a more uniform water flow between the endcaps and the soil. A polypropylene filter with a mesh

opening of  $105 \mu\text{m}$  was glued onto each endcap in order to keep fine sand particles from leaving the column. The effective column volume was accurately measured gravimetrically for each individual packing.

The columns were prepared by following this procedure: (1) Remove gas from a set amount of cleaned and dried sand by sonicating it in 3D water for 20 min. Wash the sand 3 times with 3D water to remove any fine particles. (2) Wet pack the column with special care to avoid any layering. Tamp the sand tightly with a rubber vibrator. Dry and weigh the sand left from packing to determine the net amount of sand used. (3) Dissolve any remaining air trapped during packing by flooding 3D water through the packed column until complete saturation, as judged gravimetrically, is obtained. The porosity of the column is then calculated by using measured column volume, the weight of sand used, the density of the sand, and the final weight of the fully saturated column. (4) For the preparation of the other two types of columns, thoroughly drain the column after step 3. (5) For the unsaturated columns with residual gas bubbles, imbibe a 2D solution into the medium at a low flow rate ( $\sim 6 \text{ cm/hr}$ ) in order to entrap air as a residual phase (below critical capillary and bond numbers). Weigh the column and calculate the exact gas and water saturations. (6) For the unsaturated columns with a continuous gas phase, after step 5, pump a 2D solution into the column from the top at a pumping rate which appears to result in a seepage velocity of  $10 \text{ cm/hr}$ . We define the seepage velocity  $v$  as  $v = Q/S_w n$ , where  $Q$  is the volumetric pumping rate,  $n$  is the porosity and  $S_w$  is the water saturation. In the water saturated column  $S_w = 1$  we measured  $n$  and  $S_w$  and adjusted  $Q$  to obtain a constant seepage velocity  $v$ . After a



constant flow rate was reached, we adjusted the pumping rate monotonically until the seepage velocity actually reached 10 cm/hr. Table 2 lists the parameters and their reproducibility. For example, porosity was  $0.43 \pm 0.019$  over the total of 30 columns. The gas saturation  $S_g$  ( $S_w + S_g = 1$ ) of the 10 unsaturated columns with residual gas phase was  $S_g = 15.0 \pm 0.62\%$ , and for the remaining 10 unsaturated columns with continuous gas phase, it was  $S_g = 46.0 \pm 2.4\%$ . The pH was controlled at  $6.68 \pm 0.12$  over all of the experiments. These strictly controlled physical and chemical parameters ensured the reproducibility of the column experiments.

### The Procedure for Column Experiments

(1) Set and calibrate the pumping rate (ml/hr) to match the seepage velocity of 10.0 cm/hr. (2) Obtain the desired chemical conditions and fine mineral-free conditions within the column by flooding it with a 3D solution until the pH and turbidity of the effluent reach that of the influent. (3) Inject a slug of dilute particle suspension at the seepage velocity of 10.0 cm/hr. The slug was 1 water pore volume for hydrophilic particles and 6 pore volumes for hydrophobic particles. For a total column pore volume  $V$ , a water pore volume was calculated as  $S_w V$ . The effluent was collected by a fraction collector at a rate of 6 samples per pore volume. (4) Inject 2 or 3 pore volumes of particle-free solution to replace the suspension at the same flow rate. (5) Check the weight change of the column at the end of the run, and check the pH value of the effluent. (6) Measure the particle concentration with a double beam spectrophotometer at a wave length of 260 nm.

TABLE 3.2. Parameters of Column Experiments

Parameters	Value
Size of sand grains	212 to 315 $\mu\text{m}$
Bulk density	$1.95 \pm 0.012$
Porosity	$0.43 \pm 0.019$
Residual gas saturation	$15.0 \pm 0.62\%$
Continuous gas saturation	$46.0 \pm 2.4\%$
Seepage velocity	10.0 cm/hr
Ionic strength	1.0 mM
pH	$6.68 \pm 0.12$
Column weight changes	$-0.097 \pm 0.049\%$

## RESULTS AND DISCUSSION

### Micromodel Experiment

The latex particles used in the column experiments were small and dye-free, hence not suitable for the visualization experiments (Wan and Wilson, 1993). We chose two types of larger-sized fluorescent latex particles as the surrogates for those used in the column experiments to illustrate the underlying mechanisms involved in the column experiments. Figures 3 and 4 are photomicrographs taken after slugs of 30 pore volumes of dilute particle suspensions were injected and then replaced by a particle-free solution (Wan and Wilson, 1993). The ionic strength was 1.0 mM  $\text{NaNO}_3$  and the pH was 6.6 for the solution and suspension, the same as that used in the column experiments. In Figure 3, hydrophilic latex particles (contact angle  $< 10^\circ$ ,  $0.95 \mu\text{m}$ ) preferentially sorbed onto a gas bubble trapped in a pore body, and few particles sorbed onto the adjacent pore walls. In Figure 4, hydrophobic latex particles (contact angle  $= 122^\circ$ ,  $1.05 \mu\text{m}$ ) sorbed onto both the pore-walls and the trapped bubble. Hydrophobic particles show a strong affinity for the gas-water interface.

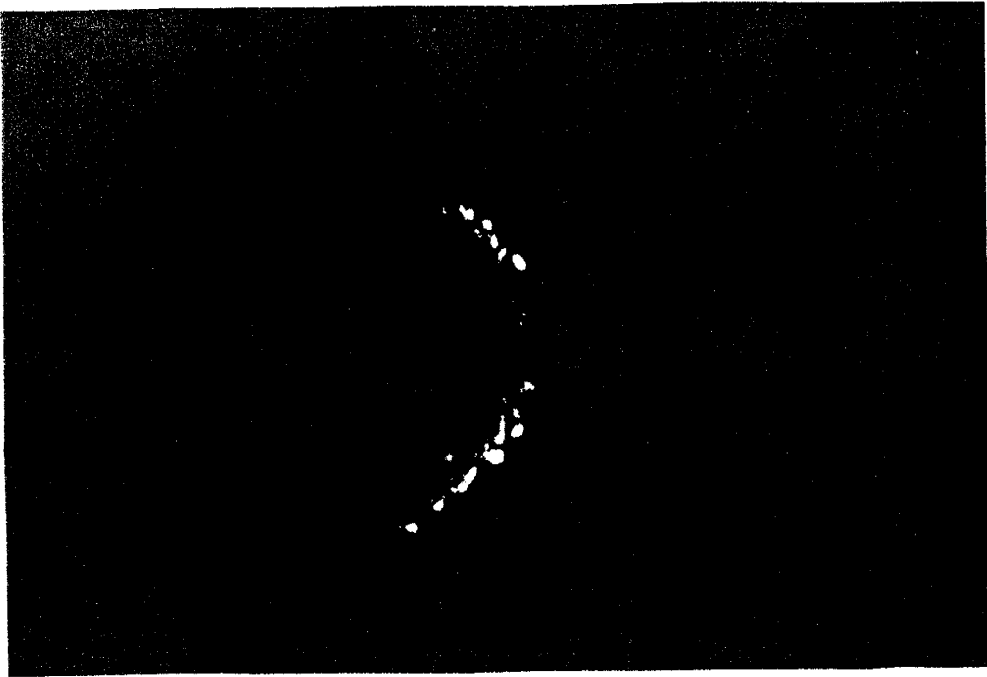


Figure 3.3. Hydrophilic negatively charged latex particles ( $0.95 \mu\text{m}$ ) preferentially sorb onto the downstream portion of an air bubble. Few particles sorb onto the pore walls. Solution ionic strength is  $1.0 \text{ mM}$ ,  $\text{pH } 6.6$ . Glass micromodel with quadrilateral network.

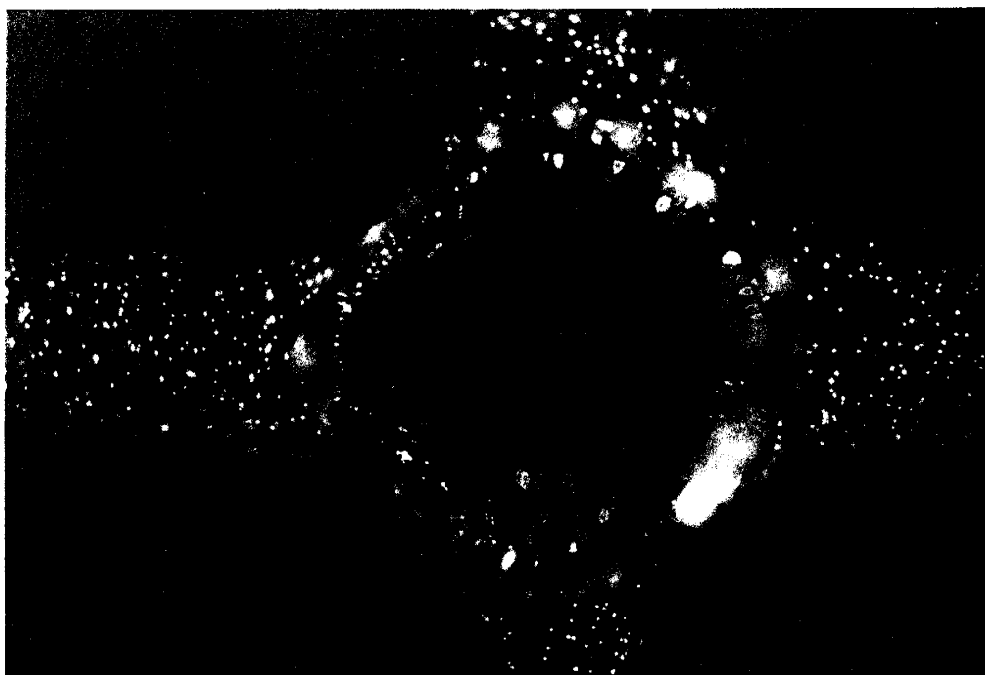


Figure 3.4. Hydrophobic negatively charged latex particles sorb onto both air-water and glass-water interfaces. Observe the effect of particle surface hydrophobicity by comparing to Figure 3.3. All the other experimental conditions are the same.

### Column Experiments using Hydrophilic Colloids

A slug of one water pore volume of hydrophilic latex particle ( $0.19 \mu\text{m}$ ,  $\theta_a = 36^\circ$ ) suspension was applied in the three types of columns, and then displaced by 2 pore volumes of particle-free solution. The chemical conditions were the same as those in the micromodel experiments shown in Figures 3 and 4. All of the other experimental conditions were kept strictly the same for the columns. Therefore, the differences in the breakthrough data were mainly caused by the presence and amount of gas. The results are presented as breakthrough curves where the fraction of the influent particle concentration ( $C/C_o$ ) leaving the packed column is a function of pore volume.  $C$  and  $C_o$ , respectively, were the effluent and influent concentrations of colloids.

Figure 5 is the summary of results from 15 columns with hydrophilic particles. The top curve is the breakthrough curve from the water saturated columns, the middle curve is from the columns with a trapped residual gas phase, and the lower curve is from the unsaturated columns with a continuous gas phase. The solid lines were drawn with the average of the data from 5 repeated experiments. The standard deviation of each point is plotted as a vertical error bar. These curves present several features. First, the standard deviations of the breakthrough curves are small, relative to the great difficulties in reproducing data in filtration experiments, indicating good reproducibility. Second, the mass recoveries decrease systematically with increasing gas saturation. The total mass recovery for each saturation is: 99% from the water saturated columns, 91% from the residual gas columns, and 82% from the continuous gas columns. The 99% mass recovery from the water saturated media was caused by the chemical conditions, which

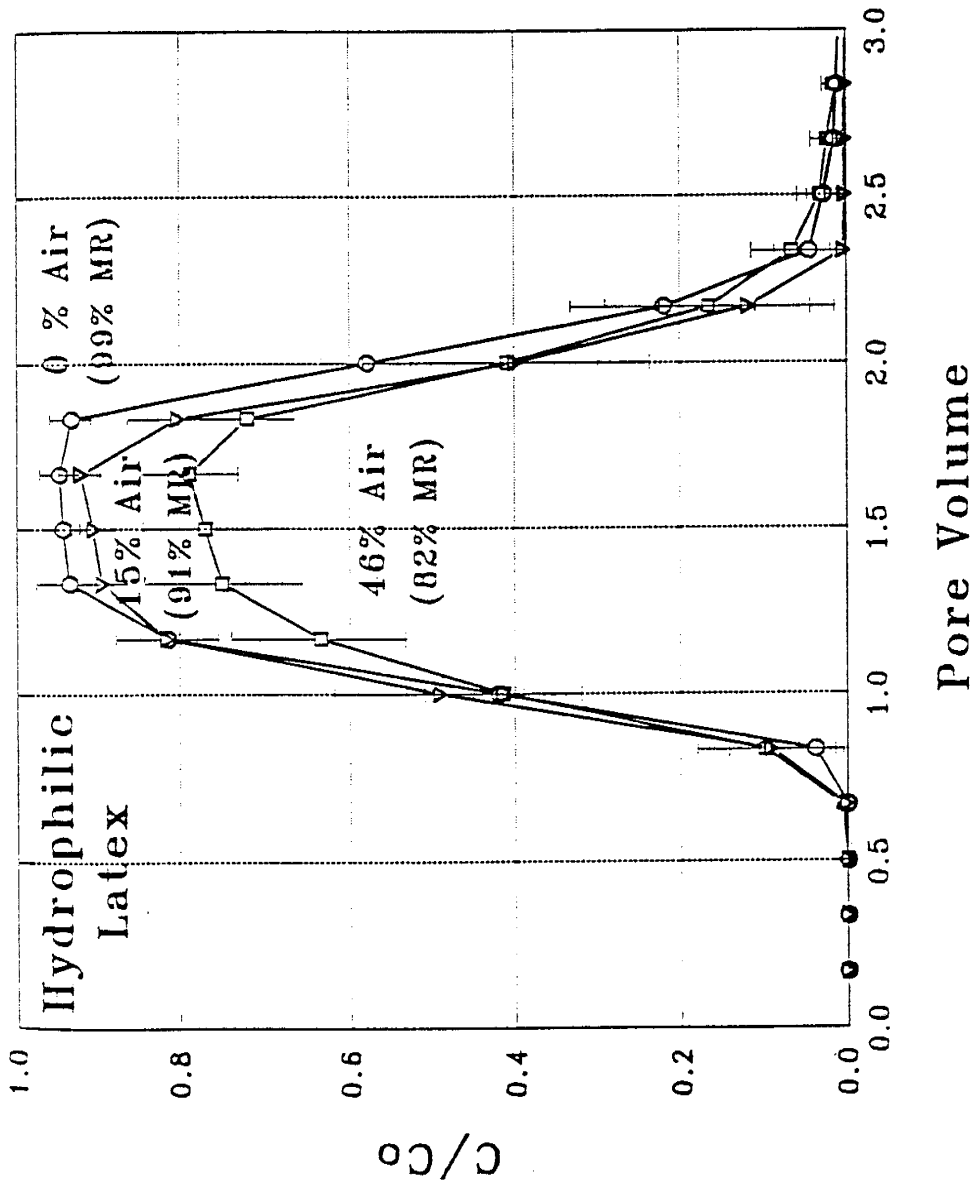


Figure 3.5. Breakthrough curves of hydrophilic latex particles from three types of columns: fully saturated, pseudo-saturated and unsaturated. Each curve shows an average of five repeated experiments and the standard deviations are plotted as error bars. Percentages show the percentage of pore volume occupied by air (% Air) as well as the percentage of total mass recovery (% MR).

were extremely unfavorable for particle deposition on solid surfaces. This curve also indicates that mechanical filtration, including caking and straining, didn't have a significant effect on the transport of the particles through the packed media, and that, therefore, all the particles retained in the columns were retained due to physical-chemical filtration. Increasing the air saturation to the non-wetting phase residual, 15.0 % of pore volume in our case, lowers the mass recovery by 8%. Where does this mass go? Figure 3 suggests the answer: the 8% mass is irreversibly sorbed by the air bubbles trapped in the pore bodies. Increasing the air saturation further to the continuous air phase condition, decreases the mass recovery by 17% compared to the water saturated condition. Clearly this was caused by the increased area of the gas-water interface, creating more sorption sites and higher collision probabilities. These retained particles were apparently all sorbed onto the gas-water interface. Third, the seepage velocity was maintained the same for the columns with different water saturation. The water pore volume of columns with different saturations was accurately measured and applied; at water pore volume = 1,  $C/C_0 \approx 0.5$  (0.4-0.5). No preferential advection was observed, even for the columns with the continuous gas phase. It appears that in these continuous gas phase columns the particles were locally trapped along the gas-water interface due to a combination of hydrodynamic and capillary forces. We speculate that the capillary forces hold the particles on the interface (Wan and Wilson, 1993), while the hydrodynamic (flowing) forces attempt to pull them into the water phase in order to progress further through the unsaturated media. Some increases of breakthrough dispersion with gas saturation can be observed in Figure 5, although they are not large.



The moderate increases may be due to the uniformly sized sand grains and the decreased significance of flow tortuosity induced by trapped gas in a uniform pore structure for the residual gas columns. The increase is larger for the continuous gas columns. Finally, the curves from unsaturated columns have no significant tailing, a fact which indicates that the sorption onto the gas-water interface is irreversible.

### Column Experiments using Hydrophobic Particles

Particle surface hydrophobicity is one of the most important factors dominating particle behavior in porous media. The behavior of hydrophobic latex particles ( $0.22 \mu\text{m}$ ,  $\theta_a = 127^\circ$ ) was tested and compared with that of the previous hydrophilic ones. A slug of 6 water pore volumes of particle suspension was fed into the columns, and then displaced by 3 water pore volumes of particle-free solution. The larger slug of suspension was applied because of the strong retention of hydrophobic particles. For a slug of 1 water pore volume suspension, no particles broke through from the unsaturated columns. All of the other experimental conditions were kept strictly the same. It is obvious from the photomicrograph in Figure 4 that particles do not enter into the areas where the gas bubbles contact the solid surface because the water film between the gas and solid is too thin for the particles to enter. The effective sorption areas of the solid medium, therefore, are roughly inversely proportional to the gas content of the medium. When we compare the mass recovery data for different saturations, the percentage of the hydrophobic particles retained by the gas-water interface is actually greater than the net differences indicated by the breakthrough curves.

Figure 6 is the summary of the results, where the breakthrough curves are from the three types of columns under different levels of saturation. Again every experiment was repeated five times and the breakthrough curves were drawn based on the average values. The total mass recoveries in Figure 6 are the integration of particles in the pore volume effluent. The actual mass recoveries were greater than these values because effluent particle concentration had not yet diminished to zero when the tests were terminated. Interpretation of the curves yields several observations. First, the top curve from water-saturated columns has 68% of mass recovery, so that 32% of the particles were retained in the columns by sorption onto the solid medium surface alone. The plateau of the curve implies that the sorption sites of the solid medium have not yet been saturated by particles, and the sorption energy of the solid surface has not been reduced by the increased coverage. The obvious tailing shows desorption of particles from the solid surface. Second, the middle curve from columns with trapped residual gas bubbles has recovered 42% and left 58% of the particles in the column by sorption onto both solid and gas bubble surfaces. At least 26% were sorbed onto the bubbles, while the reduced effective solid surface area sorbed less than 32%. The curve is smooth and has a gentle slope, which may indicate that the sorption energy of the gas-water interface decreases with surface coverage. The curve is still climbing when the influent slug is cut off. Even so, the top of the peak is higher than that from saturated columns. This suggests that the total effective sorption area of the solid surface in an unsaturated medium is smaller than that in the water saturated medium. The lower tailing compared with that from saturated columns indicates that the desorption is only from the solid-

water interface, not the gas-water interface. Third, the bottom curve for the continuous gas columns is similar to the middle one for the trapped gas. The only difference is that the total gas-water interface area is larger and retains more particles. A total of 74% of the particles were trapped in the unsaturated columns with a continuous 46% gas saturation. At least 42% of the total mass was sorbed onto the gas bubbles, while again, because of the less effective solid surface area, less than 32% were sorbed on the solid.

We also tested latex particles with higher hydrophobicity ( $0.22 \mu\text{m}$ ,  $\theta_a = 140^\circ$ ), and observed much lower mass recoveries. For example, a slug of 6 pore volume particle suspension never broke through from the columns with 46% trapped gas. Because of the poor data reproducibility (caused by formation of particle aggregates in the solution) we will not report the further results here.

Comparing the data in Figure 6 with those in Figure 5, we conclude that the degree of sorption onto the gas-water interface increases with increasing particle hydrophobicity. We believe the increased sorption onto the solid surface was caused by a reduction of electrostatic repulsive force between the particles and the solid surface; hence the van der Waals attractive force was dominant. Increased sorption onto the gas-water interface suggests a hydrophobic force between the hydrophobic particles, and the gas-water interface. If we compare Figure 6 and Figure 4, we observe the effect in one and the cause in the other. These data convincingly emphasize the importance of the gas-water interface on colloid transport in an unsaturated porous medium.

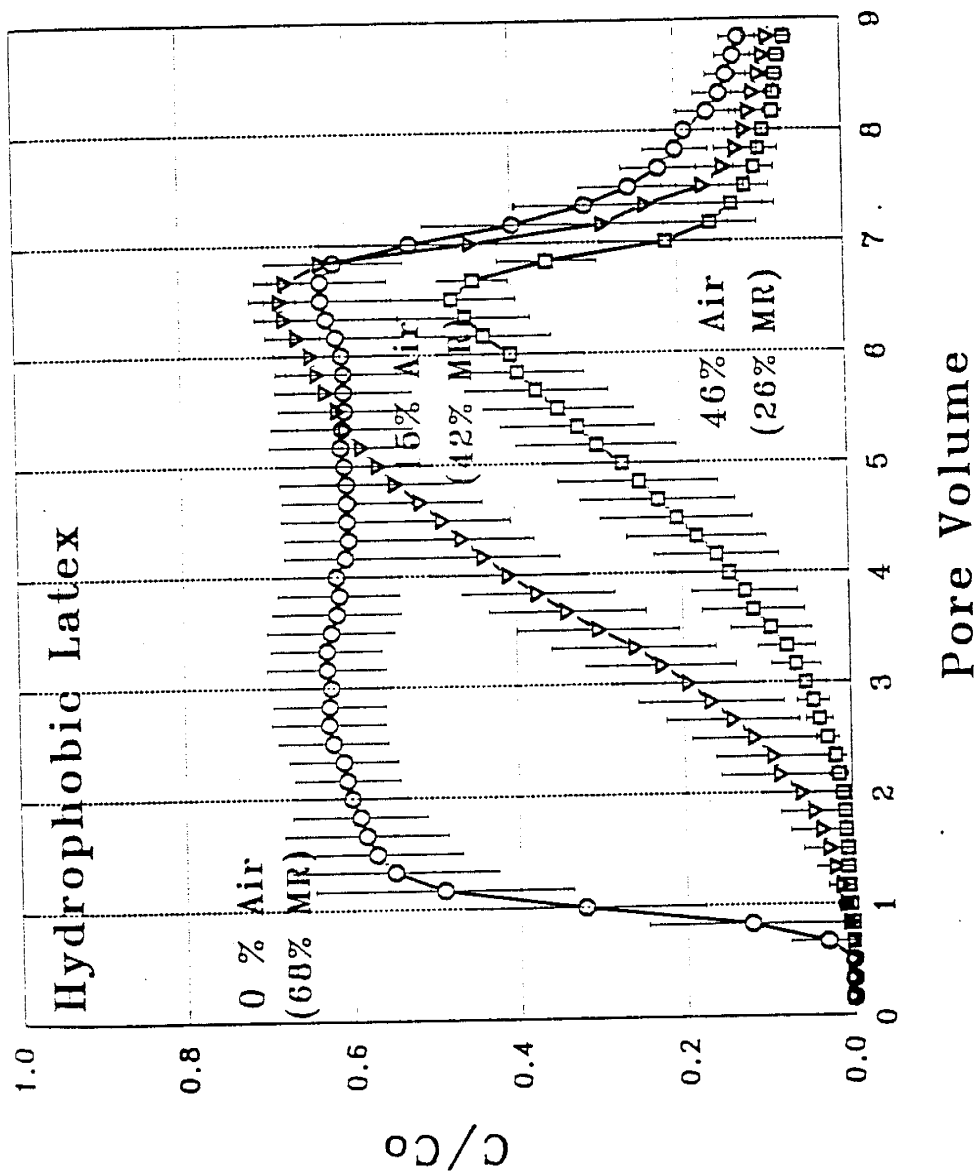


Figure 3.6. Breakthrough curves of hydrophobic latex particles from three types of columns: fully saturated, pseudo-saturated and unsaturated. Each curve shows an average of five repeated experiments and the standard deviations are plotted as error bars. Compare the effect of particle hydrophobicity on retention with Figure 3.5.

## SUMMARY AND CONCLUSIONS

We have obtained quantitative measurements of colloid sorption as a function of gas saturations. Using latex particles with different surface hydrophobicity provides a better understanding of the effect of colloid hydrophobicity on the degree of sorption. These methods may be useful tools for other related research.

The results show that: (a) The retention of colloidal particles by porous media is a function of the gas saturation of the media. Colloid particles preferentially sorbed onto the gas-water interface relative to the rock-water interface under simulated ground water conditions. (b) The gas-water interface sorbs hydrophilic particles in unfavorable filtration conditions under which the quartz-water interface does not sorb the particles. The retention of particles increases with the increasing gas saturation of a porous medium, i.e., with increasing gas-water interface area. (c) There was no preferential flow of colloids attached to the gas-water interface in the presence of continuous gas and water phases. Apparently the particles are trapped by capillary forces at the interface, in stagnation zones when hydrodynamic forces attempt but fail to carry them back into the water phase. (d) The degree of sorption onto both the gas-water and the rock-water interfaces dramatically increased with increasing colloid surface hydrophobicity. Hydrophobic particles have strong affinity to the gas-water interface. (e) The sorption onto the gas-water interface is irreversible due to the capillary force attraction (Wan and Wilson, 1993).

The preferential and irreversible sorption of colloidal particles onto the gas-water

interface suggests a significant vadose zone transport mechanism. A stationary gas phase behaves as a sorbent phase retaining the particles, thereby reducing colloid transport. However, moving interfaces occurring during drainage or imbibition may increase the movement of colloids into the deeper vadose zone and underlying aquifer.

**Acknowledgment.** We would like to express our deep appreciation to Jill Buckley, Norman Morrow, and Robert Bowman, for their helpful discussions and the use of their equipment. We would also like to acknowledge the Subsurface Science Program, Office of Health and Environmental Research, U. S. Department of Energy for supporting this work.

## REFERENCES

- Adamczyk, Z., T. Dabros, J. Czarnecki, and T. G. M. van de Ven, Particle transfer to solid surfaces, *Adv. Colloid Interface Sci.*, 19, 183-252, 1983.
- Bales, R. C., S. R. Hinkle, T. W. Kroeger, and K. Stocking, Bacteriophage adsorption during transport through porous media: chemical perturbations and reversibility, *Environ. Sci. Technol.*, 25, 2088-2095, 1991.
- Bear, J., *Dynamics of Fluids in Porous Media*, Elsevier Publishing Company, Inc., 1972.
- Bowen, B. D. and N. Epstein, Fine particle deposition in smooth parallel-plate channels, *J. Colloid Interface Sci.*, 72, 81-97, 1979.
- Buddemeier, R. W., and J. R. Hunt, Transport of colloidal contaminants in groundwater: radionuclide migration at the Nevada test site, *Appl. Geochem.*, 3, 535-548, 1988.
- Byrd, R. B., W. E. Steward, and E. N. Lightfoot, *Transport Phenomena*, Wiley, New York, 1960.
- Elimelech M., and C. R. O'Melia, Effect of particle size on collision efficiency in the deposition of Brownian particles with electrostatic energy barriers, *Langmuir*, 6, 1153-1163, 1990a.
- Elimelech M., and C. R. O'Melia, Kinetics of deposition of colloidal particles in porous media, *Envir. Sci. Technol.*, 24, 1528-1536, 1990b.
- FitzPatrick, J. A., and L. A. Spielman, Filtration of aqueous latex suspensions through beds of glass spheres, *J. Colloid Interface Sci.*, 43, 350-360, 1973.
- Friedlander, S. K., *Smoke, Dust, and Haze: Fundamentals of Aerosol Behavior*, 317 pp., Wiley-Interscience, New York, 1977.
- Gregory, J. and A. J. Wishart, Deposition of latex particles on alumina fibers, *Colloids Surf.*, 1, 313-334, 1980.
- Gschwend, P. M. and S. C. Wu, On the constancy of sediment-water partition coefficients of hydrophobic organic pollutants, *Environ. Sci. Technol.*, 19, 90-96, 1985.

- Ives, K. J., and J. Gregory, Surface forces in filtration, *Proc. Soc. Water Treat. Exam.*, 15, 93-115, 1966.
- Litton, G. M. and T. M. Olson, Colloid deposition rates on silica bed media and artifacts related to collector surface preparation methods, *Environ. Sci. Technol.*, 27, 185-193, 1993.
- McCarthy, J. F. and J. M. Zachara, Subsurface transport of contaminants, *Envir. Sci. Technol.*, 23, 496-502, 1989.
- McDowell-Boyer, L. M., J. R. Hunt, and N. Sitar, Particle transport through porous media, *Water Resour. Res.*, 22, 1901-1921, 1986.
- O'Melia, C. R., Particle-particle interactions in aquatic systems, *Colloids Surf.*, 39, 255-271, 1989.
- Ottewill, R. H. and J. N. Shaw, Electrophoretic studies of polystyrene lattices, *J. Electroanal. Chem.*, 37, 133-142, 1972.
- Powelson, D. K., J. R. Simpson, and C. P. Gerba, Virus transport and survival in saturated and unsaturated flow through soil columns, *J. Environ. Qual.*, 19, 396-401, 1990.
- Puls, R. W. and R. M. Powell, Transport of inorganic colloids through natural aquifer material: implications for contaminant transport, *Environ. Sci. Technol.*, 26, 614-621, 1992.
- Spielman, L. A., and J. A. FitzPatrick, Theory for particle collection under London and gravity forces, *J. Colloid Interface Sci.*, 42, 607-623, 1973.
- Spielman, L. A., and J. A. FitzPatrick, Role of electrical double-layer in particle deposition by convective diffusion, *J. Colloid Interface Sci.*, 46, 22-31, 1974.
- Spielman, L. A., Particle capture from low-speed laminar flow, *Annu. Rev. Fluid Mech.*, 9, 297-319, 1977.
- Tien, C., and A. C. Payatakes, Advances in deep bed filtration, *AICHE J.*, 25, 737-759, 1979.
- Tien, C., *Granular filtration of aerosols and hydrosols*, Butterworths, Stoneham, Mass, 1989.
- Tobiason J. E., and C. R. O'Melia, Physicochemical aspects of particle removal in depth filtration. *J. Am. Wat. Wks. Assoc.*, 80, 54-64, 1988.



- Wan, J., and J. L. Wilson, Colloid transport and the gas-water interface in porous media, Chap. 5, Colloid and Interfacial Aspects of Groundwater and Soil Cleanup, D. Sabatini and R. Knox (Eds), American Chemical Society, Washington, D. C., 55-70, 1992a.
- Wan, J., and J. L. Wilson, Transport of colloidal particles during gas and aqueous fluid flow in porous media, Chap. 55, Manipulation of Groundwater Colloids for Environmental Restoration, McCarthy and Wobber (Eds), CRC Press, Boca Raton, FL., 335-339, 1992b.
- Wan, J., and J. L. Wilson, New findings on particle transport within the vadose zone: the role of the gas-water interface, in Proceedings of 12th Ann. Hydrology Days, March, Colorado State Univ., Ft. Collins, CO, 402-419, 1992c.
- Wan, J., and J. L. Wilson, Visualization of the role of the gas-water interface on the fate and transport of colloids in porous media, Submitted to Water Resources Research, January, 1993.
- Yao, K. M., M. T. Habibian, and C. R. O'Melia, Water and wastewater filtration: concepts and applications, *Envir. Sci. Technol.*, 5, 1105-1112, 1971.

## APPENDIX 3A

## BREAKTHROUGH DATA OF LATEX PARTICLES

## Abbreviations:

C# = experimental number

C<sub>b</sub> = background concentration from effluent

C<sub>o</sub> = initial particle concentration

C<sub>i</sub> = effluent particle concentration

mr = total particle mass recovery

AVG = the average of repeated experiments

STD = the standard deviation of data from repeated experiments

Table 3.3. Breakthrough Data of Hydrophilic Latex Particles through Water-Saturated Columns

C89		C91		C25-1		C25-2		AVG	STD
Cb=0.009		Cb=0.013		Cb=0.004		Cb=0.005		0.000	0.000
Co=0.163		Co=0.149		Co=0.331		Co=0.342		0.000	0.000
mr=0.971		mr=1.013		mr=0.981		mr=0.995		0.000	0.000
Ci	C/Co	Ci	C/Co	Ci	C/Co	Ci	C/Co		
0.009	0.000	0.013	0.000	0.004	0.000	0.005	0.000	0.000	0.000
0.009	0.000	0.013	0.000	0.004	0.000	0.005	0.000	0.000	0.000
0.009	0.000	0.013	0.000	0.004	0.000	0.005	0.000	0.000	0.000
0.009	0.000	0.013	0.000	0.004	0.000	0.005	0.000	0.000	0.000
0.009	0.000	0.018	0.034	0.025	0.063	0.024	0.056	0.038	0.025
0.083	0.454	0.069	0.376	0.150	0.441	0.145	0.409	0.420	0.030
0.134	0.767	0.140	0.852	0.282	0.840	0.277	0.795	0.814	0.034
0.155	0.896	0.160	0.987	0.322	0.961	0.313	0.901	0.936	0.039
0.168	0.975	0.155	0.953	0.313	0.934	0.318	0.915	0.944	0.022
0.170	0.988	0.153	0.940	0.314	0.937	0.322	0.927	0.948	0.024
0.167	0.969	0.147	0.899	0.311	0.927	0.326	0.939	0.934	0.025
0.090	0.497	0.107	0.631	0.281	0.837	0.198	0.564	0.632	0.127
0.036	0.166	0.073	0.403	0.038	0.103	0.077	0.211	0.220	0.112
0.014	0.031	0.013	0.000	0.015	0.033	0.044	0.114	0.044	0.042
0.015	0.037	0.013	0.000	0.010	0.018	0.023	0.053	0.027	0.020
0.013	0.025	0.013	0.000	0.005	0.003	0.015	0.029	0.014	0.013
0.012	0.018	0.013	0.000	0.004	0.000	0.014	0.026	0.011	0.012
0.010	0.006	0.013	0.000	0.004	0.000	0.015	0.029	0.009	0.012

Table 3.4. Breakthrough Data of Hydrophilic Latex Particles through Columns with 15% Gas

C92			C89-2			C90-2			C107			C109			AVG			STD		
Cb=0.017			Cb=0.007			Cb=0.007			Cb=0.005			Cb=0.004								
Co=0.155			Co=0.155			Co=0.149			Co=0.157			Co=0.158								
mr=0.920			mr=0.882			mr=0.941			mr=0.912			mr=0.895								
Ci			Ci			Ci			Ci			Ci								
0.017	0.000		0.007	0.000		0.007	0.000		0.005	0.000		0.004	0.000							
0.017	0.000		0.007	0.000		0.007	0.000		0.005	0.000		0.004	0.000							
0.017	0.000		0.007	0.000		0.007	0.000		0.005	0.000		0.004	0.000							
0.017	0.000		0.007	0.000		0.008	0.007		0.005	0.000		0.004	0.000							
0.029	0.077		0.008	0.006		0.046	0.262		0.014	0.057		0.013	0.057							
0.085	0.439		0.092	0.548		0.113	0.711		0.062	0.363		0.067	0.399							
0.141	0.800		0.136	0.832		0.145	0.926		0.123	0.752		0.125	0.766							
0.154	0.884		0.140	0.858		0.147	0.940		0.150	0.924		0.142	0.873							
0.154	0.884		0.144	0.884		0.146	0.933		0.153	0.943		0.145	0.892							
0.154	0.884		0.155	0.955		0.145	0.926		0.153	0.943		0.147	0.905							
0.141	0.800		0.141	0.865		0.110	0.691		0.138	0.847		0.132	0.810							
0.087	0.452		0.057	0.323		0.043	0.242		0.081	0.484		0.083	0.500							
0.063	0.297		0.010	0.019		0.008	0.007		0.023	0.115		0.029	0.158							
0.017	0.000		0.007	0.000		0.007	0.000		0.007	0.013		0.005	0.006							
0.017	0.000		0.007	0.000		0.007	0.000		0.007	0.013		0.004	0.000							
0.017	0.000		0.007	0.000		0.007	0.000		0.007	0.013		0.004	0.000							
0.017	0.000		0.007	0.000		0.007	0.000		0.006	0.006		0.004	0.000							
0.017	0.000		0.007	0.000		0.007	0.000		0.005	0.000		0.004	0.000							

Table 3.5. Breakthrough Data of Hydrophilic Latex Particles through Columns with 46% Gas

C89-3		C90-3		C92-2		C113		C114		AVG	STI
Cb=0.009	C/Co	Cb=0.012	C/Co	Cb=0.022	C/Co	Cb=0.006	C/Co	Cb=0.007	C/Co	0.000	0.1
0.009	0.000	0.012	0.000	0.022	0.000	0.006	0.000	0.007	0.000	0.000	0.1
0.009	0.000	0.012	0.000	0.022	0.000	0.006	0.000	0.007	0.000	0.000	0.1
0.009	0.000	0.012	0.000	0.022	0.000	0.008	0.002	0.007	0.000	0.006	0.1
0.010	0.007	0.012	0.000	0.024	0.014	0.008	0.002	0.007	0.000	0.099	0.1
0.023	0.093	0.030	0.121	0.045	0.158	0.026	0.020	0.013	0.006	0.415	0.1
0.084	0.500	0.065	0.356	0.093	0.486	0.059	0.053	0.106	0.099	0.635	0.1
0.121	0.747	0.110	0.658	0.130	0.740	0.110	0.104	0.117	0.110	0.749	0.1
0.132	0.820	0.136	0.832	0.140	0.808	0.129	0.123	0.151	0.144	0.770	0.1
0.135	0.840	0.132	0.805	0.141	0.815	0.137	0.131	0.164	0.157	0.788	0.1
0.136	0.847	0.133	0.812	0.140	0.808	0.146	0.140	0.173	0.166	0.720	0.1
0.117	0.720	0.118	0.711	0.117	0.651	0.151	0.145	0.177	0.170	0.409	0.1
0.054	0.300	0.042	0.201	0.069	0.322	0.122	0.116	0.145	0.138	0.167	0.1
0.023	0.093	0.017	0.034	0.033	0.075	0.069	0.063	0.075	0.068	0.066	0.1
0.016	0.047	0.014	0.013	0.026	0.027	0.035	0.029	0.028	0.021	0.032	0.1
0.013	0.027	0.013	0.007	0.025	0.021	0.023	0.017	0.012	0.005	0.023	0.1
0.010	0.007	0.013	0.007	0.024	0.014	0.018	0.012	0.013	0.006	0.013	0.1
0.010	0.007	0.012	0.000	0.022	0.000	0.014	0.008	0.011	0.004	0.013	0.1
0.009	0.000	0.012	0.000	0.022	0.000	0.012	0.006	0.010	0.003	0.009	0.1



0.184	0.672	0.111	0.643	0.137	0.684	0.130	0.500	0.138	0.510	0.602	0.
0.186	0.679	0.113	0.655	0.136	0.679	0.130	0.500	0.139	0.514	0.605	0.
0.188	0.687	0.117	0.679	0.134	0.668	0.128	0.492	0.141	0.522	0.609	0.
0.189	0.691	0.115	0.667	0.134	0.668	0.128	0.492	0.139	0.514	0.606	0.
0.187	0.683	0.112	0.649	0.134	0.668	0.130	0.500	0.139	0.514	0.603	0.
0.188	0.687	0.112	0.649	0.135	0.674	0.130	0.500	0.138	0.510	0.604	0.
0.189	0.691	0.110	0.637	0.136	0.679	0.131	0.504	0.138	0.510	0.604	0.
0.190	0.694	0.110	0.637	0.136	0.679	0.130	0.500	0.140	0.518	0.606	0.
0.193	0.706	0.112	0.649	0.137	0.684	0.130	0.500	0.142	0.525	0.613	0.
0.194	0.709	0.115	0.667	0.140	0.701	0.133	0.512	0.144	0.533	0.624	0.
0.196	0.717	0.115	0.667	0.142	0.711	0.134	0.516	0.146	0.541	0.630	0.
0.200	0.732	0.116	0.673	0.134	0.668	0.135	0.520	0.150	0.557	0.630	0.
0.199	0.728	0.112	0.649	0.132	0.658	0.132	0.508	0.143	0.529	0.614	0.
0.197	0.721	0.089	0.512	0.106	0.519	0.120	0.460	0.111	0.404	0.523	0.
0.166	0.604	0.067	0.381	0.069	0.321	0.103	0.391	0.083	0.294	0.398	0.
0.124	0.445	0.057	0.321	0.047	0.203	0.090	0.339	0.071	0.247	0.311	0.
0.091	0.321	0.051	0.286	0.040	0.166	0.082	0.306	0.062	0.212	0.258	0.
0.064	0.219	0.049	0.274	0.038	0.155	0.073	0.270	0.056	0.188	0.221	0.
0.059	0.200	0.045	0.250	0.035	0.139	0.064	0.234	0.053	0.176	0.200	0.
0.056	0.189	0.043	0.238	0.034	0.134	0.060	0.218	0.050	0.165	0.189	0.
0.040	0.128	0.038	0.208	0.032	0.123	0.056	0.202	0.045	0.145	0.161	0.
0.036	0.113	0.036	0.196	0.031	0.118	0.047	0.165	0.043	0.137	0.146	0.
0.035	0.109	0.032	0.173	0.030	0.112	0.045	0.157	0.042	0.133	0.137	0.
0.034	0.106	0.031	0.167	0.029	0.107	0.040	0.137	0.040	0.125	0.128	0.
0.033	0.102	0.030	0.161	0.028	0.102	0.038	0.129	0.038	0.118	0.122	0.
0.028	0.083	0.028	0.149	0.027	0.096	0.032	0.105	0.036	0.110	0.109	0.

Table 3.7. Breakthrough Data of Hydrophobic Latex Particles through Columns with 15% Gas

C17-1	C17-2	C67	C94	C96	AVG	STI
Cb=0.010	Cb=0.010	Cb=0.009	Cb=0.009	Cb=0.009	0.000	0.0
Co=0.423	Co=0.404	Co=0.403	Co=0.254	Co=0.253	0.000	0.0
mr=0.452	mr=0.398	mr=0.470	mr=0.421	mr=0.503	0.000	0.0
Ci	Ci	Ci	Ci	Ci	C/Co	
0.010	0.010	0.009	0.009	0.009	0.000	0.0
0.010	0.010	0.009	0.009	0.009	0.000	0.0
0.010	0.010	0.009	0.009	0.009	0.000	0.0
0.010	0.010	0.009	0.009	0.014	0.020	0.0
0.011	0.010	0.009	0.010	0.016	0.028	0.0
0.013	0.011	0.009	0.009	0.020	0.043	0.0
0.014	0.009	0.011	0.010	0.025	0.063	0.0
0.016	0.013	0.011	0.010	0.031	0.087	0.0
0.019	0.016	0.012	0.009	0.036	0.107	0.0
0.022	0.019	0.012	0.010	0.040	0.123	0.0
0.026	0.022	0.014	0.012	0.048	0.154	0.0
0.029	0.027	0.022	0.013	0.066	0.225	0.0
0.034	0.027	0.032	0.015	0.067	0.229	0.0
0.040	0.034	0.030	0.018	0.076	0.265	0.0
0.046	0.040	0.040	0.022	0.085	0.300	0.0
0.051	0.049	0.052	0.028	0.095	0.340	0.0
0.057	0.060	0.067	0.032	0.103	0.372	0.0
0.057	0.070	0.083	0.038	0.110	0.399	0.0
0.065	0.080	0.101	0.048	0.120	0.439	0.0
0.073	0.092	0.121	0.051	0.130	0.478	0.0
0.083	0.107	0.138	0.069	0.137	0.506	0.0
0.093	0.122	0.154	0.083	0.144	0.534	0.0
0.106	0.135	0.170	0.095	0.153	0.569	0.0
0.119	0.147	0.186	0.107	0.160	0.597	0.0
0.131	0.158	0.200	0.113	0.163	0.609	0.0
0.144	0.171	0.213	0.118	0.166	0.621	0.0
0.157	0.186	0.221	0.123	0.170	0.636	0.0
0.169	0.199	0.226	0.134			
0.181	0.211					
	C/Co	C/Co	C/Co	C/Co		
	0.000	0.000	0.000	0.000		
	0.000	0.000	0.000	0.000		
	0.000	0.000	0.000	0.000		
	0.000	0.000	0.000	0.000		
	0.002	0.000	0.000	0.004		
	0.007	0.000	0.004	0.000		
	0.009	0.002	0.000	0.000		
	0.014	0.007	0.004	0.004		
	0.021	0.015	0.007	0.000		
	0.028	0.022	0.007	0.004		
	0.038	0.030	0.012	0.012		
	0.045	0.042	0.032	0.016		
	0.057	0.059	0.057	0.024		
	0.071	0.074	0.052	0.035		
	0.085	0.097	0.077	0.051		
	0.097	0.124	0.107	0.075		
	0.111	0.149	0.144	0.091		
	0.130	0.173	0.184	0.114		
	0.149	0.203	0.228	0.154		
	0.173	0.240	0.278	0.165		
	0.196	0.277	0.320	0.236		
	0.227	0.309	0.360	0.291		
	0.258	0.339	0.400	0.339		
	0.286	0.366	0.439	0.386		
	0.317	0.399	0.474	0.409		
	0.348	0.436	0.506	0.429		
	0.376	0.468	0.526	0.449		
	0.404	0.498	0.538	0.492		



0.193	0.433	0.222	0.525	0.230	0.548	0.151	0.559	0.175	0.656	0.544	0.0
0.204	0.459	0.231	0.547	0.235	0.561	0.160	0.594	0.176	0.660	0.564	0.0
0.215	0.485	0.240	0.569	0.240	0.573	0.167	0.622	0.179	0.672	0.584	0.0
0.227	0.513	0.249	0.592	0.242	0.578	0.172	0.642	0.182	0.684	0.602	0.0
0.237	0.537	0.254	0.604	0.246	0.588	0.175	0.654	0.181	0.680	0.612	0.0
0.253	0.574	0.261	0.621	0.251	0.600	0.177	0.661	0.179	0.672	0.626	0.0
0.257	0.584	0.267	0.636	0.254	0.608	0.180	0.673	0.181	0.680	0.636	0.0
0.261	0.593	0.271	0.646	0.255	0.610	0.182	0.681	0.182	0.684	0.643	0.0
0.277	0.631	0.278	0.663	0.260	0.623	0.184	0.689	0.183	0.688	0.659	0.0
0.286	0.652	0.285	0.681	0.267	0.640	0.187	0.701	0.185	0.696	0.674	0.0
0.292	0.667	0.291	0.696	0.270	0.648	0.185	0.693	0.184	0.692	0.679	0.0
0.299	0.683	0.295	0.705	0.274	0.658	0.174	0.650	0.178	0.668	0.673	0.0
0.288	0.657	0.267	0.636	0.275	0.660	0.172	0.642	0.150	0.557	0.630	0.0
0.236	0.534	0.157	0.364	0.167	0.392	0.166	0.618	0.095	0.340	0.450	0.1
0.152	0.336	0.078	0.168	0.080	0.176	0.154	0.571	0.059	0.198	0.290	0.1
0.103	0.220	0.065	0.136	0.060	0.127	0.148	0.547	0.049	0.158	0.238	0.1
0.098	0.208	0.065	0.136	0.053	0.109	0.071	0.244	0.044	0.138	0.167	0.0
0.089	0.187	0.063	0.131	0.048	0.097	0.052	0.169	0.041	0.126	0.142	0.0
0.080	0.165	0.062	0.129	0.044	0.087	0.043	0.134	0.038	0.115	0.126	0.0
0.074	0.151	0.059	0.121	0.041	0.079	0.040	0.122	0.036	0.107	0.116	0.0
0.072	0.147	0.056	0.114	0.039	0.074	0.037	0.110	0.035	0.103	0.110	0.0
0.071	0.144	0.057	0.116	0.037	0.069	0.035	0.102	0.032	0.091	0.105	0.0
0.069	0.139	0.057	0.116	0.034	0.062	0.031	0.087	0.030	0.083	0.097	0.0
0.068	0.137	0.056	0.114	0.032	0.057	0.029	0.079	0.027	0.071	0.092	0.0
0.066	0.132	0.056	0.114	0.031	0.055	0.025	0.063	0.026	0.067	0.086	0.0
0.064	0.128	0.056	0.114	0.030	0.052	0.022	0.051	0.024	0.059	0.081	0.0

Table 3.8. Breakthrough Data of Hydrophobic Latex Particles through Columns with 46% Gas

C18-1		C18-2		C68		C97		AVG	ATD
Ci	C/Co	Ci	C/Co	Ci	C/Co	Ci	C/Co		
0.010	0.000	0.022	0.000	0.006	0.000	0.014	0.000	0.000	0.000
0.010	0.000	0.022	0.000	0.006	0.000	0.014	0.000	0.000	0.000
0.010	0.000	0.022	0.000	0.006	0.000	0.014	0.000	0.000	0.000
0.010	0.000	0.022	0.000	0.006	0.000	0.014	0.000	0.000	0.000
0.010	0.000	0.022	0.000	0.006	0.000	0.014	0.000	0.000	0.000
0.012	0.005	0.023	0.002	0.006	0.000	0.014	0.000	0.002	0.002
0.013	0.007	0.025	0.007	0.006	0.000	0.014	0.000	0.004	0.004
0.014	0.009	0.026	0.010	0.006	0.000	0.014	0.000	0.005	0.005
0.014	0.009	0.027	0.012	0.006	0.000	0.014	0.000	0.005	0.006
0.015	0.012	0.029	0.017	0.006	0.000	0.014	0.000	0.007	0.008
0.017	0.016	0.029	0.017	0.006	0.000	0.014	0.000	0.008	0.008
0.019	0.021	0.029	0.017	0.006	0.000	0.014	0.000	0.010	0.010
0.022	0.028	0.030	0.020	0.007	0.003	0.015	0.004	0.014	0.011
0.025	0.035	0.033	0.027	0.008	0.005	0.015	0.004	0.018	0.013
0.028	0.042	0.037	0.037	0.008	0.005	0.019	0.022	0.027	0.014
0.030	0.046	0.040	0.045	0.009	0.008	0.024	0.045	0.036	0.016
0.035	0.058	0.042	0.050	0.010	0.010	0.026	0.054	0.043	0.019
0.040	0.069	0.045	0.057	0.010	0.010	0.030	0.072	0.052	0.025
0.045	0.081	0.049	0.067	0.011	0.013	0.034	0.090	0.063	0.030
0.053	0.099	0.054	0.079	0.012	0.015	0.037	0.103	0.074	0.035
0.059	0.113	0.060	0.094	0.012	0.015	0.047	0.148	0.093	0.049
0.066	0.129	0.068	0.114	0.014	0.020	0.057	0.193	0.114	0.062
0.073	0.145	0.075	0.131	0.014	0.020	0.058	0.197	0.124	0.064
0.081	0.164	0.093	0.176	0.016	0.025	0.060	0.206	0.143	0.070
0.091	0.187	0.095	0.181	0.018	0.031	0.066	0.233	0.158	0.076
0.101	0.210	0.104	0.203	0.023	0.043	0.075	0.274	0.182	0.085
0.111	0.233	0.115	0.230	0.028	0.056	0.082	0.305	0.206	0.092
0.122	0.259	0.126	0.257	0.035	0.074	0.086	0.323	0.228	0.093

0.132	0.282	0.138	0.287	0.042	0.092	0.091	0.345	0.251	0.096
0.142	0.305	0.149	0.314	0.050	0.112	0.093	0.354	0.271	0.094
0.153	0.330	0.161	0.344	0.061	0.140	0.101	0.390	0.301	0.096
0.165	0.358	0.173	0.374	0.071	0.165	0.102	0.395	0.323	0.092
0.176	0.383	0.183	0.399	0.081	0.191	0.106	0.413	0.346	0.090
0.186	0.406	0.198	0.436	0.094	0.224	0.108	0.422	0.372	0.086
0.191	0.418	0.211	0.468	0.108	0.260	0.110	0.430	0.394	0.080
0.195	0.427	0.221	0.493	0.106	0.254	0.111	0.435	0.402	0.089
0.213	0.469	0.235	0.527	0.125	0.303	0.112	0.439	0.435	0.082
0.223	0.492	0.245	0.552	0.138	0.336	0.114	0.448	0.457	0.079
0.230	0.508	0.253	0.572	0.147	0.359	0.115	0.453	0.473	0.078
0.203	0.446	0.224	0.500	0.156	0.382	0.117	0.462	0.447	0.043
0.136	0.291	0.146	0.307	0.161	0.394	0.111	0.435	0.357	0.060
0.087	0.178	0.088	0.163	0.071	0.165	0.092	0.350	0.214	0.079
0.072	0.143	0.073	0.126	0.050	0.112	0.071	0.256	0.159	0.057
0.065	0.127	0.067	0.111	0.044	0.097	0.058	0.197	0.133	0.039
0.061	0.118	0.062	0.099	0.040	0.087	0.051	0.166	0.117	0.030
0.056	0.106	0.059	0.092	0.037	0.079	0.046	0.143	0.105	0.024
0.052	0.097	0.057	0.087	0.035	0.074	0.045	0.139	0.099	0.024
0.050	0.092	0.056	0.084	0.033	0.069	0.042	0.126	0.093	0.021
0.048	0.088	0.055	0.082	0.030	0.061	0.035	0.094	0.081	0.012
0.046	0.083	0.055	0.082	0.030	0.061	0.034	0.090	0.079	0.011
0.045	0.081	0.054	0.079	0.029	0.059	0.034	0.090	0.077	0.011
0.045	0.081	0.052	0.074	0.028	0.056	0.033	0.085	0.074	0.011
0.043	0.076	0.050	0.069	0.026	0.051	0.029	0.067	0.066	0.009
0.041	0.072	0.050	0.069	0.024	0.046	0.027	0.058	0.061	0.010

APPENDIX 3B

BREAKTHROUGH CURVES OF LATEX PARTICLES

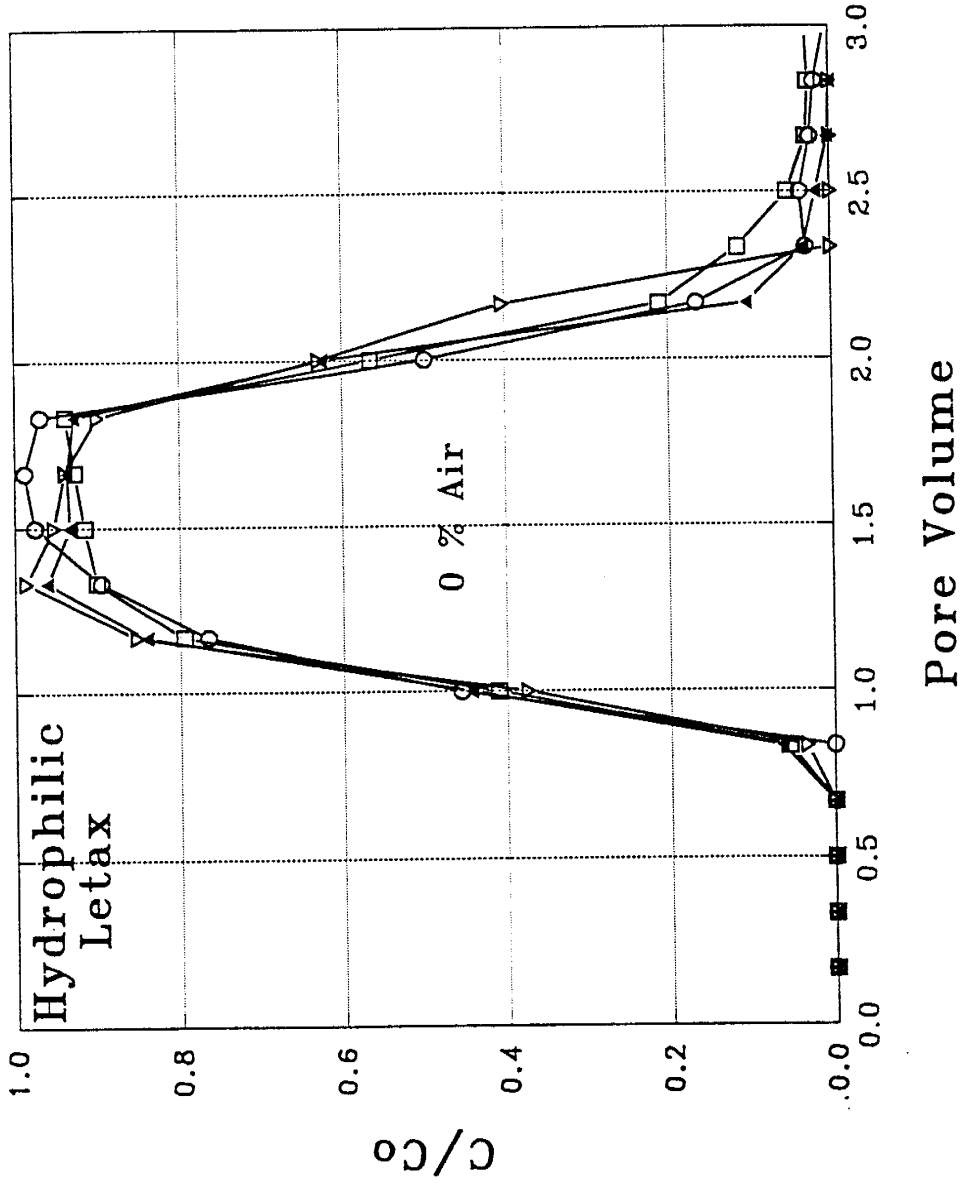


Figure 3.7. Breakthrough curves of hydrophilic latex particles from water-saturated columns.

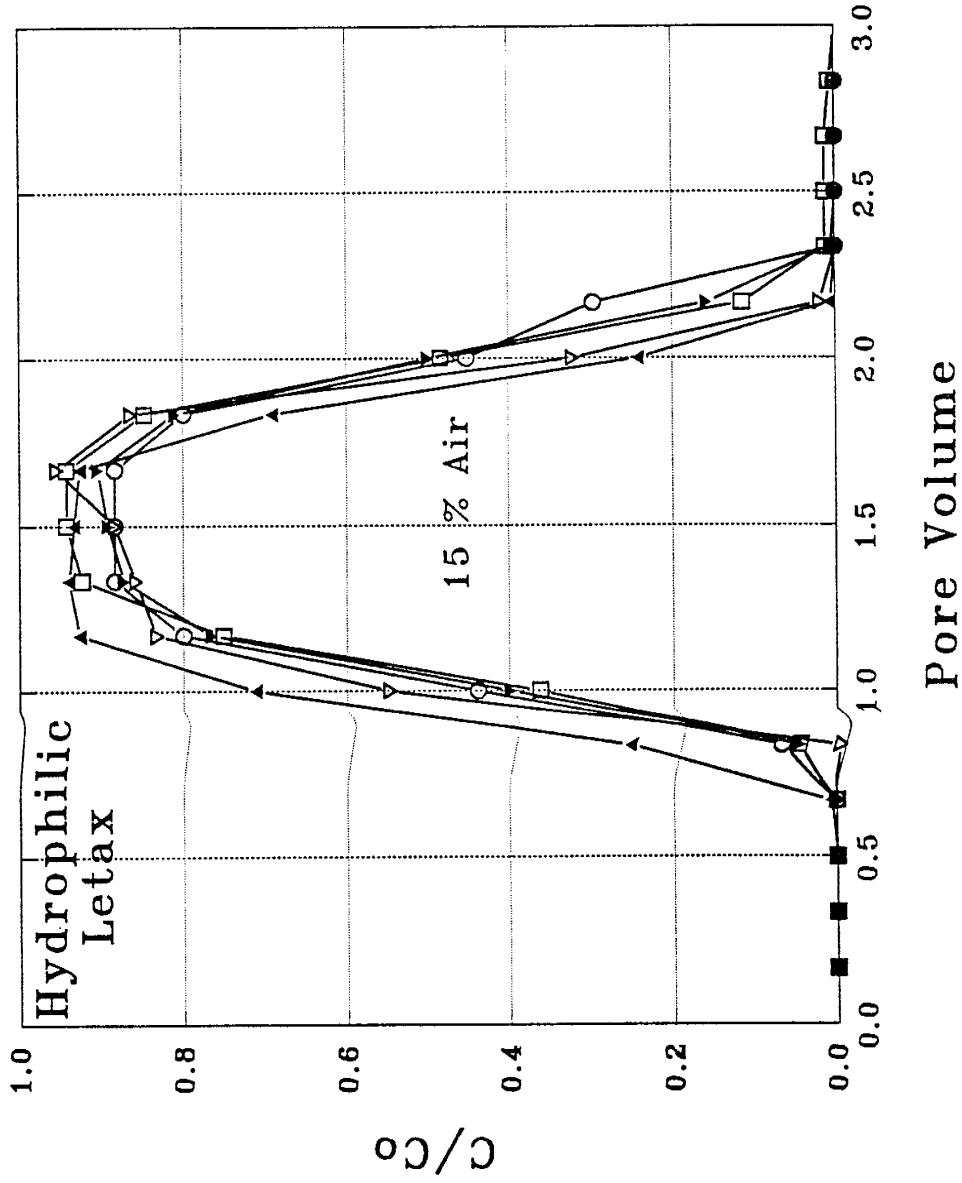


Figure 3.8. Breakthrough curves of hydrophilic latex particles from columns with 15% gas.

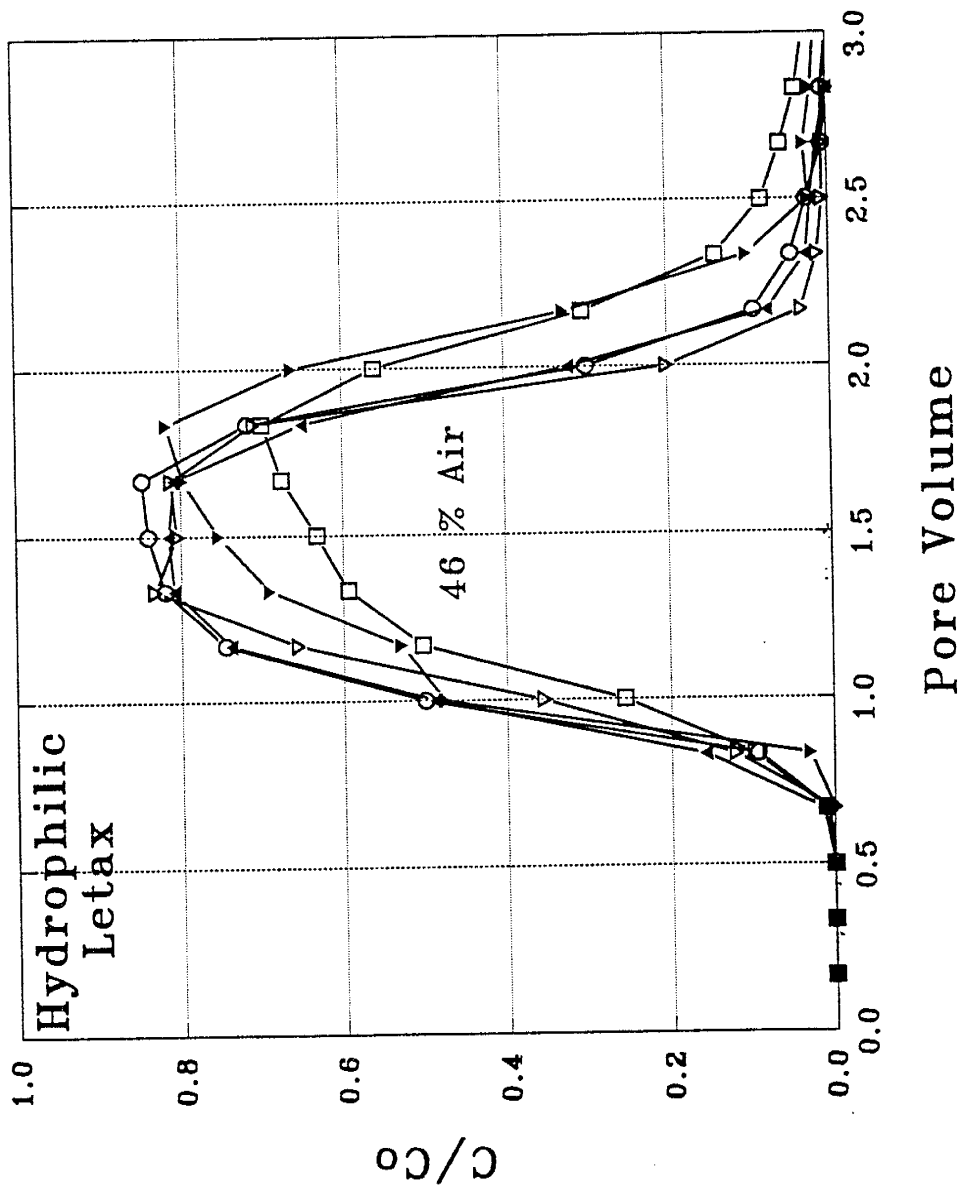


Figure 3.9. Breakthrough curves of hydrophilic latex particles from columns with 46% gas.

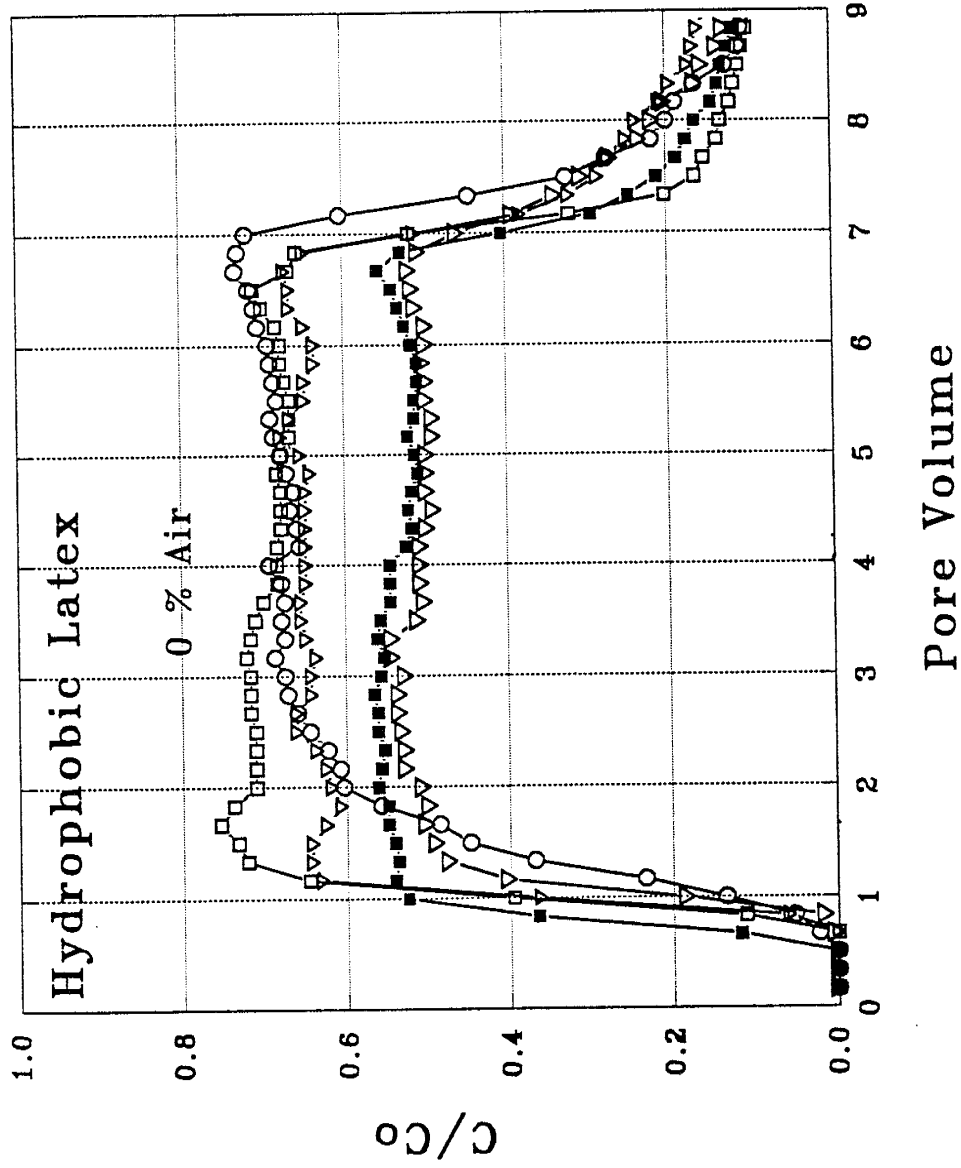


Figure 3.10. Breakthrough curves of hydrophobic latex particles from water-saturated columns.



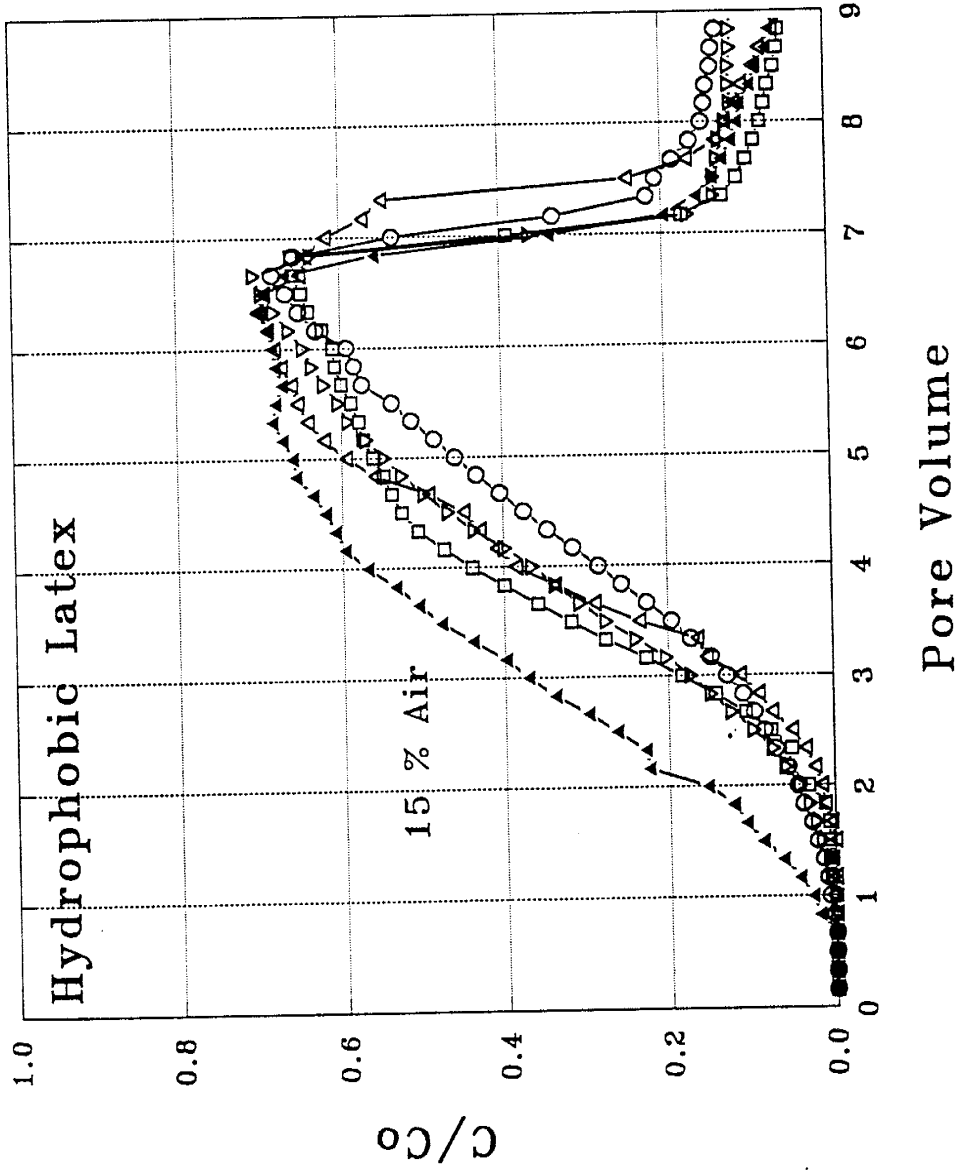


Figure 3.11. Breakthrough curves of hydrophobic latex particles from columns with 15% gas.

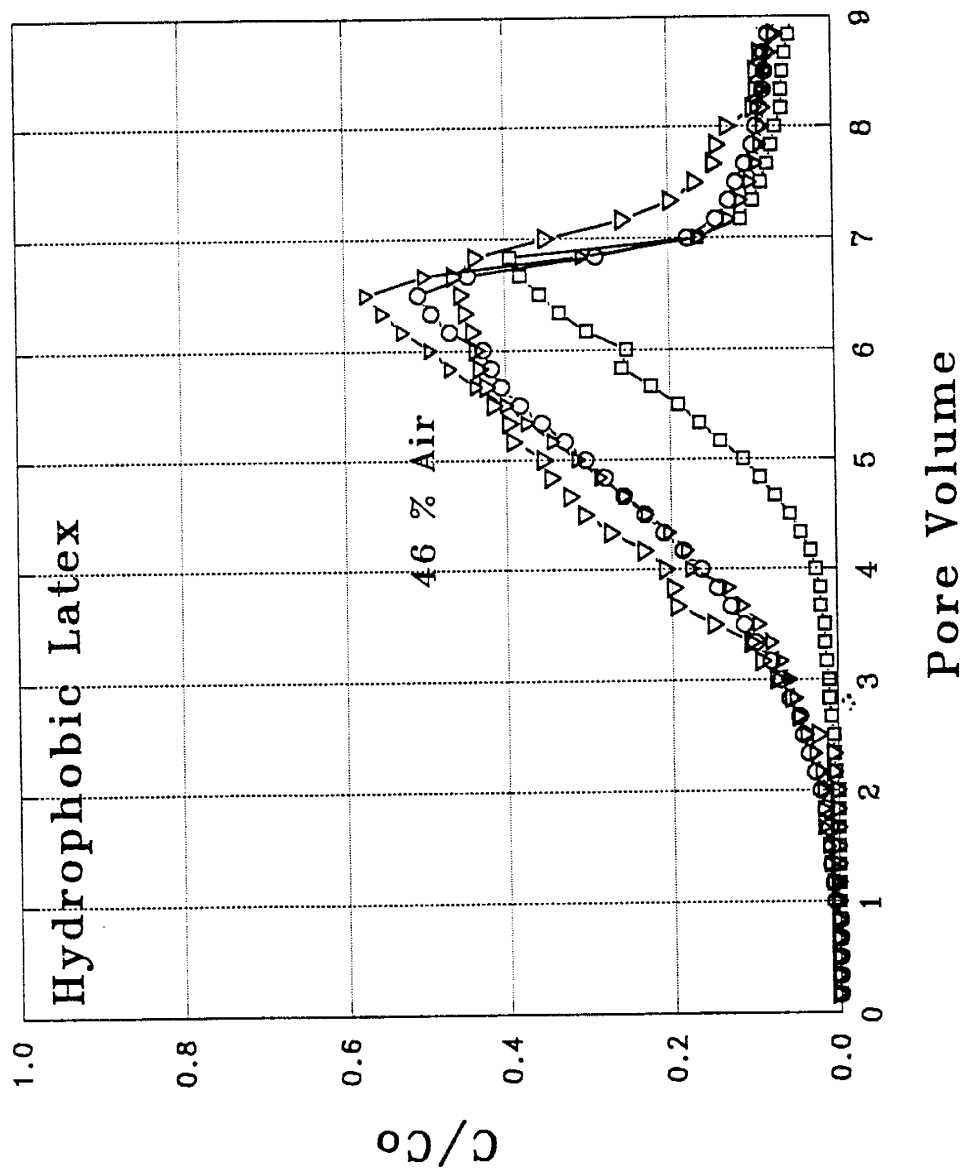


Figure 3.12. Breakthrough curves of hydrophobic latex particles from columns with 46% gas.

APPENDIX 3C

PARAMETERS OF COLUMNS IN LATEX

PARTICLE EXPERIMENTS

Table 3.9. Parameters of Columns in Experiments with Hydrophilic Latex Particles

Column	Gas%	n	$\rho_b$	pH	$\Delta$ Weight	$\Sigma$ Mass
C89	0.0	0.47	1.97	$6.50 \pm 0.05$	NA	0.971
C91	0.0	0.43	1.97	$6.43 \pm 0.18$	-0.08%	1.013
C25-1	0.0	0.45	1.94	$6.66 \pm 0.05$	NA	0.981
C25-2	0.0	0.45	1.94	$6.64 \pm 0.02$	NA	0.995
avg	0.0					0.990
C92	15.5	0.42	1.96	$6.64 \pm 0.04$	-0.08%	0.920
C89-2	14.0	0.47	1.97	$6.79 \pm 0.08$	+0.09%	0.882
C90-2	13.5	0.47	1.95	$6.51 \pm 0.06$	+0.09%	0.941
C107	15.4	0.43	1.94	$6.69 \pm 0.03$	-0.03%	0.912
C109	15.3	0.43	1.93	$6.81 \pm 0.01$	-0.00%	0.895
avg	$14.7 \pm 0.8$					0.910
C89-3	47.8	0.47	1.97	$6.67 \pm 0.10$	+0.02%	0.842
C90-3	46.8	0.47	1.95	$6.61 \pm 0.06$	+0.03%	0.760
C92-2	49.1	0.42	1.96	$6.86 \pm 0.05$	+0.10%	0.823
C113	42.9	0.43	1.94	$6.66 \pm 0.06$	+0.00%	0.784
C114	44.3	0.42	1.95	$6.81 \pm 0.10$	-0.00%	0.881
avg	$46.2 \pm 2.3$					0.818
AVG		$0.44 \pm 0.022$	$1.95 \pm 0.012$	$6.66 \pm 0.12$	$0.013 \pm 0.06\%$	

Table 3.10. Parameters of Columns in Experiments with Hydrophobic Latex Particles

Column	Gas%	n	$\rho_b$	pH	$\Delta$ Weight	$\Sigma$ Mass
C95	0.0	0.42	1.96	$6.59 \pm 0.06$	-0.07%	0.721
C101	0.0	0.42	1.96	$6.77 \pm 0.03$	-0.15%	0.733
C102	0.0	0.42	1.95	$6.67 \pm 0.07$	-0.16%	0.754
C105	0.0	0.41	1.95	$6.77 \pm 0.07$	-0.04%	0.585
C106	0.0	0.41	1.95	$6.82 \pm 0.02$	-0.06%	0.619
avg	0.0					0.682
C17-1	15.2	0.41	1.98	NA	NA	0.452
C17-2	15.6	0.41	1.98	NA	NA	0.398
C67	15.4	0.43	1.95	$6.57 \pm 0.05$	NA	0.470
C94	16.0	0.42	1.96	NA	-0.04%	0.421
C96	14.7	0.42	1.96	$6.59 \pm 0.03$	-0.16%	0.503
avg	$15.4 \pm 0.43$	0.47	1.97	$6.67 \pm 0.10$		0.449
C18-1	46.8	0.47	1.95	$6.61 \pm 0.06$	NA	0.281
C18-2	49.1	0.42	1.96	$6.86 \pm 0.05$	NA	0.288
C68	42.9	0.43	1.94	$6.66 \pm 0.06$	-0.10%	0.153
C97	44.3	0.42	1.95	$6.81 \pm 0.10$	NA	0.265
avg	$45.8 \pm 2.4$					0.247
AVG		$0.43 \pm 0.019$	$1.96 \pm 0.011$	$6.70 \pm 0.10$	$-0.097 \pm 0.049\%$	

---

**CHAPTER 4**

---

**THE GAS-WATER INTERFACE AS AN INFLUENCE ON  
TRANSPORT OF MICROORGANISMS THROUGH  
UNSATURATED POROUS MEDIA**

(Submitted to Applied and Environmental Microbiology, April 5, 1993)

**ABSTRACT**

In this paper a new mechanism influencing the transport of microorganisms through unsaturated-porous media is examined, and a new method for directly visualizing bacterial behavior within a porous medium under controlled chemical and flow conditions is introduced. Resting-cells of hydrophilic and relatively hydrophobic bacterial strains isolated from groundwater were used as model microorganisms. The degree of hydrophobicity was determined by contact angle measurements. Glass micromodels allowed the direct observation of bacterial behavior on a pore scale, and three types of sand columns with different gas saturations provided quantitative measurements of the observed phenomena on a porous medium scale. The reproducibility of each breakthrough curve was established in 5 repeated experiments. The data collected from the column experiments can be explained by phenomena directly observed in the micromodel experiments. The retention rate of bacteria is proportional to the gas saturation in porous media, due to the preferential sorption of bacteria onto the gas-water

interface over the solid-water interface. The degree of sorption is mainly controlled by cell surface hydrophobicity under the simulated groundwater conditions, due to hydrophobic forces between the organisms and the interfaces. The sorption onto the gas-water interface is essentially irreversible due to capillary forces. This preferential and irreversible sorption at the gas-water interface strongly influences the movement and spatial distribution of microorganisms.

## INTRODUCTION

Research on the fate and transport of microorganisms in the subsurface environment has been stimulated by interest in in-situ biodegradation of contaminated soils and groundwater (Lee, et al., 1988; Thomas and Ward, 1989), colloid facilitated transport of radionuclides (Camp, 1986), and the enhancement of crude-oil recovery (Chase, et al., 1990), etc. A traditional and important concern is also the disposal of sewage by infiltration through soil to remove pathogenic microorganisms. In studies of microorganisms as pollutants, researchers (Gerba and Goyal, 1981; Gerba, 1985) have pointed out that microorganisms travel from a contamination source through unsaturated soil to groundwater. In studies of microorganisms as bioremediation agents (Claus and Walder, 1964; Wilson, et al., 1990) introduced microbes are required to be transported to and throughout the contaminated site, perhaps including transport through the unsaturated zone. All of these cases demand the ability to accurately predict the rate and extent of microbial transport through porous media. Predictive mathematical models need

to build on a better understanding of the behavior of microorganisms in soils and groundwater.

Transport of microorganisms is governed by sorption to immobile substrates, and also by inactivation (Bales, 1991; Yates, et al., 1987). Many factors contributing to sorption have been studied: the nature of the porous medium including soil type, grain size, heterogeneity, and clay and organic matter content (Bales, et al., 1989; Baven and Germann, 1982; Fontes, et al., 1991; Powelson, et al., 1991); water chemistry including pH and ionic strength (Bales, et al., 1991; Martln, et al., 1992); cell types including size and surface hydrophobicity (Duncan-Hewitt, 1990; Fontes, et al., 1991; Grotenhuis, et al., 1992; van Loosdrecht, et al., 1987); infiltration rate (Vaughn, et al., 1981); and clogging efficiency (Vandevivere and Baveye, 1992). Most transport studies have focused on saturated porous media, but a few have focused on unsaturated conditions. Lance and Gerba (1984) found that unsaturated flow resulted in a lower degree of virus mass recovery through loamy sand. Powelson, et al. (1990) reported that viruses were more strongly removed from the soil water under unsaturated than saturated conditions, and they suggested that the unrecovered viruses were inactivated. Yates, et al. (1985) found temperature to be the only measured water characteristic significantly correlated with viral inactivation. The approaches currently used for modeling bacterial transport all involve using an advection-dispersion equation modified to include growth, death, and a number of other processes (Corapcioglu and Haridas, 1984 & 1985; Martln et al., 1992; Peterson and Ward, 1989). The models are difficult to test empirically due to the large number of parameters describing geological and bacterial variability, the exact



determination of which is impractical (Fontes et al., 1991).

In unsaturated subsurface environments, gas is one of three major phases: solid, water, and gas. There are basically two interfaces: the gas-water and solid-water. The interactions of microorganisms with the solid-water interface have been studied for decades, but the gas-water interface has been ignored. The objectives of this project were to reveal the roles of the gas-water interface on microbial transport, and to examine the causes of increased retention of microorganisms in unsaturated porous media.

The approach taken in this research combines visualization with quantification. Two major variables were examined: cell surface hydrophobicity, and gas saturation of media. Two strains of bacteria with different surface hydrophobicities were used to examine the effect of cell surface hydrophobicity on sorption. Three types of columns with strictly controlled gas saturations were used to test the effect of the gas-water interface on microbial retention. Cell suspensions were injected at one end of the column and cell breakthrough was measured at the other end. Fully water-saturated columns served as controls; unsaturated columns with a continuous gas phase (~46% gas saturation) represented the vadose zone condition. Columns with capillary trapped residual gas bubbles (~15% gas saturation) were used to illustrate the differences between fully-saturated and pseudo-saturated conditions. We found from the literature that some of the laboratory soil columns and field sites which were referred to as water-saturated might actually contain capillary trapped gas as a residual non-wetting fluid phase; the large discrepancy in some of the previously published results may be caused by the presence of residual gas bubbles.

The phenomena responsible for the data collected in the columns were observed in micromodels, a new method for directly visualizing bacterial behavior within a porous medium. Glass micromodels are transparent and have a network of etched flow channels which enable observation of fluid flow and related transport processes by microscopy (Buckley, 1991; Chatzis, et al., 1983; Conrad, et al., 1992; Wan and Wilson, 1993a; Wilson, et al., 1990). Water-saturated micromodels served as controls, while micromodels with capillary trapped residual gas bubbles permitted direct observation of the interaction of bacteria with the gas-water interface.

In addition to the gas-water system, we present an example of a NAPL-water (non-aqueous phase liquid) system to demonstrate more potential applications of the micromodel technique. The oil-water interface has been studied since 1924 (Lee, et al., 1988; Morrow, et al., 1988; Mudd and Mudd, 1924a), but our method allows studies under dynamic fluid conditions. We tested the behavior of a strain with intermediate hydrophobicity on the NAPL-water interface by culturing the cells in the micromodel, and then displacing the cell suspension by a cell-free solution.

## MATERIALS AND METHODS

**Glass Micromodels.** A pore network is composed of pore bodies connected by pore throats. In a micromodel these pores have a complex three-dimensional structure although the network is only two-dimensional. Conventional micromodels have pore sizes ranging from 0.1 to a few millimeters. The smaller pores are more difficult to fabricate.

Previous techniques were modified in this research. We reduced pore size to a few micrometers. Four micromodels with the same pore network pattern were generated in one glass plate with the improved technique (Figure 1). Including four models on one plate allows us to repeat an experiment by simply shifting to the adjacent identical network. Figure 2 shows three pore network patterns: Figure 2(a) is a saturated hexagonal pore network with pore sizes of 20-250  $\mu\text{m}$ ; Figure 2(b) is an unsaturated quadrilateral pore network showing air trapped as residual air bubbles (the pore sizes are 40-200  $\mu\text{m}$ ). These two network patterns contain 1250 pore bodies, respectively. A wider pore size distribution with random pore network connections is closer to that of the natural porous media. Figure 2(c) is an unsaturated heterogeneous network showing continuous gas and water phases (pore sizes vary from 20 to 400  $\mu\text{m}$ ). These micromodels contain only 0.1 ml pore volume. The glass encloses each of the pores at the top and bottom, as well as along the sides as shown in the photographs. This third dimension is best visualized in Figure 2c, along the tops of the air filled pore channels (Wan and Wilson 1993a).

**Solutions and Cell Suspensions.** To simulate typical groundwater conditions (low ionic strength and about neutral pH), ionic strength was 1.0 mM and pH was 6.6 for all of the cell-free solutions and cell suspensions in all of the experiments. These conditions are unfavorable for cell attachment at the solid-water interface. The ionic strength of the solutions was adjusted using  $\text{NaNO}_3$ , and pH was buffered by  $\text{NaHCO}_3$ . All chemicals used were analytical grade. Solutions were filtered through a 0.22  $\mu\text{m}$  pore size filter

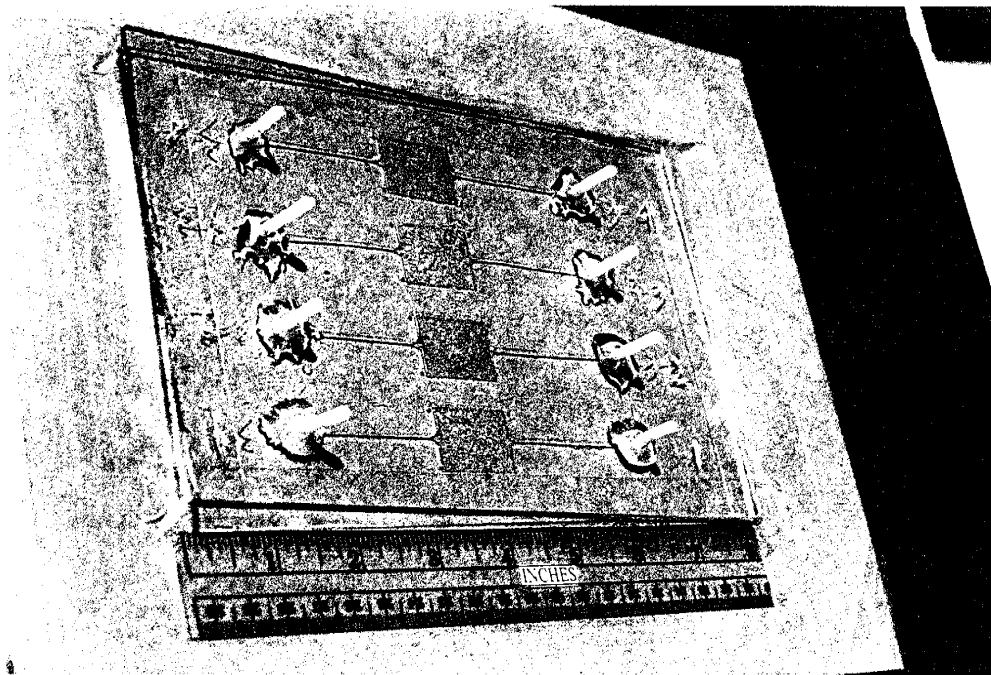


Figure 4.1. Photo of a glass multi-micromodel plate containing four micromodels with a heterogeneous network pattern.

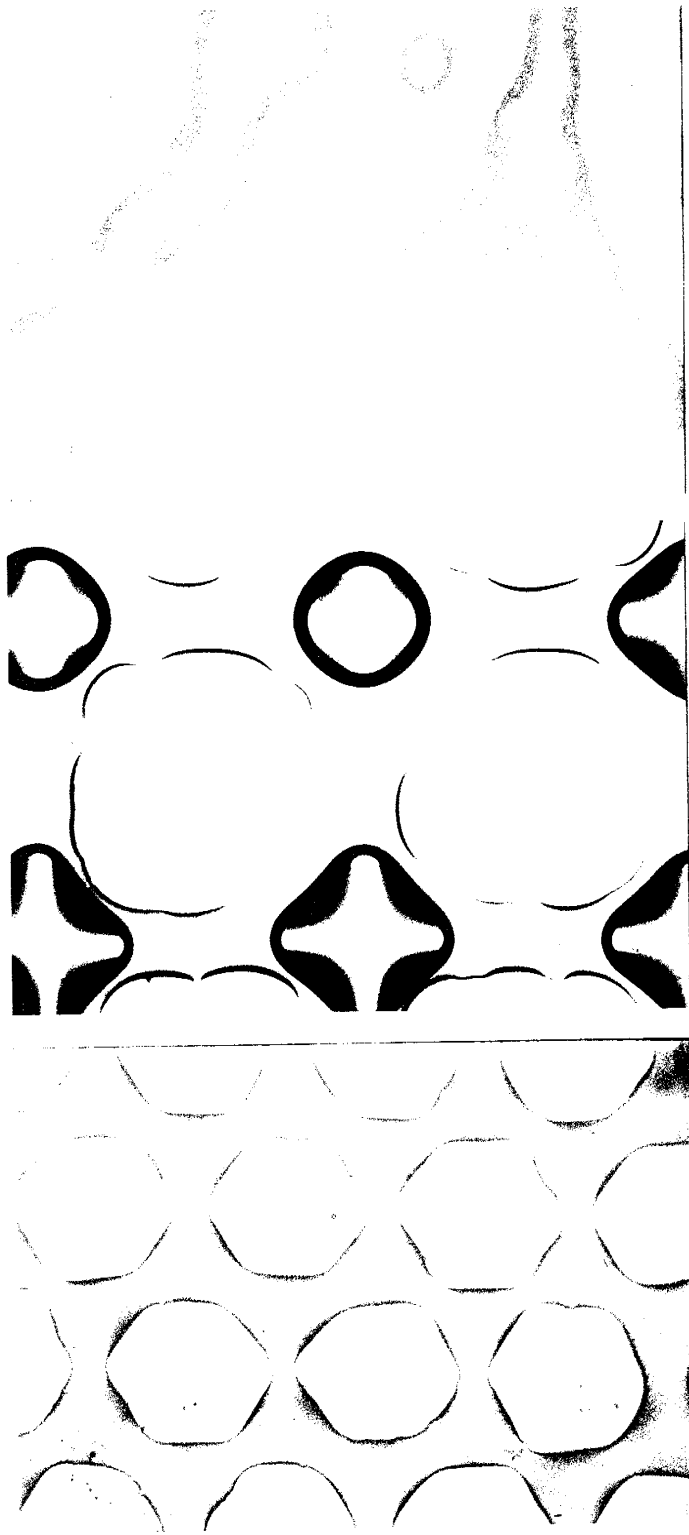


Figure 4.2. Microphotographs of 3 types of networks showing different saturations: (a) saturated hexagonal network, pore size 20-250  $\mu\text{m}$ ; (b) unsaturated quadrilateral network with capillary trapped air bubbles, pore size 20-200  $\mu\text{m}$ ; (c) unsaturated heterogeneous network with continuous gas phase, pore size 20-400  $\mu\text{m}$ .

before use. Cell suspensions were made in a filtered and autoclaved solution. Air was used as the gas phase, and isooctane as the NAPL.

**Bacterial Strains.** Three bacterial strains were used in this research. Arthrobacter sp. (Subsurface Microbiology Culture Collection, ZAL001, Florida State University) was isolated by Kieft (1991) from subsurface sediments (324 m depth). Pseudomonas cepacia 3N3A was isolated by Brockman et al. (1989) from sediment samples at a depth of 203 m. These two strains were isolated from samples collected near the Savannah River Plant, South Carolina. Arthrobacter sp. S-139 was isolated by A. Mills et al. from a shallow groundwater aquifer. All three strains were used in micromodel experiments, but only 3N3A and S-139 were used in the column experiments. Cell size and cell surface characteristics are listed in Table 1. All of the measurements were carried during late stationary phase of growth. Cell size was measured with phase-contrast optical microscope. Electrophoretic mobility was measured with a Coulter DELSA 440 (Doppler Electrophoretic Light Scattering Analyzer) in a solution of 1.0 mM NaNO<sub>3</sub> at pH 6.6. Mobility data were converted to Zeta potentials (the surface potential within the double layer) calculated from the measured mean electrophoretic mobilities by using the tabulated numerical calculations of Ottewill and Shaw (1972). We used a modification of the contact angle method of van Oss and Gillman (1987), employing a filter layer-captive drop technique (Wan and Wilson, 1993a,b). A "flat" layer of bacteria, 50-100  $\mu\text{m}$  thick, was air dried at room temperature until the layer began to crack. An aqueous solution of 1.0 mM NaNO<sub>3</sub> (pH 6.6) was used as the third phase at 24 °C.

Table 4.1. Bacteria Used in the Experiments

Experiments	Bacterial Strain	Size ( $\mu\text{m}$ )	Contact Angle $\theta_a$	Zeta Potential (mV)
Air-water Micromodel & Column	<u>Pseudomonas</u> <u>cepacia</u> 3N3A	1.3x0.8	$24.7 \pm 3.1^\circ$	-12.1
Air-water Micromodel & Column	<u>Arthrobacter</u> sp. S-139	1.0x0.8	$77.1 \pm 2.5^\circ$	-56.3
Isooctane-water Micromodel	<u>Arthrobacter</u> sp. ZAL001	1.1x0.8	$48.2 \pm 2.4^\circ$	-46.2

Bacteria were grown in a 10% PTYG broth at 27°C on a shaker. The broth contained the following ingredients per liter of distilled water (Balkwill and Ghiorse, 1985): 1.0 g glucose, 1.0 g yeast extract, 0.5 g peptone, 0.5 g trypticase, 0.6 g  $\text{MgSO}_4 \cdot 7\text{H}_2\text{O}$ , and 0.07g  $\text{CaCl}_2 \cdot 2\text{H}_2\text{O}$ . When the culture reached a late logarithmic stage of growth (48 h), cells were harvested by centrifugation (5,000 x g, for 10 minutes) and washed three times in a sterile solution of 1.0 mM  $\text{NaNO}_3$  (pH 6.6). Cells were suspended in the same solution to a final concentration of about  $5 \times 10^{10}$  cell/ml, and stored at 5 °C. This concentrated cell suspension was used to make the cell film on a filter for the contact angle measurement. In the micromodel and column experiments the suspension was diluted to about  $5 \times 10^7$  cell/ml in a solution of 1.0 mM  $\text{NaNO}_3$  and pH 6.6.

**Apparatus and Procedure for the Micromodel Experiments.** A high-resolution optical microscope with fluorescent lighting system, dark field image and long-working distance objectives was used (Zeiss Axiophot). During experiments a prepared micromodel was mounted horizontally on the stage of the microscope. Flow rate was controlled by a syringe pump (Harvard Apparatus, Model 4400-001). Photomicrographs and a video record were taken simultaneously.

Micromodel experiments followed this procedure: (a) A new, clean micromodel was saturated by pumping through distilled, deionized and degassed water at as high a pumping rate as possible, until all of the gas was removed or dissolved. (b) A selected number of pore volumes of particle-free solution was pumped through the saturated micromodel to obtain the desired chemical conditions for the pore network. (c) The non-

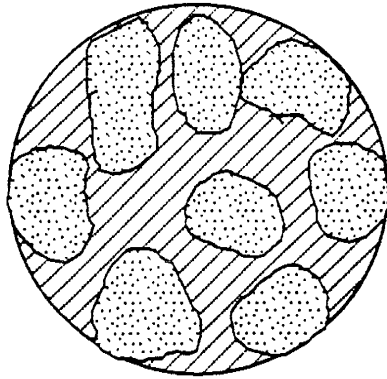
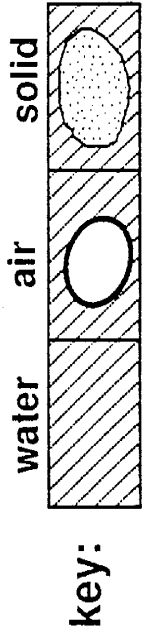


wetting gas phase was trapped in the micromodel as residual bubbles by draining the micromodel with a non-wetting fluid and then reimbibing the wetting fluid (Chatzis, et al., 1983; Conrad, et al., 1992; Wilson, et al., 1990). (d) The micromodel was set on the microscope stage. A dilute cell suspension ( $\sim 5 \times 10^7$  cell/ml) was injected at a constant rate (1.5 ml/hr) for a pre-selected number of pore volumes (usually 30 pore volumes). The behavior of the bacteria was observed and recorded. (e) The cell suspension was replaced with a cell-free solution at the same flow rate until all the free cells were displaced from the micromodel and only cells attached to solid-water and gas-water interfaces were left. (f) The trapped gas bubbles were mobilized and subsequently removed from the network by increasing the pressure gradient (increasing the velocity of wetting fluid). (g) In the NAPL-water experiments, bacteria were cultured in a micromodel after step c above in a solution of 1% PTYG broth for 48 h, then followed by step e (1% PTYG broth contained 0.1x the concentration of organic components used in 10% PTYG broth, but the same concentration of inorganic constituents).

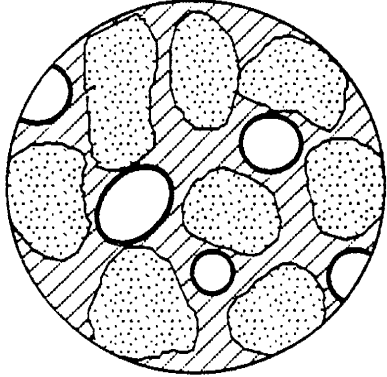
**Materials and Procedure for the Column Experiments.** Cylindrical glass columns (ACE glass Inc.), 30 cm long and 2.5 cm in diameter, were used. The columns were packed with high purity quartz sand (Unimin Co., New Canaan, CT), in grain sizes ranging from 212 to 315  $\mu\text{m}$  in diameter. The purpose of choosing a narrow range of grain size was to gain relatively homogeneous packing and avoid layering. Using quartz sand instead of glass beads, we had better control of the chemical conditions of the solution. A clean medium surface is one of the most important factors controlling the reproducibility of cell breakthrough data. The procedures for sand cleaning and column

packing were presented in Wan and Wilson (1993b). Figure 3 is a schematic illustration of the cross sections of three differently saturated columns. In Figure 3a the column is fully water saturated, and the quartz-water interface is the only interface present. In Figure 3b the column has about 15% gas saturation, with gas trapped as isolated bubbles. Two interfaces, the gas-water and the rock-water interface are present. In Figure 3c the column has about 46% gas saturation; both gas and water are interconnected and two interfaces exist. There were three to five repeated experiments for each combination of saturation and the two bacterial strains, for a total of almost thirty columns. Column parameters and their standard deviations are listed in Table 2. These exact physical and chemical conditions ensured good reproducibility of breakthrough data. Each prepared column had precisely measured porosity ( $n$ ), gas saturation ( $S_g$ ) and water saturation ( $S_w$ ).  $S_g$  and  $S_w$  represent proportions of the void volume of a medium ( $S_g + S_w = 1$ ) occupied by gas and water, respectively. A prepared column also had equilibrium chemical conditions (pH and turbidity of the effluent reached that of the influent).

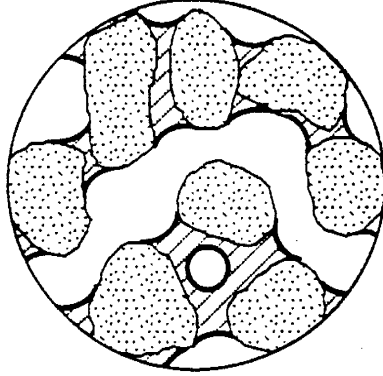
In each experiment the pumping rate  $Q$  (ml/hr) was set to match a pre-selected seepage velocity  $v = Q/nS_w = 10$  cm/hr. A slug of 1 water pore volume of dilute cell suspension ( $\sim 5 \times 10^7$  cell/ml) was injected at the seepage velocity. A water pore volume was calculated as  $S_w V$ , where  $V$  was the total column pore volume. The effluent was collected by a fraction collector at a rate of 6 samples per pore volume. Two water pore volumes of cell-free solution were injected to replace the cell suspension at the same flow rate. Cell concentrations were measured as soon as possible after collection, with a double beam spectrophotometer at a wave length of 260 nm. The weight change of the



(a) Water Saturated



(b) Residual Gas



(c) Continuous Gas

Figure 4.3. Cross-sectional sketch of 3 column types with different saturations.

Table-4.2. Parameters for the Column Experiments

Parameters	Value
Size of sand grains	212 to 315 $\mu\text{m}$
Bulk density	$1.96 \pm 0.021 \text{ g/cm}^3$
Porosity	$0.41 \pm 0.005$
Residual gas saturation	$15.5 \pm 1.1\%$
Continuous gas saturation	$46.5 \pm 2.0\%$
Seepage velocity	10.0 cm/hr
Ionic strength	1.0 mM
pH	$6.65 \pm 0.11$
Column weight changes	$-0.06 \pm 0.053\%$

column at the end of a run was checked, as well as the pH of the effluent. Each of our column experiments ran 9 h and sample analyses required approximately 1 h. A test of conditions conducted before the experiment showed that the cell concentration of the suspensions remained constant over 24 h at a room temperature of 24 °C. This ensured that time was not a factor altering cell concentration during the experiment.

## RESULTS AND DISCUSSION

**Cell Surface Hydrophobicity.** It has previously been suggested that the overall tendency of microorganisms to exhibit hydrophobic surface properties is determined by a complex interplay of polar and apolar outer surface components (Rosenberg and Rosenberg, 1981). Surface moieties that promote or reduce hydrophobicity appear to coexist on the cell surface. It is thus their relative concentration, distribution, configuration, and juxtaposition which determine the tendency of the cell to exhibit hydrophobic surface properties (Rosenberg and Doyle, 1990). Cell surface hydrophobicity is one of the most important factors governing the transport of microorganisms. During the past decade investigators have implicated cell surface hydrophobicity in a wide variety of adhesion phenomena, but have not related it to adhesion on gas-water interfaces. Cell surface hydrophobicity is poorly defined. The absence of a commonly accepted technique for the characterization of cell surface hydrophobicity is a potential problem in current research. If we use a 90° water contact angle as the criterion for separating hydrophobic and hydrophilic surfaces, then the

bacteria studied to date all fall into the hydrophilic range. Obviously, this definition does not serve our purpose. In this paper, we use water-air contact angles of cell surfaces to characterize the relative hydrophobicity. Table 1 lists the advancing contact angles,  $\theta_a$ , and electrostatic mobility data. Each water contact angle value was a mean of 15-24 measurements. Contact angles are roughly inversely proportional to electrostatic mobilities.

**Micromodel Experiments.** In the gas-water system experiments, we used two bacterial strains: hydrophilic strain 3N3A ( $\theta_a = 25^\circ$ ) and the relatively hydrophobic strain S-139 ( $\theta_a = 77^\circ$ ). Their behaviors at the gas-water and glass-water interfaces were visualized and recorded on video tape and photomicrographs. Figures 4 and 5 are photomicrographs taken after slugs of 30 pore volumes of a dilute cell suspensions were injected and then replaced by a cell-free solution. Both photographs were taken under transparent light and a bright field. Bacteria are shown as dark grey spots on the dark air bubble surface (see Figure 2b to see a clean gas bubble and glass surface under the same lighting conditions). The ionic strength was 1.0 mM NaNO<sub>3</sub>, pH 6.6, and flow rate was 1.5 ml/hr. In Figure 4, hydrophilic bacteria are preferentially sorbed onto a trapped gas bubble, relative to the nearby glass pore walls. Only a few cells are sorbed onto the glass surface, mostly where the bubble and the pore walls formed narrow throats. It is clear that there is an adhesion force on the gas-water interface which the glass-water interface does not have. In other words the pair interaction energy of cell/air bubble is attractive, but that of cell/glass is repulsive. For the pair of cell/air bubble, both the electrostatic and van der Waals forces are repulsive; the only attractive force is the hydrophobic force



Figure 4.4. Hydrophilic bacteria 3N3A ( $1.3 \times 0.8 \mu\text{m}$ ) preferentially sorbed on air bubble trapped in a pore body of hexagonal network. The air bubble is at the center and top, filling much of the frame. Bacteria are dark grey spots under the bright field transparent light.

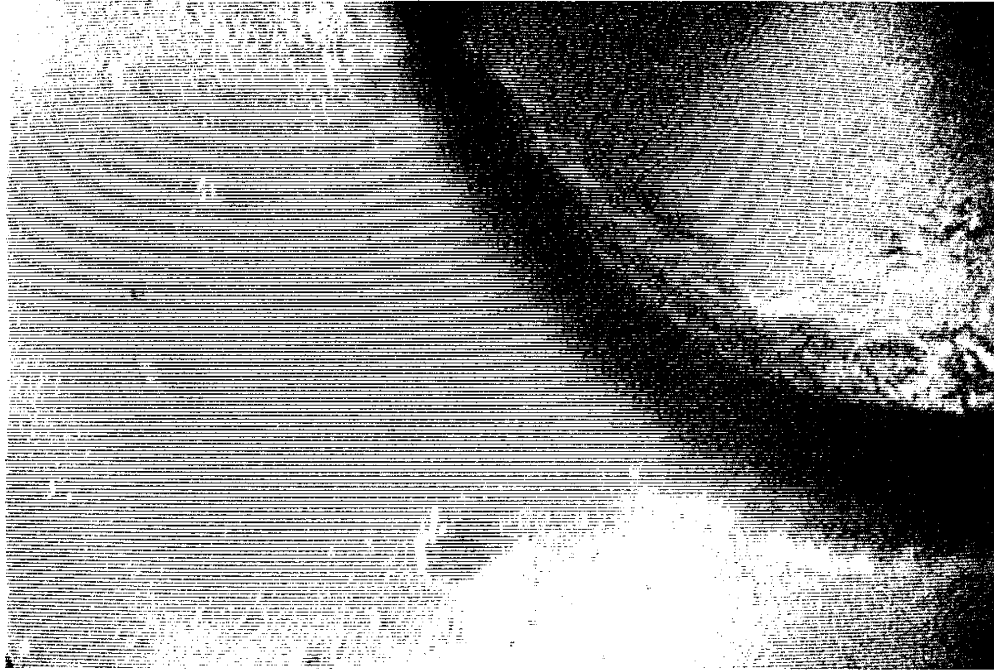


Figure 4.5. Relatively hydrophobic bacteria S-139 ( $1.0 \times 0.8 \mu\text{m}$ ) accumulated on an air bubble and sorbed onto the pore wall in the pore body of a hexagonal network. The air bubble is on the upper right. Bright field and transparent light.



(Wan and Wilson, 1993a), and its absolute value is greater than the sum of the repulsive forces. For the pair of hydrophilic cell/glass, the electrostatic repulsive force is dominant and the total interaction energy is repulsive. The few cells sorbed on the narrow throats may be due to the high momentum energy and high collision rate. Cells with high momentum energy may overcome the energy barrier and fall into the energy valley where van der Waals forces dominate. In Figure 5, relatively hydrophobic cells obviously have a greater affinity for the gas bubble as well as the glass surface, compared with the hydrophilic cells in Figure 4. The pair energy of cell/bubble is more attractive due to the greater hydrophobic force between a cell and a gas bubble, as the cell surface hydrophobicity increases. On the glass surface the total interaction energy changes sign due to the increased hydrophobic force. In Figure 5 the relatively hydrophobic cells have formed aggregates on both the gas-water and glass-water interfaces. This formation is also due to the increased cell surface hydrophobicity.

In Figure 6 relatively hydrophobic bacteria S-139 are shown in white under a dark field. Figure 2c shows this same heterogenous pore network under transparent light. In Figure 6a, a large air bubble is trapped and almost covered by bacteria. This photo was taken after the cell suspension was flooded for 24 hours ( $\sim 240$  pore volumes) through the micromodel, and then displaced by a cell-free solution. Some bacteria have sorbed on the pore walls, especially the side walls. This photo convincingly demonstrates that bacteria prefer the gas-water interface to the glass-water interface. In Figure 6b the trapped air bubble with its sorbed bacteria has disappeared from the network and left behind a few cells sorbed onto the glass surface. This photograph was taken after step f; the residual air bubbles have been mobilized and carried away from the network by

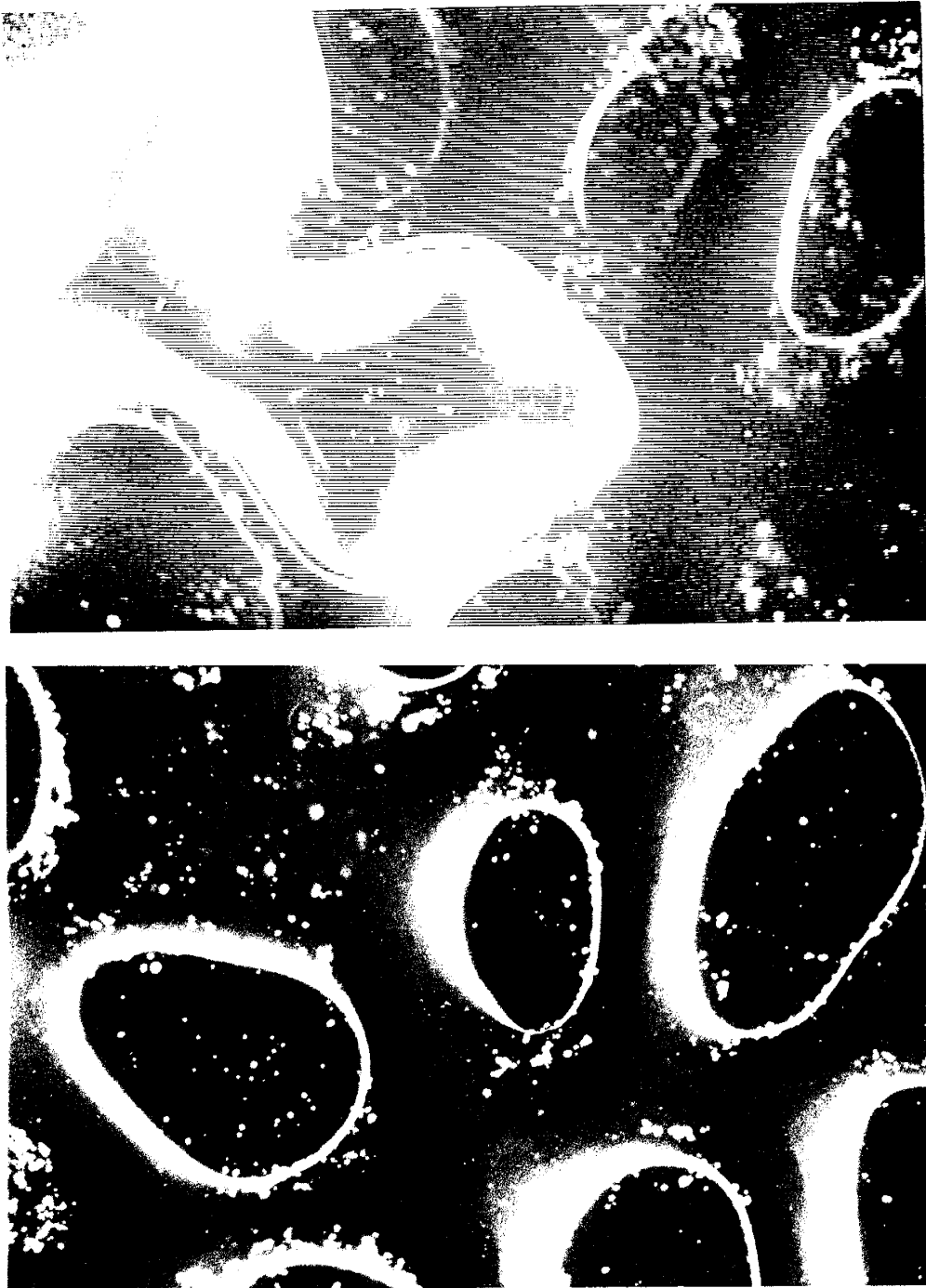


Figure 4.6. Dark field photographs; bacteria are in white; heterogeneous network. (a) A large number of bacteria S-139 ( $1.0 \times 0.8 \mu\text{m}$ ) sorbed on a trapped air bubble, and fewer bacteria sorbed on the pore walls. (b) The air bubble with sorbed bacteria removed by increasing water flow rate.

increasing the water flow rate (Morrow, et al., 1988; Wilson, et al., 1990). This experiment demonstrates that, with increasing shear stress (e.g., during rain events), both the residual gas and continuous gas may be redistributed, thereby enhancing the transport of microorganisms.

Trapping isooctane in a quadrilateral network as the non-wetting phase and using bacterial strain ZAL001 ( $\theta_a=48^\circ$ ), we have studied the behavior of microorganisms on the NAPL-water interface. In the dark field photographs of Figure 7, bacteria are in white surround an oil drop trapped in a pore body. Figure 7a was taken after cells were cultured in a network in a solution of 1% PTYG for 48 hours (we suggest a much lower concentration of PTYG in future experiments). This photo indicates that bacteria prefer the aqueous phase to the oil phase. The bulk population of bacteria has not partitioned into the oil drop. Some of them have passed the three-phase contact line (glass, oil and water). This might be because of the roughness of the glass surface where the water film between glass and oil is thick enough for the bacteria to enter. We also see a higher population of bacteria at the oil-water interface than in the bulk aqueous solution. This might be because of the combination of the attractive pair energy of cell-oil bubble, and the capillary force holding some cells on the oil-water interface (Wan and Wilson, 1993a). The capillary force holds the cells on the interface as long as the cells attach to the interface. In Figure 7b, the cell suspension has been displaced by a cell-free solution. The cells on the oil-water interface remain; only the cells suspended in the aqueous solution have been removed. Some cells sorbed on the glass also remain behind. This photo indicates that under these conditions bacteria prefer the oil-water interface rather than the glass-water interface.



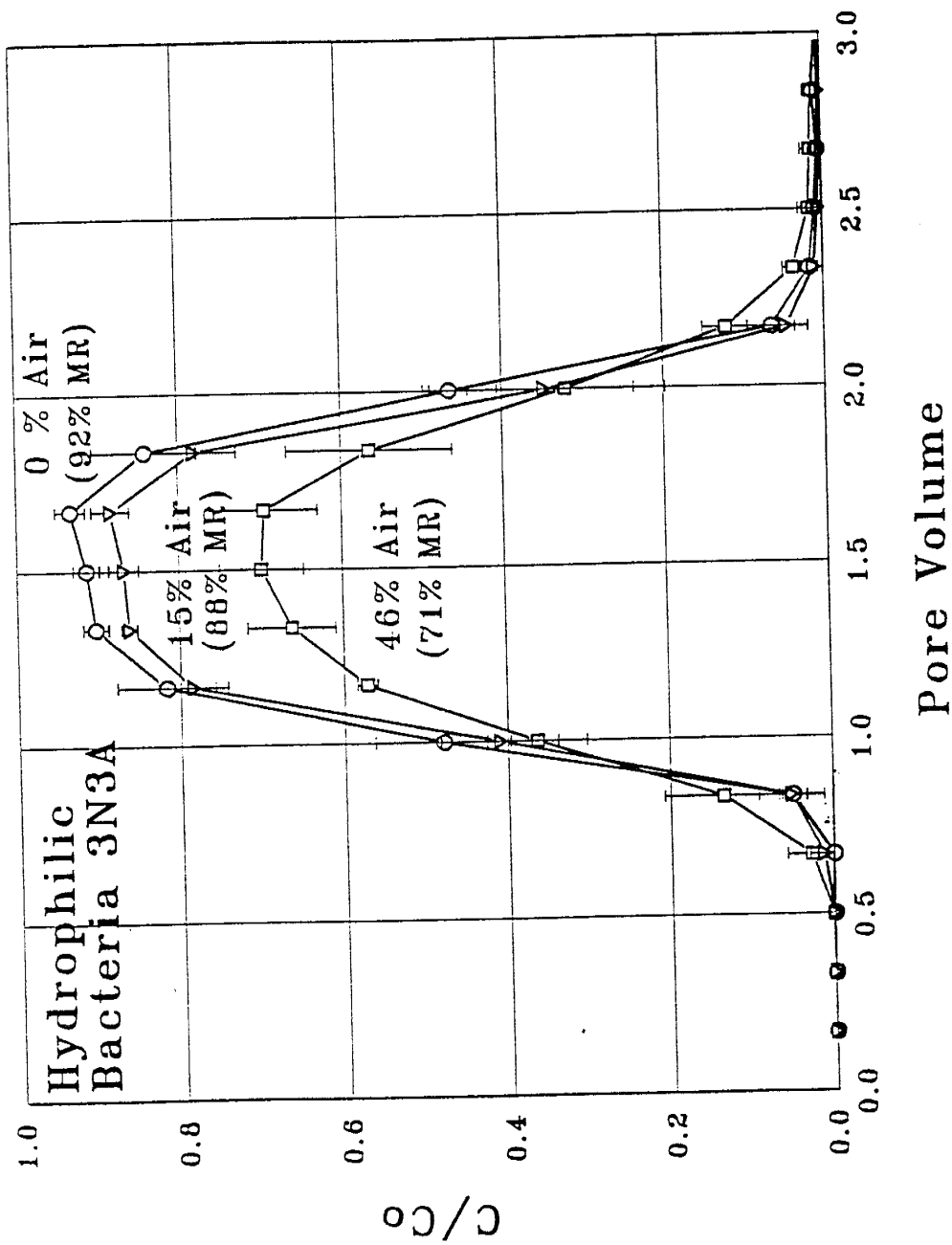
Figure 4.7. Bacterial strain ZAL001 ( $1.1 \times 0.8 \mu\text{m}$ ) with a strong affinity to the organic carbon liquid-water interface. Dark field. (a) Bacteria cultured in a quadrilateral network; (b) Bacteria suspension was displaced by bacteria-free solution after (a). Bacteria remain on the oil-water interface.

**Column Experiments.** The same two strains used in the gas-water system micromodel experiments were used in the column experiments. A slug of 1 water pore volume of cell suspension was pumped from the top into the columns, and then displaced by 2 water pore volumes of a particle-free solution at the same flow rate. Each strain was injected into the three types of columns with different saturations as shown in Figure 3. The results are presented as breakthrough curves where the fraction of the influent cell concentration leaving the packed column ( $C/C_0$ ) is a function of actual water pore volume.  $C$  and  $C_0$ , respectively, are the effluent and influent cell concentrations. The chemical conditions are the same as those in the micromodel experiments. For the three different saturation conditions, all the other experimental conditions are kept the same. Therefore, for a particular bacterial strain the differences among the breakthrough curves are mainly caused by the presence and amount of gas.

Figures 8 and 9 summarize of the data of the two respective strains, 3N3A and S-139. The solid lines have been drawn with the average of the data from 3-5 repeated experiments. The standard deviation of each point is plotted as a vertical error bar. Figure 8 shows the breakthrough curves of hydrophilic 3N3A. The top curve is from the water-saturated columns, the middle curve is from the columns with a trapped residual gas phase, and the lower curve is from the columns with a continuous gas phase. The data show the following features: (a) The mass recoveries are inversely proportional to the gas saturations (correlation coefficient =  $-0.99$ ). Only 8% of the cells were lost in the fully-water saturated columns, indicating unfavorable conditions for cell attachment to the solid surface, a fact which was consistent with the visualization demonstrated by

the clean glass surface in Figure 4. The 8% mass lost might have been caused by a mechanical filtration process, possibly by straining. Increasing the air saturation to the non-wetting phase residual (15.0%) lowered the mass recovery by 4%. Figure 4 suggests that the 4% mass has been irreversibly sorbed by the air bubbles trapped in the pore bodies. Increasing the air saturation further to a continuous air phase decreased the mass recovery by 21% compared to that for water-saturated conditions. This difference was evidently caused by the increased area of the gas-water interface. These retained cells were sorbed onto the gas-water interface and in the narrow pore throats. (b) The standard deviations in repeated experiments were small, relative to the difficulties usually encountered in reproducing data in filtration experiments. (c) The seepage velocity was constant for the columns with different levels of water saturation. Columns were well-packed (homogeneous) and no preferential advection was observed, even for the columns with a continuous gas phase. (d) Slightly increased cell dispersion with increased gas saturation is shown in Figure 8. The moderate increase may have been due to a slight increase in water phase flow tortuosity induced by the presence of the gas. (e) The curves showed no tailing, indicating that sorption onto the gas-water interface is irreversible; in addition any mechanically strained cells were not released. The irreversibility of sorption at the gas-water interface is presumably due to strong capillary forces (Wan and Wilson, 1993a).

Figure 9 shows the breakthrough curves of relatively hydrophobic bacteria from the three types of columns. All of the other experimental conditions were the same as for the hydrophilic cells, and the cell sizes of the two strains were similar. The data indicate



Figures 4.8. Breakthrough curves of bacterial strain 3N3A from columns with three different saturations (3 to 5 replications each). Percentages show the percentage of pore volume occupied by air (% Air) and the percentage of total cell mass recovery (% MR).

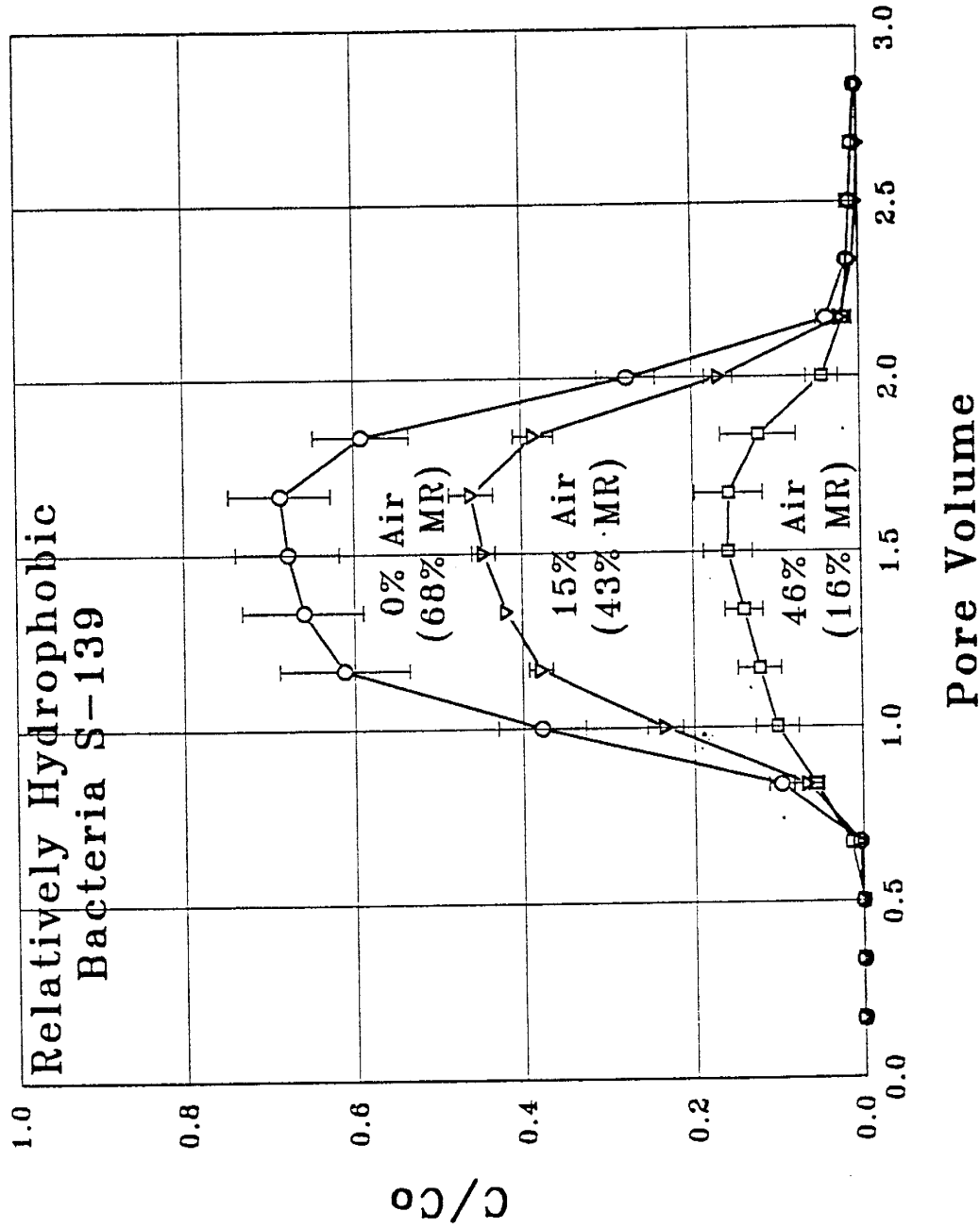


Figure 4.9. Breakthrough curves of bacterial strain S-139 from columns with three different saturations (3 to 5 replications each). Compare the effect of particle hydrophobicity on retention with Figure 4.8.



the following characteristics: (a) A higher proportion of hydrophobic cells than hydrophilic cells were retained in the columns. In the saturated conditions 32% of the total cells were retained by sorption onto the solid surface of the medium as well as by mechanical straining. In the columns of trapped residual air, at least 25% of the cells sorbed onto the gas-water interface. In the columns with a continuous gas phase, at least 52% of the total mass were sorbed onto the gas-water interface. (b) The lack of tailing indicates that sorption onto both interfaces, as well as straining, are irreversible. (c) The relatively small error bars indicate the reproducibility of the data.

If we put Figures 8 and 4; Figures 9 and 5 together, we can observe the effect in one and the cause in the other. The data emphasize the importance of the gas-water interface on the transport of microorganisms in unsaturated porous media.

The glass micromodel technique allows us to determine the effect of the gas-water interface on the fate and transport of bacteria. This technique has the advantage of permitting direct observation of the behavior of bacteria on a pore and network scale under strictly controlled chemical and flow conditions. It has great potential to be used and further developed for additional purposes such as the optimization and monitoring of bioremediation processes, and monitoring the functional activity of bacteria.

Although the column method has been commonly used in laboratory research, the effect of an inadvertent capillary trapped gas phase has been neglected. We have demonstrated that certain conditions previously thought to be saturated may actually be pseudo-saturated and contain gas trapped as a residual phase. For a relatively hydrophobic strain of bacteria, even a small amount of residual gas can dramatically

reduce the transport. We have quantified bacterial sorption as a function of saturation conditions. In addition, the accurately controlled physical and chemical conditions of the column experiments have allowed us to achieve a greater degree of reproducibility than has been previously attained by other researchers using the column methods.

The retention of microorganisms by porous media is in part a function of gas saturation, due to preferential sorption onto the gas-water interface. Even hydrophilic bacteria, which do not sorb onto the solid-water interface under unfavorable chemical conditions, are sorbed by the gas-water interface. The sorption is due to the hydrophobic force: sorption at the gas-water interface increases with increasing particle hydrophobicity. The sorption onto the gas-water interface is also irreversible due to capillary forces. A static gas-water interface sorbs and retains microorganisms, thereby reducing their transport. A gas-water interface with previously sorbed cells can be mobilized and redistributed by the increased shear stress; the mobilized gas-water interface may thus increase the movement of microorganisms. The gas-water interface is a significant factor governing the movement and distribution of microorganisms in the subsurface environment, with potential applications that include in-situ bioremediation, microbially enhanced oil recovery, and wastewater disposal.

**Acknowledgment.** The authors would like to acknowledge Dr. John McCarthy, Dr. Aaron Mills and Dr. Jim Fredrickson for sharing their bacterial cultures, and for their helpful discussion. We thank LuAnn Pavletich for help with editing this manuscript; and we would also like to acknowledge the Subsurface Science Program, Office of Health and Environmental Research, U. S. Department of Energy for supporting this work. DOE Grant Number DE-FG04-89ER60829.

## REFERENCES

- Bales, R. C., C. P. Gerba, G.H. Grondin, and S.L. Jensen. 1989. Bacteriophage transport in sandy soil and fractured tuff. *Appl. Environ. Microbiol.* 55:2061-2067.
- Bales, R. C., S. R. Hinkle, T. W. Kroeger, and K. Stocking. 1991. Bacteriophage adsorption during transport through porous media: chemical perturbations and reversibility. *Environ. Sci. Technol.* 25:2088-2095.
- Balkwill, D. L., and W. C. Ghiorse. 1985. Characterization of subsurface bacteria associated with two shallow aquifers in Oklahoma. *Appl. Environ. Microbiol.* 50:580-588.
- Baven, K., and P. F. Germann. 1982. Macropores and water flow in soils. *Water Resour. Res.* 18:1311-1325.
- Brockman, F. J., B. A. Denovan, R. J. Hicks, and J.K. Fredrickson. 1989. Isolation and characterization of quinoline-degrading bacteria from subsurface sediments. *Appl. Environ. Microbiol.* 55:1029-1032.
- Buckley, J. S. 1991. Multiphase displacements in micromodels. p. 157-189. in *Interfacial Phenomena in Petroleum Recovery*. N.R. Morrow (ed). Marcel Dekker, Inc. New York and Basel.
- Champ, D. R. 1986. Microbial mediation of radionuclide transport. p. 17. In F.H. Molz, J. W. Mercer, and J. T. Wilson (ed.), *Abstracts of the AGU Chapman Conference on Microbial Processes in the Transport, Fate, and In-situ Treatment of Subsurface Contaminants*. Snowbird, Utah. American Geophysical Union, Washington, D.C.
- Chase, K. L., R. S. Bryant, K. M. Bertus, and A. K. Stepp. 1990. Investigations of mechanisms of microbial enhanced oil recovery by microbes and their metabolic products. Dept. of Energy Report No. NIPER-483. Bartlesville, OK.
- Chatzis, I., N. R. Morrow, and H. T. Lim. 1983. Magnitude and detailed structure of residual oil saturation, *Soc. Pet. Eng.* 23:311-325.
- Claus, D. and N. Walder. 1964. The decomposition of toluene by soil bacteria. *J. Gen. Microbiol.* 36:107-122.
- Conrad, S. H., J. L. Wilson, W. R. Mason, and W. J. Peplinski. 1992. Visualization of residual organic liquid trapped in aquifers. *Water Resour. Res.* 28:467-478.
- Corapcioglu, M. Y. and A. Haridas. 1984. Transport and fate of microorganisms in porous media: a theoretical investigation. *J. Hydrol.* 72:149-169.

- Corapcioglu, M. Y. and A. Haridas. 1985. Microbial transport in soils and groundwater: a numerical model. *Adv. Water Resour.* 8:188-200.
- Duncan-Hewitt, W. C. 1990. Nature of the hydrophobic effect, p. 39-74. In *Microbial Cell Surface Hydrophobicity*. R. J. Doyle and Mel Rosinger (eds). American Society for Microbiology. Washington, DC.
- Fontes, D. E., A. L. Mills, G. M. Hornberger, and J. A. Herman. 1991. Physical and chemical factors influencing transport of microorganisms through porous media. *Appl. Environ. Microbiol.* 57:2473-2481.
- Gannon, J. T., V. B. Manlial, and M. Alexander. 1991. Relationship between cell surface properties and transport of bacteria through soil. *Appl. Environ. Microbiol.* 57:190-193.
- Gerba, C. P. and S. M. Goyal. 1981. Quantitative assessment of the adsorptive behavior of viruses to soils. *Environ. Sci. Technol.* 15:940-944.
- Gerba, C. P. 1985. Microbial contamination of the subsurface, p. 53-67. In C. H. Ward, W. Giger, and P. L. McCarty (ed.), *Groundwater quality*. John Wiley & Sons, Inc., New York.
- Grotenhuis, J. T. C., C. M. Plugge, A. J. M. Stams, and A. J. B. Zehnder. 1992. Hydrophobicities and electrophoretic mobilities of anaerobic bacterial isolates from methanogenic granular sludge. *Appl. Environ. Microbiol.* 58:1054-1056.
- Kieft, T. L., and L. L. Rosacker. 1991. Application of respiration- and adenylate-based soil microbiological assays to deep subsurface terrestrial sediments. *Soil Biol. Biochem.* 23:563-568.
- Lance, J. C., and C. P. Gerba. 1984. Virus movement in soil during saturated and unsaturated flow. *Appl. Environ. Microbiol.* 47:335-337.
- Lee, M. D., J. M. Thomas, R. C. Borden, P. B. Bedient, J. T. Wilson, and C. H. Ward. 1988. Bioremediation of aquifers contaminated with organic compounds. *Crit. Rev. Environ. Control.* 18:29-89.
- Marshall, K. C., and R. H. Cruickshank. 1973. Cell surface hydrophobicity and the orientation of certain bacteria at interfaces. *Arch. Microbiol.* 91:29-40.
- Martln, R. E., E. J. Bouwer, and L. M. Hanna. 1992. Application of clean-bed filtration theory to bacterial deposition in porous media. *Environ. Sci. Technol.* 26:1053-1058.

- Morrow, N. R., I. Chatzis, and J. J. Taber. 1988. Entrapment and mobilization of residual oil in bead packs. *SPE Reservoir Engineering*. 3:927-934.
- Mudd, S. and E. B. H. Mudd. 1924a. The penetration of bacteria through capillary spaces. IV. A kinetic mechanism in interfaces. *J. Exp. Med.* 40:633-645.
- Mudd, S. and E. B. H. Mudd. 1924b. Certain interfacial tension relations and the behavior of bacteria in films. *J. Exp. Med.* 40:647-660.
- Ottewill, R. H., and J. N. Shaw. 1972. Electrophoretic studies of polystyrene lattices. *J. Electroanal. Chem.* 37:133-142.
- Peterson, T. C., and R. C. Ward. 1989. Development of a bacterial transport model for coarse soils. *Water Resour. Bull.* 25:349-357.
- Powelson, D. K., J. R. Simpson, and P. Gerba. 1990. Virus transport and survival in saturated and unsaturated flow through soil columns. *J. Environ. Qual.* 19:396-401.
- Powelson, D. K., J. R. Simpson, and P. Gerba. 1991. Effects of organic matter on virus transport in unsaturated flow. *Appl. Environ. Microbiol.* 57:2192-2196.
- Rosenberg, M. and E. Rosenberg. 1981. Role of adherence in growth of Acinetobacter calcoaceticus on hexadecane. *J. Bacteriol.* 148:51-57.
- Rosenberg, M. and R. J. Doyle. 1990. Microbial cell surface hydrophobicity: history, measurement, and significance, p.1-38. In *Microbial Cell Surface Hydrophobicity*. R. J. Doyle and Mel Rosenberg (eds). American Society for Microbiology. Washington, DC.
- Thomas, J. M., and C. H. Ward. 1989. In situ bioremediation of organic contaminants in the subsurface. *Environ. Sci. Technol.* 23:760-766.
- Vandevivere, P., and P. Baveye. 1992. Relationship between transport of bacteria and their clogging efficiency in sand columns. *Appl. Environ. Microbiol.* 58:2523-2530.
- Van Loosdrecht, M. C. M., J. Lyklema, W. Norde, G. Schraa, and A. J. B. Zehnder. 1987. Electrophoretic mobility and hydrophobicity as a measure to predict the initial steps of bacterial adhesion. *Appl. Environ. Microbiol.* 53:1898-1901.
- Van Oss, C. J., and C. F. Gillman. 1972. Phagocytosis as a surface phenomenon. I. Contact angles and phagocytosis of non-opsonized bacteria. *J. Reticuloendothel. Soc.* 12:283-292.

- Vaughn, J. M., E. F. Landry, C. L. Beckwith, and M. C. Thomas. 1981. Virus removal during groundwater recharge: effects of infiltration rate on adsorption of poliovirus to soil. *Appl. Environ. Microbiol.* 41:139-147.
- Wan, J., and J. L. Wilson. 1993a. Visualization of the role of the gas-water interface on the fate and transport of colloids in porous media. Submitted to *Water Resources Research*.
- Wan, J., and J. L. Wilson. 1993b. Colloid transport in unsaturated porous media. Submitted to *Water Resources Research*.
- Wilson, J. L., S. H. Conrad, W. R. Mason, W. Peplinski, and E. Hagan. 1990. Laboratory investigation of residual liquid organics from spills, leaks, and the disposal of hazardous waters in groundwater. R. S. Kerr Environmental Research Laboratory. EPA/600/690/004.
- Wilson, J. T., L. E. Leach, M. Henson, and J. N. Jones. 1986. In situ bioremediation as a ground water remediation technique. *Ground Water Monit. Rev.* 6:56-64.
- Yates, M. V., C. P. Gerba, and L. M. Kelly. 1985. Virus persistence in groundwater. *Appl. Environ. Microbiol.* 49:778-781.
- Yates, M. V., S. R. Yates, J. Wagner, and C. P. Gerba. 1987. Modeling virus survival and transport in the subsurface. *J. Contam. Hydrol.* 1:329-345.

## APPENDIX 4A

### BREAKTHROUGH DATA OF BACTERIA

Abbreviations:

C# = experimental number

C<sub>b</sub> = background of effluent

C<sub>o</sub> = initial cell concentration

C<sub>i</sub> = effluent cell concentration

mr = total cell mass recovery

AVG = the average of repeated experiments

STD = the standard deviation of data from repeated experiments



Table 4.3. Breakthrough Data of Hydrophilic Strain 3N3A through Water-Saturated Columns

C51	C53	C59	C61	AVG	STD
Cb=0.007	Cb=0.005	Cb=0.005	Cb=0.012	0.000	0.000
Co=0.193	Co=0.195	Co=0.199	Co=0.192	0.000	0.000
mr=0.918	mr=0.972	mr=0.887	mr=0.904	0.000	0.000
Ci	Ci	Ci	Ci	C/Co	C/Co
0.007	0.005	0.005	0.012	0.000	0.000
0.007	0.005	0.005	0.012	0.000	0.000
0.007	0.005	0.005	0.012	0.000	0.000
0.007	0.005	0.005	0.012	0.000	0.000
0.014	0.012	0.014	0.027	0.049	0.017
0.085	0.126	0.093	0.099	0.480	0.083
0.154	0.183	0.158	0.171	0.818	0.061
0.182	0.186	0.181	0.184	0.904	0.016
0.185	0.188	0.185	0.184	0.915	0.016
0.188	0.193	0.188	0.188	0.935	0.019
0.176	0.185	0.168	0.156	0.842	0.065
0.101	0.099	0.090	0.102	0.466	0.024
0.027	0.010	0.021	0.022	0.065	0.029
0.012	0.005	0.008	0.017	0.017	0.011
0.009	0.005	0.006	0.016	0.009	0.008
0.008	0.005	0.005	0.015	0.005	0.006
0.011	0.005	0.006	0.014	0.009	0.008
0.009	0.005	0.006	0.014	0.006	0.004

Table 4.4. Breakthrough Data of Hydrophilic Strain 3N3A through Columns with 15% Gas

C52		C56		C63		C/Co		AVG	STD
Cb=0.004	Ci	Cb=0.005	Ci	Cb=0.007	Ci	C/Co	C/Co	0.0000	0.0000
Co=0.200	0.0040	Co=0.194	0.0050	Co=0.168	0.0070	0.0000	0.0000	0.0000	0.0000
mr=0.828	0.0040	mr=0.876	0.0050	mr=0.835	0.0070	0.0000	0.0000	0.0000	0.0000
	0.0040		0.0050		0.0130	0.0357	0.0357	0.0119	0.0168
	0.0100		0.0080		0.0250	0.1071	0.1071	0.0509	0.0402
	0.1060		0.0710		0.0710	0.3810	0.3810	0.4104	0.0724
	0.1730		0.1540		0.1320	0.7440	0.7440	0.7857	0.0431
	0.1790		0.1700		0.1520	0.8631	0.8631	0.8629	0.0100
	0.1820		0.1740		0.1490	0.8452	0.8452	0.8688	0.0183
	0.1840		0.1800		0.1500	0.8512	0.8512	0.8844	0.0235
	0.1530		0.1710		0.1320	0.7440	0.7440	0.7816	0.0524
	0.0350		0.1060		0.0690	0.3690	0.3690	0.3482	0.1500
	0.0060		0.0200		0.0160	0.0536	0.0536	0.0470	0.0279
	0.0050		0.0070		0.0100	0.0179	0.0179	0.0111	0.0053
	0.0050		0.0070		0.0070	0.0000	0.0000	0.0051	0.0042
	0.0040		0.0070		0.0070	0.0000	0.0000	0.0034	0.0049
	0.0040		0.0070		0.0070	0.0000	0.0000	0.0034	0.0049
	0.0040		0.0070		0.0070	0.0000	0.0000	0.0034	0.0049

Table 4.5. Breakthrough Data of Hydrophilic Strain 3N3A through Columns with 46% Gas

C60		C62		C64		AVG
Ci	C/Co	Ci	C/Co	Ci	C/Co	
0.0050	0.0000	0.0100	0.0000	0.0070	0.0000	0.0000
0.0050	0.0000	0.0100	0.0000	0.0070	0.0000	0.0000
0.0060	0.0049	0.0100	0.0000	0.0070	0.0000	0.0016
0.0190	0.0686	0.0100	0.0000	0.0090	0.0114	0.0267
0.0520	0.2304	0.0210	0.0539	0.0280	0.1200	0.1348
0.0940	0.4363	0.0680	0.2843	0.0720	0.3714	0.3640
0.1240	0.5833	0.1280	0.5784	0.1040	0.5543	0.5720
0.1420	0.6716	0.1580	0.7255	0.1110	0.5943	0.6638
0.1490	0.7059	0.1650	0.7598	0.1180	0.6343	0.7000
0.1360	0.6422	0.1710	0.7892	0.1220	0.6571	0.6962
0.1000	0.4657	0.1540	0.7059	0.0990	0.5257	0.5658
0.0560	0.2500	0.1000	0.4412	0.0550	0.2743	0.3218
0.0270	0.1078	0.0430	0.1618	0.0240	0.0971	0.1223
0.0160	0.0539	0.0150	0.0245	0.0130	0.0343	0.0376
0.0120	0.0343	0.0110	0.0049	0.0090	0.0114	0.0169
0.0110	0.0294	0.0100	0.0000	0.0090	0.0114	0.0136
0.0100	0.0245	0.0100	0.0000	0.0090	0.0114	0.0120
0.0070	0.0098	0.0100	0.0000	0.0080	0.0057	0.0052

Table 4.6. Breakthrough Data of Hydrophobic Strain S-139 through Water-Saturated Columns

C79	C81	C82	C85	AVG	STD
Cb=0.005	Cb=0.006	Cb=0.006	Cb=0.006	0.000	0.000
Co=0.222	Co=0.220	Co=0.218	Co=0.208	0.000	0.000
mr=0.674	mr=0.767	mr=0.603	mr=0.666	0.001	0.002
Ci	Ci	Ci	Ci	0.003	0.006
C/Co	C/Co	C/Co	C/Co	0.097	0.015
0.005	0.006	0.005	0.006	0.378	0.052
0.005	0.006	0.005	0.006	0.613	0.077
0.005	0.006	0.006	0.006	0.661	0.072
0.005	0.006	0.008	0.006	0.679	0.061
0.024	0.033	0.025	0.024	0.689	0.060
0.087	0.106	0.072	0.085	0.592	0.057
0.145	0.159	0.111	0.139	0.276	0.034
0.158	0.167	0.123	0.148	0.039	0.012
0.161	0.171	0.132	0.148	0.015	0.005
0.159	0.177	0.138	0.146	0.010	0.005
0.129	0.158	0.127	0.122	0.010	0.005
0.060	0.077	0.069	0.056	0.007	0.004
0.012	0.014	0.018	0.012	0.000	0.000
0.008	0.009	0.010	0.008	0.000	0.000
0.007	0.007	0.009	0.008	0.000	0.000
0.007	0.006	0.008	0.007	0.000	0.000
0.006	0.006	0.007	0.006	0.000	0.000
0.005	0.006	0.005	0.006	0.000	0.000

Table 4.7. Breakthrough Data of Hydrophobic Strian S-139 through Columns with 15% Gas

C75			C76			C80			C86			AVG	STD
Cb=0.006			Cb=0.005			Cb=0.005			Cb=0.006			0.000	0.000
Co=0.124			Co=0.121			Co=0.222			Co=0.208			0.000	0.000
mr=0.422			mr=0.428			mr=0.436			mr=0.445			0.000	0.000
Ci	C/Co		Ci	C/Co		Ci	C/Co		Ci	C/Co		0.004	0.007
0.006	0.000		0.005	0.000		0.005	0.000		0.006	0.000		0.065	0.017
0.006	0.000		0.005	0.000		0.005	0.000		0.006	0.000		0.234	0.021
0.006	0.000		0.005	0.000		0.005	0.000		0.006	0.000		0.378	0.014
0.008	0.016		0.005	0.000		0.005	0.000		0.006	0.000		0.420	0.008
0.013	0.056		0.010	0.041		0.024	0.086		0.022	0.077		0.447	0.014
0.032	0.210		0.032	0.223		0.064	0.266		0.055	0.236		0.461	0.026
0.051	0.363		0.052	0.388		0.093	0.396		0.082	0.365		0.386	0.025
0.057	0.411		0.055	0.413		0.101	0.432		0.094	0.423		0.169	0.017
0.060	0.435		0.057	0.430		0.107	0.459		0.102	0.462		0.023	0.002
0.060	0.435		0.060	0.455		0.105	0.450		0.111	0.505		0.008	0.006
0.054	0.387		0.053	0.397		0.082	0.347		0.092	0.413		0.003	0.003
0.030	0.194		0.026	0.174		0.038	0.149		0.039	0.159		0.000	0.000
0.009	0.024		0.008	0.025		0.010	0.023		0.010	0.019		0.000	0.000
0.006	0.000		0.007	0.017		0.007	0.009		0.007	0.005		0.000	0.000
0.006	0.000		0.006	0.008		0.005	0.000		0.007	0.005		0.000	0.000
0.006	0.000		0.005	0.000		0.005	0.000		0.006	0.000		0.000	0.000
0.006	0.000		0.005	0.000		0.005	0.000		0.006	0.000		0.000	0.000
0.006	0.000		0.005	0.000		0.005	0.000		0.006	0.000		0.000	0.000

Table 4.8. Breakthrough Data of Hydrophobic Strain S-139 through Columns with 46% Gas

C83		C84		C87		C88		AVG	STD
Cb=0.006	0.006	Cb=0.005	0.005	Cb=0.006	0.006	Cb=0.006	0.006	0.000	0.000
Co=0.221	0.000	Co=0.218	0.000	Co=0.212	0.000	Co=0.217	0.000	0.000	0.000
mr=0.128	0.000	mr=0.129	0.000	mr=0.135	0.000	mr=0.153	0.000	0.000	0.000
Ci	C/Co	Ci	C/Co	Ci	C/Co	Ci	C/Co	0.014	0.003
0.009	0.014	0.008	0.014	0.008	0.009	0.010	0.018	0.014	0.003
0.020	0.063	0.014	0.041	0.017	0.052	0.020	0.065	0.055	0.009
0.036	0.136	0.019	0.064	0.026	0.094	0.030	0.111	0.101	0.026
0.036	0.136	0.023	0.083	0.031	0.118	0.035	0.134	0.117	0.021
0.037	0.140	0.029	0.110	0.034	0.132	0.038	0.147	0.132	0.014
0.056	0.226	0.034	0.133	0.036	0.142	0.039	0.152	0.163	0.037
0.062	0.253	0.035	0.138	0.034	0.132	0.036	0.138	0.165	0.051
0.050	0.199	0.025	0.092	0.024	0.085	0.025	0.088	0.116	0.048
0.023	0.077	0.013	0.037	0.013	0.033	0.013	0.032	0.045	0.019
0.014	0.036	0.009	0.018	0.008	0.009	0.009	0.014	0.019	0.010
0.011	0.023	0.009	0.018	0.007	0.005	0.008	0.009	0.014	0.007
0.012	0.027	0.008	0.014	0.006	0.000	0.007	0.005	0.011	0.010
0.011	0.023	0.007	0.009	0.006	0.000	0.007	0.005	0.009	0.008
0.009	0.014	0.006	0.005	0.006	0.000	0.006	0.000	0.005	0.006
0.006	0.000	0.005	0.000	0.006	0.000	0.006	0.000	0.000	0.000

APPENDIX 4B

BREAKTHROUGH CURVES OF BACTERIA

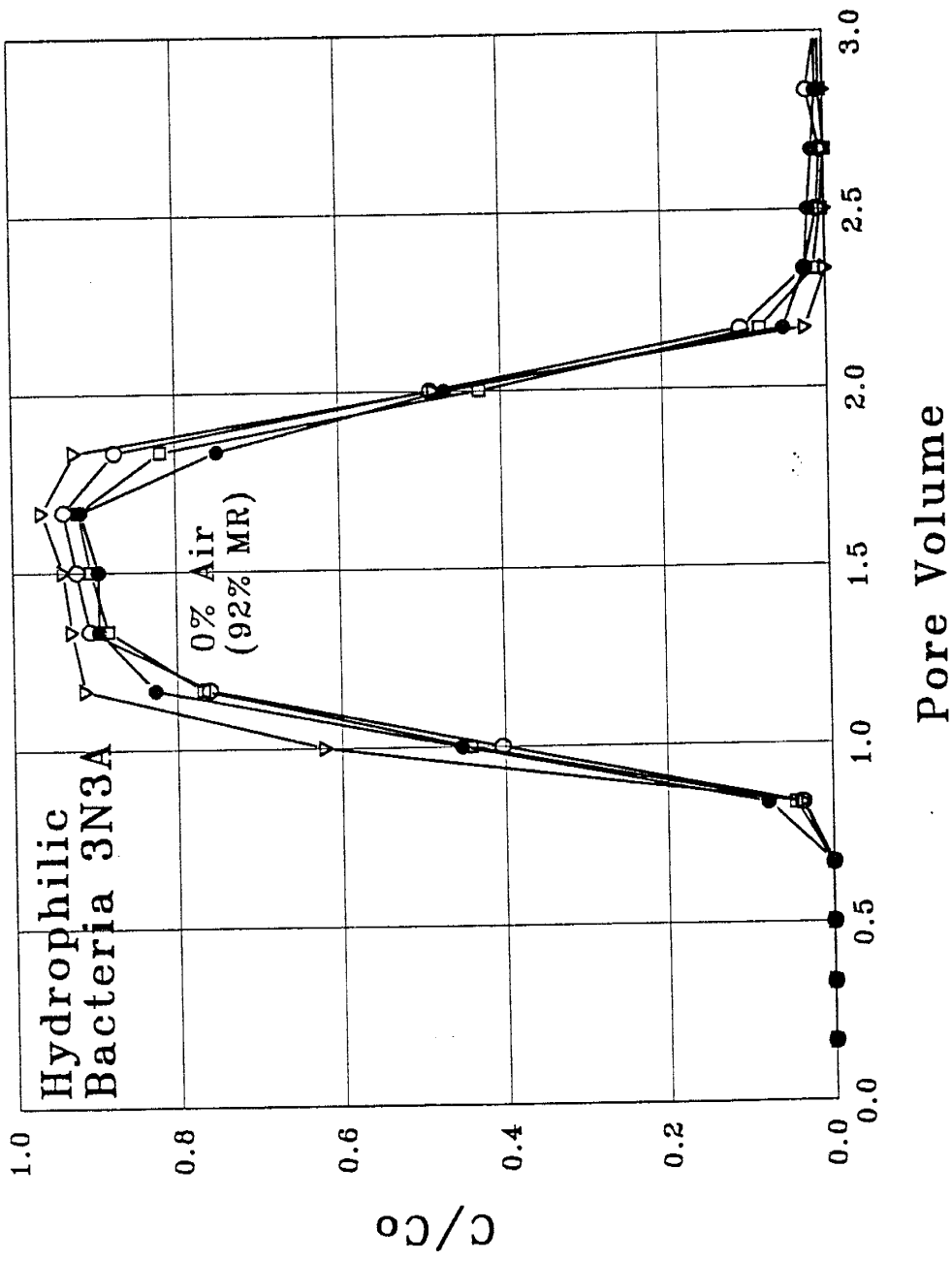


Figure 4.10. Breakthrough curves of hydrophilic strain 3N3A from water-saturated columns.



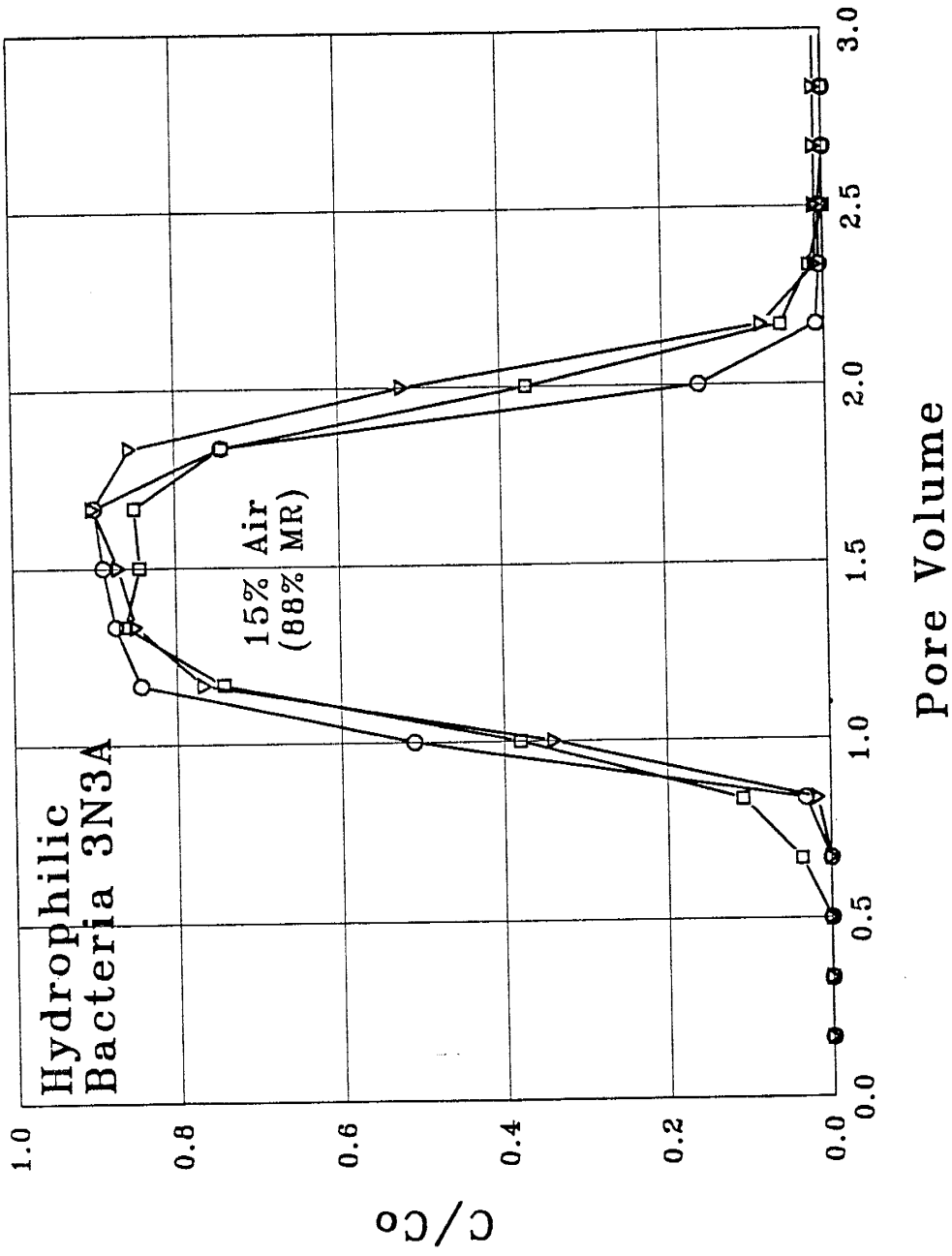


Figure 4.11. Breakthrough curves of hydrophilic strain 3N3A from columns with 15% gas.

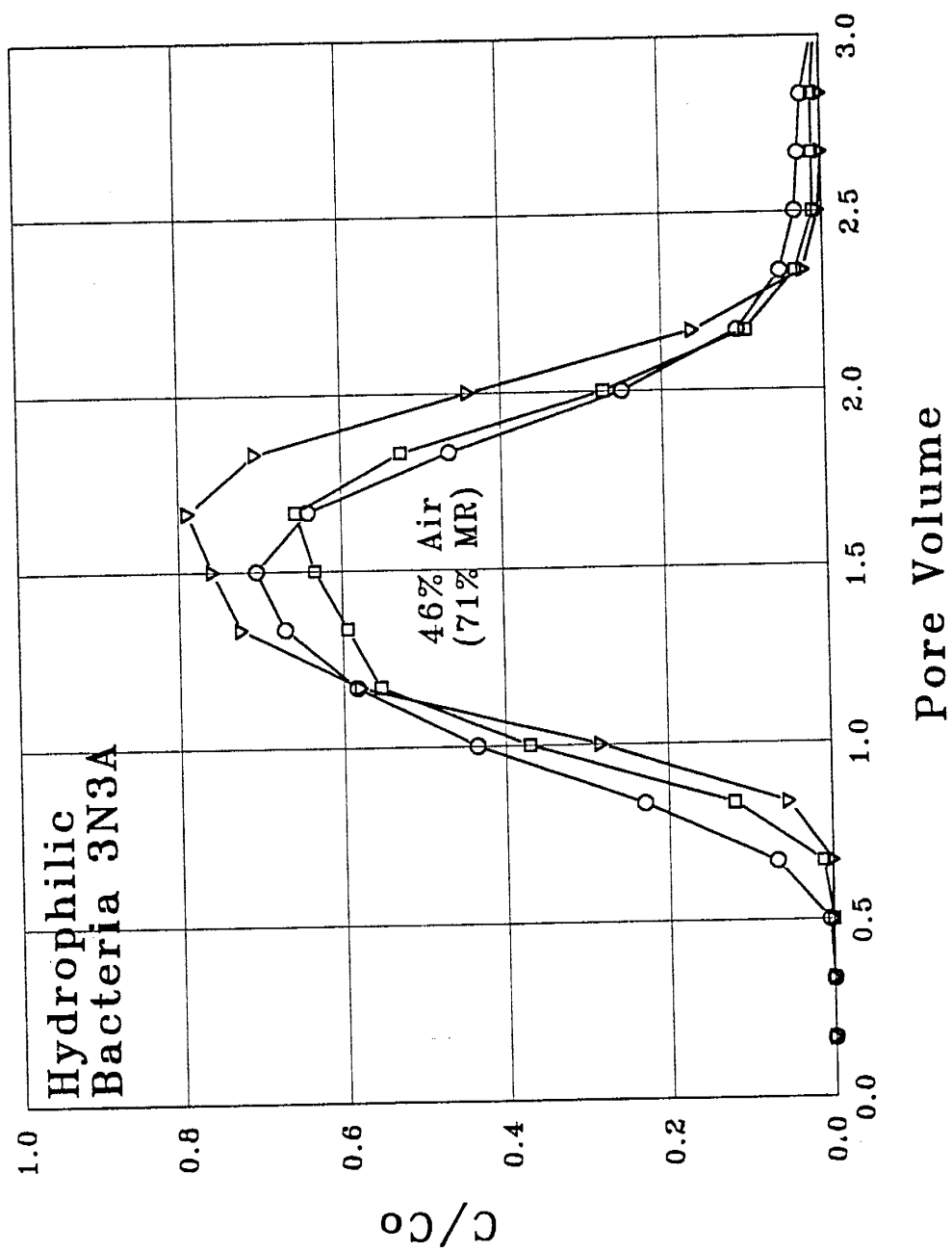


Figure 4.12. Breakthrough curves of hydrophilic strain 3N3A from columns with 46% gas.

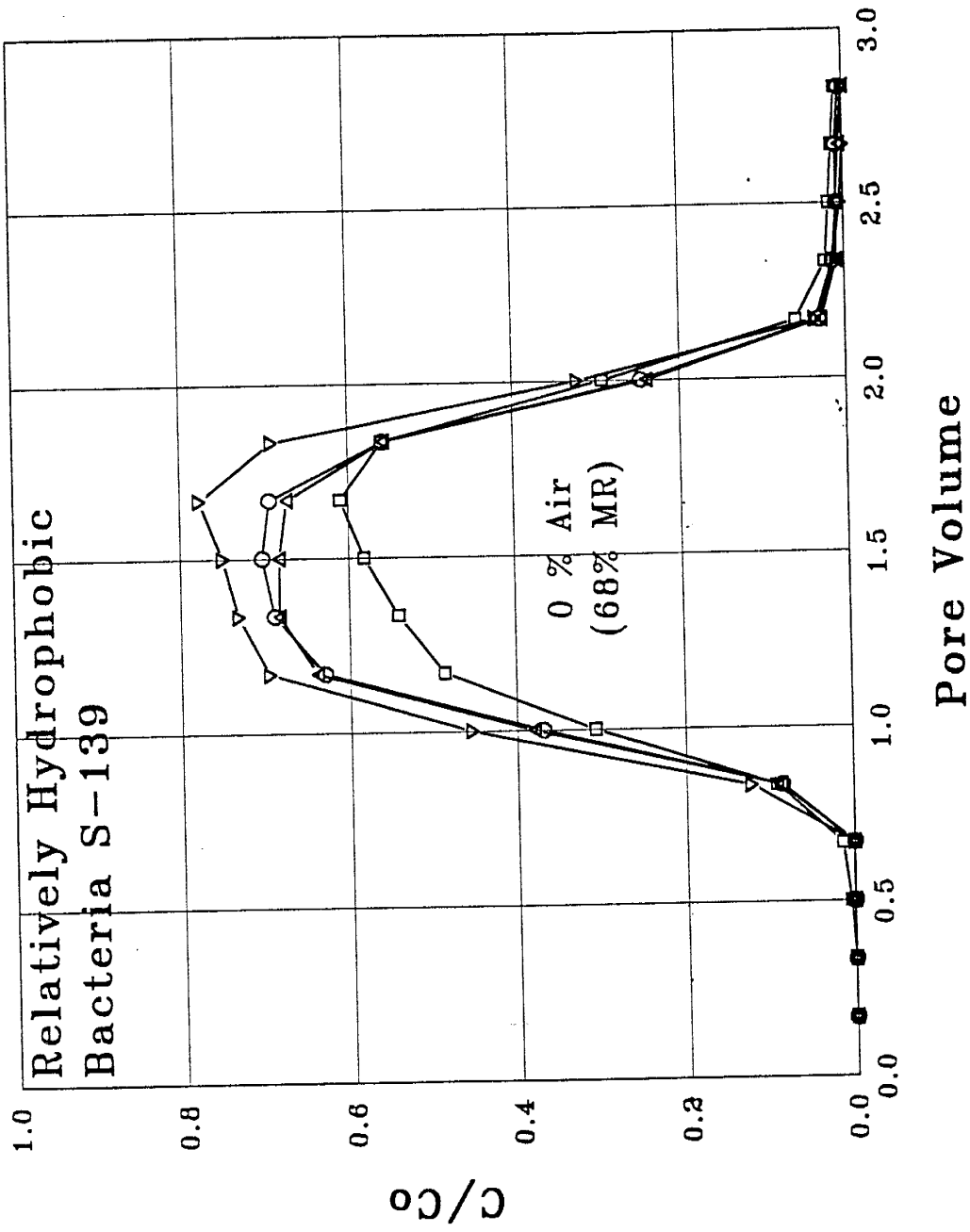


Figure 4.13. Breakthrough curves of relatively hydrophobic strain S-139 from water-saturated columns.

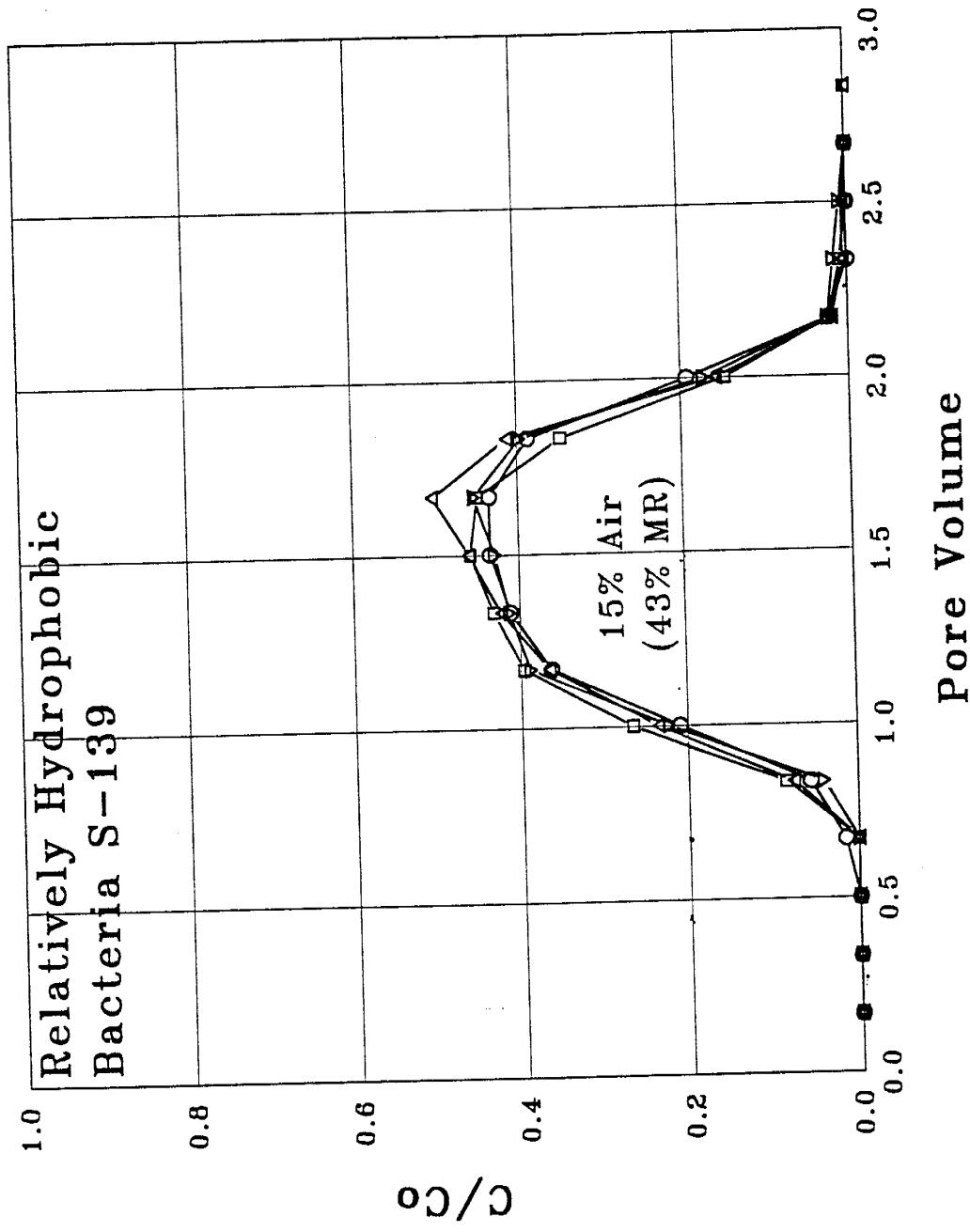


Figure 4.14. Breakthrough curves of relatively hydrophobic strain S-139 from columns with 15% gas.

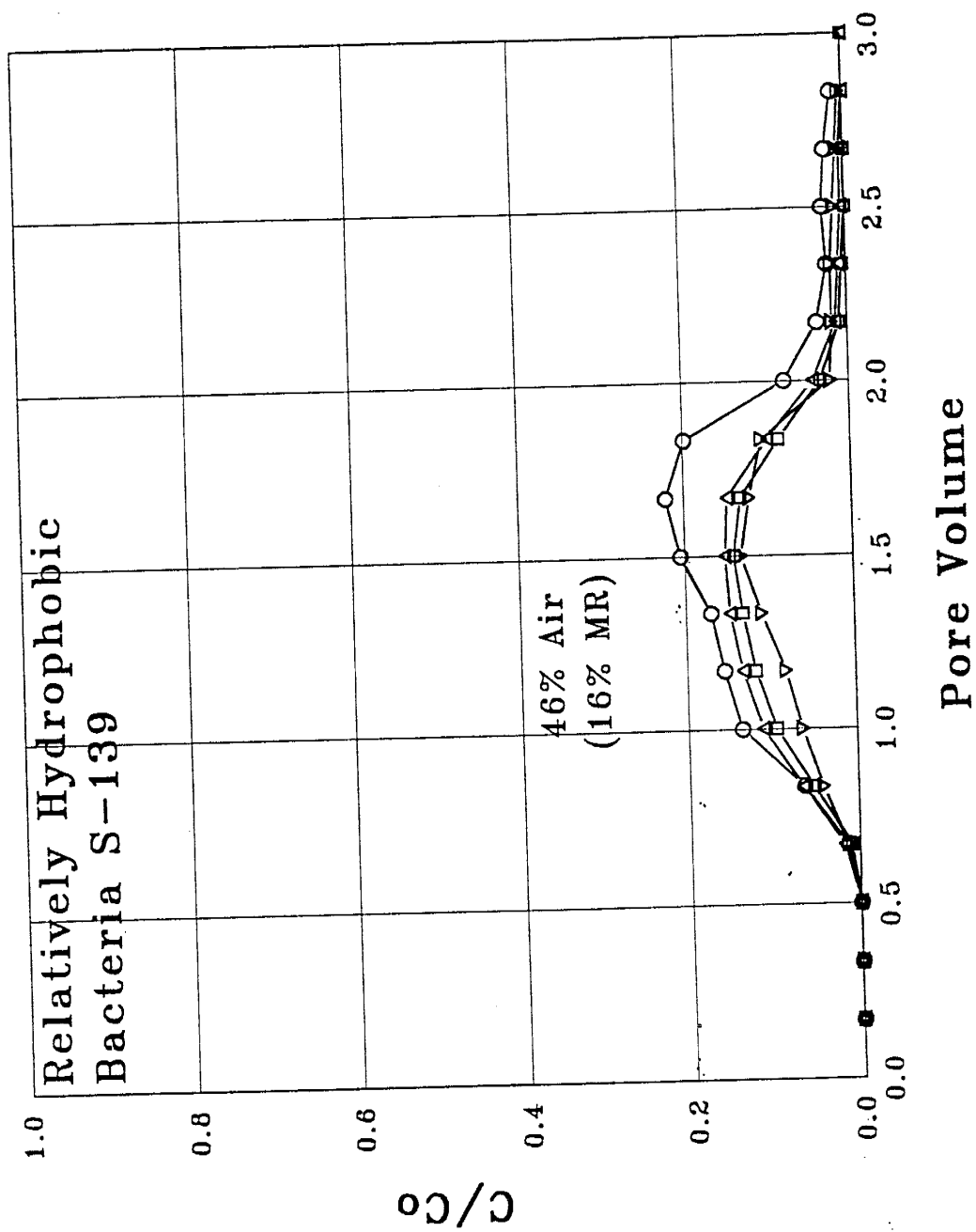


Figure 4.15. Breakthrough curves of relatively hydrophobic strain S-139 from columns with 46% gas.

APPENDIX 4C

PARAMETERS OF COLUMNS IN BACTERIAL  
EXPERIMENTS

Table 4.9. Parameters of Columns in Experiments with Hydrophilic Bacteria

Column	Gas%	n	$\rho_b$	pH	$\Delta$ Weight	$\Sigma$ Mass
C51	0.0	0.421	1.937	$6.60 \pm 0.12$	-0.02%	0.918
C53	0.0	0.412	1.954	$6.41 \pm 0.19$	-0.03%	0.972
C59	0.0	0.402	1.976	$6.55 \pm 0.11$	-0.15%	0.887
C61	0.0	0.413	1.960	$6.38 \pm 0.17$	NA	0.904
avg	0.0					0.921
C52	14.6	0.424	1.937	$6.63 \pm 0.11$	-0.01%	0.828
C56	14.3	0.423	1.937	$6.58 \pm 0.07$	+0.10%	0.876
C63	17.5	0.419	1.966	$6.45 \pm 0.22$	-0.03%	0.835
avg	$15.5 \pm 1.4$					0.846
C60	44.9	0.412	1.906	$6.65 \pm 0.04$	-0.00%	0.720
C62	44.0	0.414	1.907	$6.41 \pm 0.06$	-0.02%	0.755
C64	50.3	0.418	1.906	$6.51 \pm 0.05$	-0.03%	0.652
avg	$46.4 \pm 2.8$					0.709
AVG		$0.416 \pm 0.006$	$1.936 \pm 0.023$	$6.52 \pm 0.094$	$-0.02 \pm 0.067$	

Table 4.10. Parameters of Columns in Experiments with Hydrophobic Bacteria

Column	Gas%	n	$\rho_b$	pH	$\Delta$ Weight	$\Sigma$ Mass
C79	0.0	0.406	1.973	$6.67 \pm 0.13$	-0.04%	0.674
C81	0.0	0.404	2.019	$6.88 \pm 0.07$	-0.15%	0.767
C82	0.0	0.412	1.980	$6.86 \pm 0.07$	-0.04	0.603
C85	0.0	0.403	1.981	$6.89 \pm 0.07$	-0.11%	0.666
avg	0.0					0.677
C75	14.3	0.406	1.940	$6.65 \pm 0.18$	NA	0.422
C76	15.4	0.407	1.948	$7.05 \pm 0.19$	NA	0.428
C80	16.2	0.404	1.974	$6.80 \pm 0.12$	-0.12%	0.436
C86	16.3	0.402	1.988	$6.69 \pm 0.02$	+0.00%	0.445
avg	$15.5 \pm 0.8$					0.433
C83	46.5	0.407	1.978	$6.62 \pm 0.06$	-0.13%	0.128
C84	47.7	0.402	1.980	$6.64 \pm 0.06$	-0.15%	0.129
C87	47.9	0.395	1.991	$6.83 \pm 0.17$	NA	0.135
C88	44.8	0.406	1.980	$6.85 \pm 0.11$	NA	0.153
avg	$46.7 \pm 1.2$					0.136
AVG		$0.404 \pm 0.004$	$1.978 \pm 0.019$	$6.78 \pm 0.13$	$0.10 \pm 0.04$	



---

## CHAPTER 5

---

### SUMMARY AND RECOMMENDATIONS

The major findings of this work and its contribution to the understanding of the behavior of colloids and bacteria at the gas-water interface in a groundwater system may be summarized as follows:

1. The preferential and irreversible sorption of colloids onto the gas-water interface suggests a mechanism for vadose zone transport. A stationary gas-water interface behaves as a sorbent phase retaining the particles and reducing colloid transport. However, moving interfaces occurring during drainage or imbibition may increase the movement of colloids into the deeper vadose zone and underlying aquifer (see Appendix 5A).
2. The glass micromodel technique developed in this dissertation allows us to directly visualize the behavior of colloids and bacteria at interfaces within individual pores and pore networks under strictly controlled chemical and flow conditions. It has great potential to be used and further developed for additional purposes such as the optimization and monitoring of bioremediation processes, and the monitoring of the functional activity of particulate contaminants.
3. The phenomenon of the capillary trapping non-wetting phase in laboratory and

field experiments has not attracted enough attention. Many porous media previously thought to be saturated may actually be pseudo-saturated and contain gas trapped as a residual phase. It has been demonstrated in this research that for relatively hydrophobic particles, even a small amount of residual gas can dramatically affect transport.

4. Although the column method has been commonly used in laboratory research, it has been demonstrated in this research that under accurately controlled physical and chemical conditions, a greater degree of reproducibility than has been previously attained by other researchers, is achievable.

On the basis of the research that has been conducted during this investigation, the following areas for future research are suggested:

1. The work on dynamic gas-water interfaces needs to be completed by conducting quantification and further visualization experiments.

2. To better predict the vadose zone transport of particulate contaminants and microorganisms, new mathematical models involving the effects of the gas-water interfaces should be considered and the data from column experiments can be used to validate the models.

3. Similar to that of colloidal particles, dissolved hydrophobic organic matter behavior at the gas-water interface is a significant question requiring investigation.

4. The behavior of colloids at NAPL-water interfaces should be investigated. In particular, the interfacial tension variation due to particle accumulation onto the interface, and the subsequent effects on mobilization and redistribution of residual NAPL, would be extremely interesting to investigate.

## APPENDIX 5A

### A DYNAMIC VS. A STATIC GAS-WATER INTERFACE

The subject of dynamic gas-water interfaces is not included in this submitted paper, because it is unfinished and has potential to be further developed as a independent subject. I plan to continue this research in the near future. The primary result is presented in this appendix.

In steady and slow flow conditions, the gas-water interface is static, suspended particles approach the gas-water interface by diffusion and advection, and the DLVO and structural forces control the sorption. However, in many cases the gas-water interface is dynamic, such as during an infiltration event following a heavy rainfall, and during a natural drying-wetting process. The gas-water interface takes the initiative to approach the particles sorbed on the pore walls. In these cases DLVO forces are no longer important, and the capillary forces are the governing forces. Therefore the sorption of particles onto the gas-water interface should be more efficient. This idea has been tested and the result is shown in Figure 5.1.

Positively charged polystyrene latex particles were used. Ionic strength of the solution and suspension was 1.0 mM and pH was 6.6. At the first step particles were sorbed onto the pore walls and the residual air bubbles by flooding through 30 pore volumes of particle suspension; then the suspension was replaced with particle-free solution. In Figure 5.1a, the entire pore and air bubble surfaces are covered by particles. Next, moving gas-water interfaces were created by injecting air to displace the

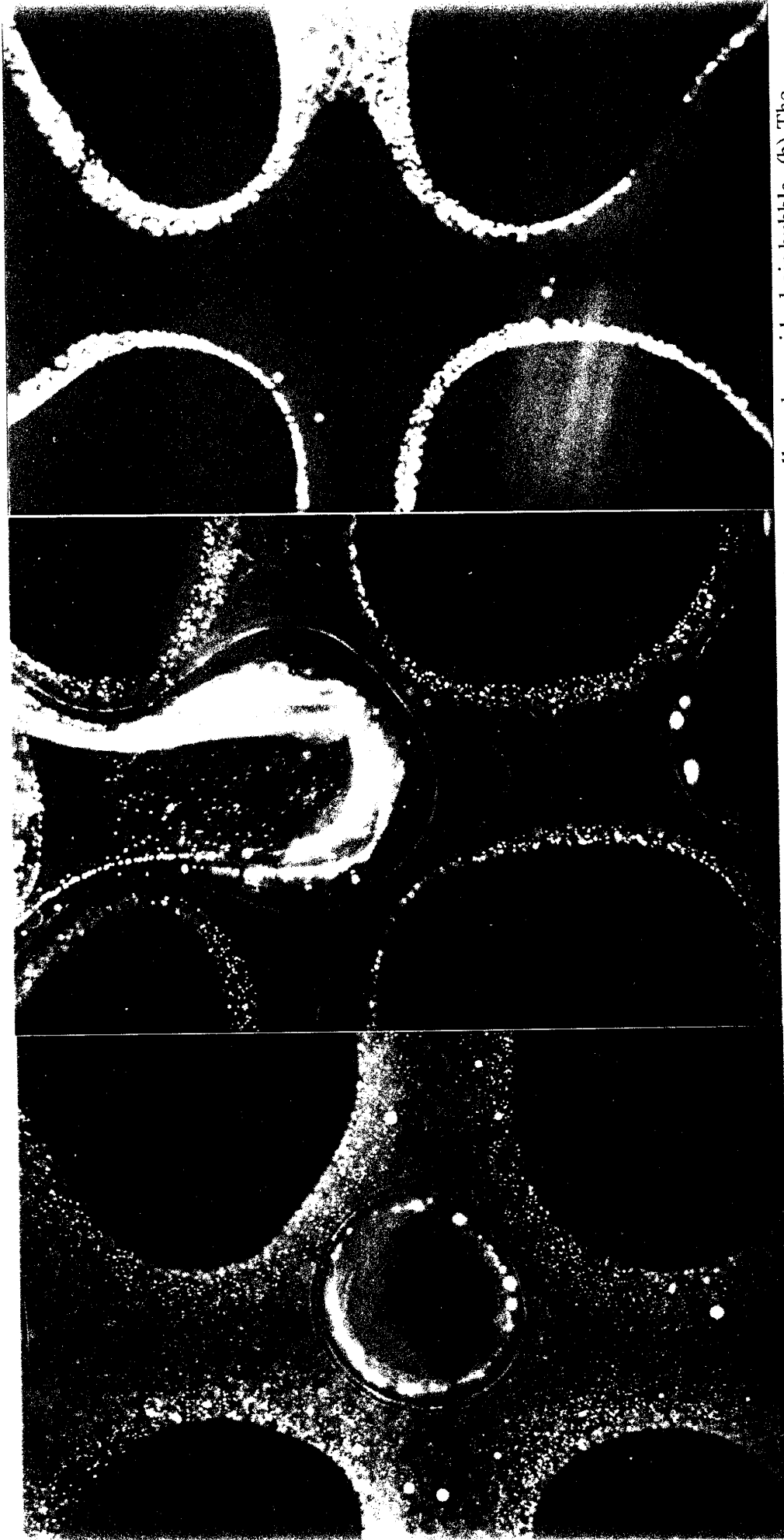


Figure 5.1. Effect of a moving gas-water interface. (a) Particles sorbed on the pore walls and a residual air bubble. (b) The front of a moving gas-water interface, which strips, sorbs and carries particles along with it. (c) The detachment is complemented from the walls of the ore body, but particles are left in pore wedges and dead zones, where the interface is not able to reach.

aqueous phase. The moving interface detached all of the particles sorbed on the pore walls anywhere it reached. Figure 5.1b shows the front of a moving interface. Finally, the solution was injected to displace the air phase and carry the interface away. Figure 5.1c shows that the detachment is completed in the pore bodies, but particles remain in pore wedges and dead zones. In real porous media, these are the grain-grain contacts.